High spatial resolution mapping of African wetlands using multi-sensor data analysis

Sani Idris Garba

Submitted in accordance with the requirements for the degree of

Doctor of Philosophy

The University of Leeds

School of Geography

November 2024

The candidate confirms that the work submitted is his own, except where work which has formed part of jointly authored publications has been included. The contribution of the candidate and the other authors to this work has been explicitly indicated below. The candidate confirms that appropriate credit has been given within the thesis where reference has been made to the work of others.

The work in Chapter four of the thesis has appeared in a publication as follows:

Garba, S.I., Ebmeier, S.K., Bastin, J.F., Mollicone, D. and Holden, J. 2023. Wetland mapping at 10 m resolution reveals fragmentation in southern Nigeria. Wetlands Ecology and Management. ***31****(3), pp.329–345.*

The work in Chapter five of the thesis has been submitted, reviewed, revised and resubmitted with the same authors as above.

In both cases I was responsible for the study design, data collection and analysis, preparation of figures, and writing the manuscript. Professor Joseph Holden and Dr Susanna Ebmeier are my supervisors and oversaw the work. They provided conceptual direction, advised on study design, analyses and discussion. Some ground truth data were provided by co-authors Bastin and Mollicone. All authors contributed to review and editing of the research papers.

Acknowledgements

Firstly, I would like to thank Almighty God for giving the me health and blessing me with wonderful supervisors for my research work. Words cannot express my gratitude to my PhD supervisors Professor Joseph Holden and Dr. Susanna Ebmeier for their support, guidance and encouragement throughout the whole project. Their enthusiasm and patience inspired me a lot. Above all, their caring approach and kindness are the source of my motivation especially during difficult times in my research journey. I will never forget your support and friendly gestures.

I would like to thank the PTDF for funding my research project and support throughout my research years. I also want to thank my transfer examiners Professor Alexis Comber and Dr Paul Morris who used their precious time to review my early work and gave helpful comments and suggestions about this research. I want to thank all members of the River Basins research cluster and water@leeds for creating good times and friendship. Thanks also to everybody in the University of Leeds Peat Club for sharing their knowledge, advice and friendship. It has been a real pleasure to be part of the School of Geography for the past five years and I thank the wonderful people in the department, including Andy Turner for his advice, guidance and willingness to support at any time.

I also want to thank the Graduate School Senior Officer Jacqui Manton for valuable assistance from the beginning of my project application to the completion of this project. I want to thank Jean-François Bastin for providing me with some valuable data and suggestions during my project. Thanks to all researchers and institutions who provided data or any support I used in this project. The thesis presented here has only been possible with your generous freely available datasets. I also want to thank Jiren Xu and all the students under Professor Holden's supervision for their friendship and support.

I am thankful to all my family and friends for all wishes and support. Many thanks to my wife for her endurance and kindness. Thanks to my mother and father-in-law for their support and goodwill prayers. My special gratitude goes to my Mum and Dad for their tireless support and unconditional love - I am really indebted to you forever.

Abstract

This thesis integrates optical indices and SAR polarimetric features obtained from Sentinel-1 SAR and Sentinel-2 optical imagery from different seasons using a Random Forest classification algorithm to produce a detailed wetland map, first for southern Nigeria, and then for the whole of the main continent of Africa at 10 m resolution. Wetlands of southern Nigeria cover a total area of 29,924 km^2 and those of Africa cover 947,750 km^2, larger than that indicated in previous coarser global wetland maps, excluding open water bodies. A wetland fragmentation and population density index was developed indicating that ~13,021 km^2 of wetlands are potentially threatened by human activity within Africa. Using the new map and compiled wetland carbon inventory data, it was estimated that African wetland contains about 54.30 Gt of carbon which is around 5% to 9% of wetland soil carbon stored globally. Calculations across a range of climate zones suggest that drained peatland, mangrove and marsh in Africa could emit 260Mt C yr^{-1} (936Mt CO_2 yr^{-1} equivalents) which is equivalent to 2.4% of global net annual CO_2 emissions. Field sampling across Africa is required in order to include emissions from other wetland types. Long-term assessment of changes within the wetlands of the Lake Chad region for 2000-2020 showed that there was a net loss of wetland area. The greatest wetland decline occurred between 2000 – 2005 with a net loss of 277 km^2 (±12 km^2). However, there was wetland loss for all periods studied, including during a wetter period when it was anticipated that wetland extent would increase. The most significant change occurred around the northern pool of the lake. The tools developed by this study pave the way for ongoing high-resolution monitoring and assessment of African and global wetlands.

Table of Contents

List of Figures

List of Tables

Abbreviations

ANN	Artificial Neural Network
AVIRIS	Airborne Visible and Infrared Imaging Spectrometer
BTU	Built Up
CASI	Compact Airborne Spectrographic Imager
CIFOR	Center for International Forestry Research
CO	Carbon dioxide
CTL	Cultivated land
CVA	Change Vector Analysis
DPW	Deep water
DT	Decision Tree
DVI	Difference Vegetation Index
DVWI	Difference between vegetation and water
DWAF	Department of Water and Sanitation
EM	Expectation–Maximization
EO	Earth Observation
ETM	Enhanced Thematic Mapper
FAO	Food and Agriculture Organisation
FREL	Forest Emission Reference Level
FRST	Forest
GEE	Google Earth Engine

GHG	Green House Gases
GIS	Geographical Information System
GLC	Global Land Cover
GLWD	Global Lake and Water Database
GLWD	Global Lake and Wetland Database
GS	Gramm–Schmidt
IPCC	Intergovernmental Panel on Climate Changes
IRS	Indian Remote Sensing Satellite
ISODATA	Iterative Self Organizing Data Technique
JULES	Joint UK Land Environment Simulator
KNN	K Nearest Neighbour
LISS	Linear Imaging Self
LULC	Land Use Land Cover
MLC	Maximum Likelihood Classification
MNDWI	Modified Normalized Difference Water Index
MNG	Mangrove
MODIS	Moderate Resolution Imaging Spectro
MSAVI	Modified Soil Adjusted Vegetation Index
MSI	Multispectral Instrument
MSI	Moisture Stress Index

MSS	Multi Spectral Scanner
NASA	National Aeronautics and Space Administration
NDMI	Normalized Difference Moisture Index
NDVI	Normalized Difference Vegetation Index
NDWI	Normalized Difference Water Index
NIR	Near Infrared
NWI	National Wetland Inventory
PCA	Principal Component Analysis
PCC	Post Classification Comparison
RF	Random Forest
SAR	Synthetic Aparture Radar
SAVI	Soil Adjusted Vegetation Index
SHW	Shallow Water,
SMM	Spectral Mixture Models
SPOT	Systeme Pour l'Observation de la Terre
SR	Simple Ratio
SRTM	Shuttle Radar Topography Mapper
SVM	Support Vector Machine
SWIR	Shortwave Infrared
SWP	Swamp
TCWI	Tessled Cap Wetness Indices
TM	Landsat Thematic Mapper

US	United States
WFPI	Wetland fragmentation and population index

Chapter 1
Introduction

1.1 Problem statement

African wetlands include some of the most productive ecosystems in the world, and in many cases serve as the exclusive source of natural resources upon which rural economies depend (Amler et al., 2015; Nsengimana et al., 2017; Musasa and Marambanyika, 2022), providing food, energy, medicine and building materials for large human populations (Metz, 2017; Igu and Marchant, 2017; Ondiek et al., 2020). In addition to water purification (Salimi and Scholz, 2021), flood attenuation, carbon storage and sequestration, wetlands provide unique and highly productive landscapes for fodder, fibre and fuel (Nhamo et al., 2017; Steinbach et al., 2021). Wetlands, with their abundant store of freshwater, generally organic-rich soils, and high productivity, play a central role in the economy of all large African river basins and coastal zones (Adekola et al., 2012; Ondiek et al., 2020; Steinbach et al., 2021; Matema et al., 2022). African wetlands are thought to store over 30 Pg of carbon but are increasingly threatened by climate change, watershed development, agricultural expansion, invasive species, and pollution (Ouyang and Lee, 2020; Ballut-Dajud et al., 2022). Human interference in combination with effects of climate change, may compromise the functionality of these socio-ecological systems (Amler et al., 2015; Mandishona and Knight, 2022; Li et al., 2022). Recent studies estimate 30-50% loss of some African wetland types in recent decades, underscoring the need for improved conservation efforts (Rebelo et al., 2010; Bootsma et al., 2019).

Yet, information about African wetlands is far from complete. The existing wetland mapping products on a global scale, such as the Ramsar site database, only contain information on wetlands that have been classified as of ‘international importance’. The Global Lakes and Wetlands Database (GLWD) has information that is dated and probably incomplete (Gumbricht et al., 2017; Hu, Niu and Chen, 2017; Steinbach et al., 2021). Other recent mapping products such as PEATMAP (Xu et al., 2018) are typically based on secondary data of varying quality and age with a mix of spatial resolutions. An obvious example can be seen in the centre of Figure 1.1 where there is a sudden discontinuity in peatland coverage between country borders. GLWD and PEATMAP also do not provide information on the dynamic condition of African wetlands. Consequently, this makes it more difficult to assess the impact of human activities on the surrounding wetland ecosystem. Furthermore, in recognition of the climate change problem, the IPCC (2013) Wetland Supplement shows that there is a need to understand the distributions of wetlands and their interactions with the climate system much more. There is also a need to investigate the result of human interaction with wetlands, especially in densely populated regions of Africa.

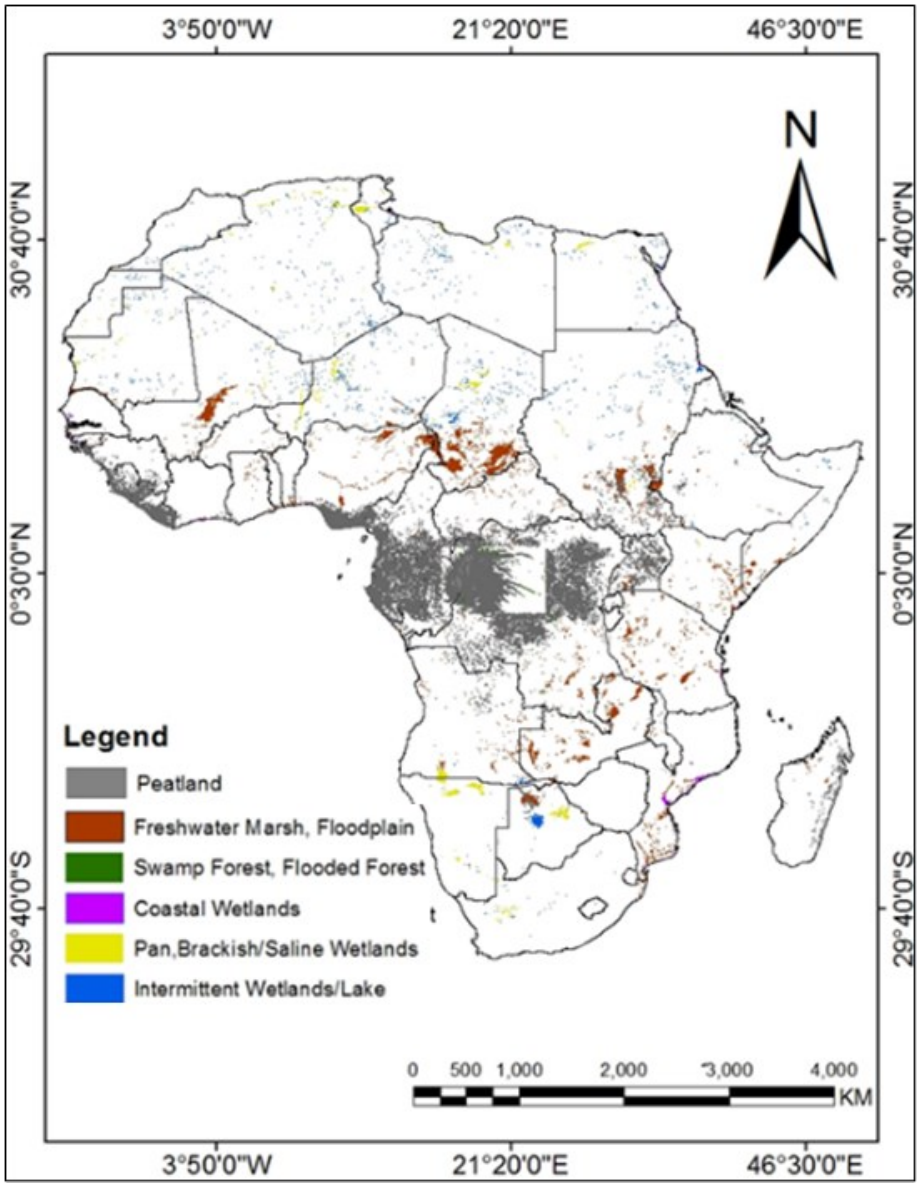

Figure 1.1. Distribution of African wetlands based on a combination of data from the Global Lakes and Wetlands Database GLWD (Lehner and Döll, 2004) (1km^2 resolution) and PEATMAP (Xu et al., 2018).

1.2 Research gap

Many existing continental and regional wetland maps rely on coarse resolution sensors unable to differentiate wetland types and missing small/narrow wetlands (Mahdianpari et al., 2018; Slagter et al., 2020). Continental products overlook newer

high-resolution data that could improve mapping accuracy if leveraged (Kaplan et al., 2019; Gulácsi and Kovács, 2020). Studies utilizing high resolution data have focused only on individual wetland sites rather than undertaken continental approaches (Sahour et al., 2022). Studies to date have not fully exploited synergies from multi-sensor integration of current high resolution optical and radar data for continental-scale wetland mapping especially for African regions (Li et al., 2022). Optical data alone has limitations for wetland classification while frequent cloud cover restricts multi-temporal analysis in the tropics (Amani et al., 2017; Mahdavi et al., 2018). The validation and calibration of remote sensing data often rely on limited ground truthing, leading to uncertainties in the accuracy of wetland maps. Robust ground-truth data collection is essential for improving the reliability of mapping results (Jamali and Mahdianpari, 2022). The lack of a recent accurate continental wetland baseline hampers monitoring of status, threats, and changes across Africa.

In this thesis, I seek to improve the mapping of African wetlands using a range of up-to-date, high-resolution, remote sensing techniques and ground control data. This approach serves as the foundation for improving our understanding of these wetlands and supporting more informed conservation decisions. Through this mapping, I will assess the characteristics of current African wetlands, their fragmentation, and their potential as carbon stores. Additionally, I aim to study wetland change over time in a case study region. Below, I provide an overview of the study's research questions and methods.

1.3 Research aim and objectives

The overall aim of the study is to develop combined approaches that enable the production of a map and the associated assessment of the extent and types of wetlands in Africa, at high spatial resolution, by employing a variety of remote sensing techniques. In doing so, I seek to produce and interrogate a novel high resolution wetland map for the whole continent. To achieve the general aim of the research, the following research questions are defined:

1. What is the current extent of wetland area in southern Nigeria and how is this broken down into different wetland types? (Method prototype, described in Chapter 4)
2. What is the current extent of wetland coverage across Africa? How is this distributed across different wetland types and climate zones? What is the estimated carbon storage in African wetlands, and how might greenhouse gas emissions vary under different degradation scenarios? Additionally, what is the relationship between population density and highly fragmented wetland areas? (Chapter 5)
3. What is the trend of change in Lake Chad region wetlands (as a regional case study) over two decades and can these changes be linked to clear human drivers of change? This region is one of the most important transboundary wetland regions in Africa (Chapter 6)

1.4 Summary of methods

To address the challenge of mapping African wetlands at high spatial resolution (10 m), to estimate the current distribution and extent of different wetland types and

assess the association of human population with surrounding wetland fragmentation in Africa, I took a remote sensing approach. However, I first gathered information on the location and characteristics of wetlands in Africa from various sources. My reference data were obtained from the Food and Agriculture Organization (FAO) global dryland assessment (Bastin et al., 2017), Ramsar Sites database (2019), other organization reports, journal papers, and academic theses (both PhD and MSc). In this study, I make use of Google Earth Engine (GEE) computational power and the availability of advanced remote sensing data collected by Copernicus Sentinels and other earth observation data. The whole study involved the extraction of spectral indices such as Normalized Differential Vegetation Indices (NDVI), Normalized Differential Water Indices (NDWI), Modified Normalized Differential Water Indices (MNDWI) and Tessled Cap Wetness Indices (TCWI). The classification was performed using random forest (RF) classifications. Once the maps were produced, I then developed an index of wetland fragmentation and a population index to analyze the relationship between wetland fragmentation and population at 10 km grid scale. This was performed by overlaying the gridded fragmentation layer with the gridded population layer to quantify the coincidence of wetland fragments and human population. In addition, for Chapter 6, multi-year time series Landsat data composites were used to map the spatial distribution and temporal changes of wetland area in the Lake Chad region for the last two decades. Change Vector Analysis (CVA) was used to assess the changes from wetland and to different landcover type in Lake Chad region.

Chapter 2
Remote sensing of wetlands

2.1 Overview

In this chapter I provides a general review of wetland characteristics and research that has been conducted on the remote sensing of wetlands**.** I firstly outlines wetland types before describing the significant role played by African wetlands and the threats facing these ecosystems. I then review the applications of different remote sensing datasets and techniques, highlighting their advantages and limitations for mapping different wetland types. I then discuss different change detection methods, their strengths and limitations, before outlining the most suitable approaches for my study.

2.2 Wetland definitions

Wetlands are ecosystems that exist at the boundary between terrestrial and aquatic environments. Wetlands occur where the water table is usually at, or near, the surface, or in a region periodically inundated with shallow water and where, under normal circumstances, the system is covered by active vegetation typically adapted to life in waterlogged conditions (Oberholster et al., 2014; Wulder et al., 2018; Mahdianpari et al., 2020; Mandishona and Knight, 2022). The Ramsar Convention (1971) defines wetlands as "areas of marsh, fen, peatland, or water, whether natural or artificial, permanent or temporary, with water that is static or flowing, fresh, brackish, or salt, including marine areas where the depth at low tide does not exceed six meters."

Wetlands can be grouped into mineral-soil systems and organic-soil systems. Sometimes lakes are also classified as wetlands. Mineral soil systems include marshes and some swamps. Marshes can often be found at the edges of lakes and streams and are dominated by herbaceous rather than woody plant species (Li et al., 2022; Zhang et al., 2023). The main source of water for marshes is by direct flow from lakes or streams (Woodson, 2012), or sometimes from direct rainfall (Herbst, 2015). Marshes can also be found in the coastal zone between land and open saltwater and these are known as salt or tidal marshes (Sun et al., 2016). Saltmarshes are characterized by distinct vegetation types, highly dependent upon soil salinity and being regularly flooded by tides (Van Beijma et al., 2014; Mitsch and Gosselink, 2015; LaRocque et al., 2020). Mangroves are another dominant coastal wetland ecosystem characterized by trees and shrubs that are salt-tolerant. Mangroves are mostly evergreen forests that grow in sheltered low lying coasts estuaries, and lagoons of tropical and subtropical regions (Adekanmbi and Ogundipe, 2009; Lee and Yeh, 2009; Kuenzer et al., 2011; Dan et al., 2016; Navarro et al., 2021). Swamps are forested wetlands (Jones, 1997; Lehner and Döll, 2004a; Gumbricht et al., 2017) which occur along large rivers or on the shores of large lakes where they are critically dependent upon natural water level fluctuations with permanently or seasonally flooded mineral soil (Jones, 1997). Some swamps have hummocks, or dry-land protrusions. Swamps are dominated by woody vegetation that tolerates periodic inundation and waterlogging (Mahdianpari et al., 2017). Some wetland classifications include swamps that occur on organic soils, often called peat

swamps (Connolly and Holden, 2017; Langan et al., 2018; Elshehawi et al., 2019). Others, however, only refer to swamps on mineral soils.

Peatlands occur where the soil is formed predominately from dead plant material that has not decayed, due to waterlogging. Bogs are peatlands that have no significant groundwater inflow and receive water mostly through precipitation (Connolly and Holden, 2017; Chico et al., 2019). Because the main source of water is from precipitation, the nutrient content of bogs is low. The peat is generally waterlogged, with low permeability reported from temperate at high latitude sites, except for within a few cm close to the peat surface (Acreman and Holden, 2013) and is associated with very slow rates of plant decomposition (Clarkson et al., 2012). Tropical peatlands tend to have higher permeability (Baird et al., 2017). Fens are mildly acidic or alkaline peatlands that receive their water primarily from groundwater sources and a little from precipitation. They are more nutrient-rich than bogs and support a wider variety of species because of their connection to groundwater (Clarkson et al., 2012).

2.3 Importance of wetlands

Wetland ecosystems are important providers of multiple values to humans, including socio-esthetical value, intrinsic value and economic value (Hu, Niu and Chen, 2017; Gumbricht et al., 2017; Slagter et al., 2020; Musasa and Marambanyika, 2022). The global contribution of wetland ecosystem services in monetary terms has been estimated to be around 14 trillion US dollars every year, thereby making a vital contribution to human livelihoods (Turpie and Kleynhans, 2010; Musasa and

Marambanyika, 2021). Wetlands are thought to directly supply freshwater to around 1.5 to 3 billion people as well as provide 40% and 20% of water requirements for industrial use and irrigation respectively (François et al., 2005; White et al., 2015; Klemas, 2016; Salimi and Scholz, 2021).

Wetlands are highly productive in terms of biological diversity supporting a richness of flora and fauna (Junk et al., 2013; Mahdianpari et al., 2020; Mao et al., 2020). They play key roles in regulating biogeochemical cycles, including water flows and associated nutrients, flood and storm-damage protection, water-quality improvement, aquatic and plant-biomass productivity, and shoreline stabilization (Acreman and Holden, 2013; Junk et al., 2013; Mahdianpari et al., 2018; Lu and Chang, 2023). One of the most important roles of wetlands is in regulation of global climate through sequestering and long-term storage of carbon from the atmosphere – globally they contain over 30% of terrestrial carbon (Mitsch et al., 2013; Hassan et al., 2014; Gumbricht et al., 2017; Mahdianpari et al., 2018; Mitsch and Mander, 2018; Xiu et al., 2019). Undisturbed wetlands are known to moderate or to counterbalance their positive climate forcing via methane (CH_4) and nitrous oxide (N_2O) emissions with sufficient uptake of carbon dioxide (CO_2) so that they have a net cooling effect, while also acting as long-term soil carbon stores (Petrescu et al., 2015; Zou et al., 2022).

2.3.1 Wetlands in Africa

Wetlands are common across Africa's diverse biomes, including major floodplains, swamps, mangroves, peatlands, and riparian zones (Kariyasa and Dewi, 2011;

Metz, 2017; Mandishona and Knight, 2022). Large wetland complexes include the Sudd wetlands of South Sudan, Okavango Delta in Botswana, and Bangweulu Swamps in Zambia. The percentage of wetland area in Africa has been estimated at lying in a range of approximately 1% to 16% of the total area of the continent (Amler et al., 2015; Li et al., 2022; Mandishona and Knight, 2022) though clearly with such a range, there is very high uncertainty: a research gap that needs to be filled. For example, in Equatorial Africa, the three largest wetland systems are believed to be the Zaire swamps, spanning 80,000 km^2, and the Sudd in the Upper Nile, covering over 50,000 km^2 and the wetlands of the Lake Victoria Basin (about 50,000 km^2) (Vinet and Zhedanov, 2010). However, Dargie et al (2017) reported the discovery of the Congo basin peatlands covering an estimated 145,500 km^2. Other major wetland areas in Africa are thought to include the floodplains of the Niger and Zambezi Rivers, and the Chad Basin which cover around 20,000 km^2, and a further 12,000 km^2 of wetlands in southern Africa (Vinet and Zhedanov, 2010). However, due to a lack of scientific investigation and inconsistent mapping policies in Africa, an exact estimate of the total extent of wetlands in Africa is poorly constrained. According to the Global Lakes and Wetlands Database (GLWD) the total area covered by wetlands in Africa, excluding rivers, lakes and reservoirs, has been estimated as 1,514,804 km^2. These wetlands vary in type from saline coastal lagoons in West Africa to fresh and brackish water lakes in East Africa (Metz, 2017). The greatest concentration of wetlands in Africa is thought to be roughly between 15ºN and 20ºS (see Chapter 1, Figure 1.1). Despite widespread distribution across Africa, knowledge of the African wetland extent and resources could be improved to support management needs (Dixon et al., 2016; Davidson, 2017; Taylor et al., 2018).

2.3.2 Threat to African wetlands

African wetlands face escalating threats from climate change, agricultural expansion, pollution, invasive species, and infrastructure projects (Gumbricht et al., 2017). Climate change such as rising temperatures, altered precipitation patterns, and sea-level rise contribute to wetland loss and degradation. As the climate changes, some regions experience prolonged and severe droughts (Meng et al., 2016). Climate change will continue to impact, and exacerbate, changes in water depth and flooding patterns. Irregular rainfall patterns have led to exceptionally dry years during which wetlands are affected by low water flows that facilitate more intense human exploitation, as observed, for example, in Nyando wetland, Kenya, during 2004-2005 (Rongoei et al., 2013). The floodplains of Hadejia Jam'are and the Zambezi basin have been affected as a result of reduced inflow caused by drought (Olalekan et al., 2014). Climate change is recognized as a major threat to the survival of species and integrity of ecosystems worldwide (Hulme, 2005; Halabisky et al., 2016; Gitau et al., 2017; Penfound and Vaz, 2021). Wetlands represent a land cover that is sensitive to climate change (Hu, Niu and Chen, 2017; Wu et al., 2021), and vulnerable to changes in quantity and quality of their water supply. Climate change may have a pronounced effect on wetlands through alterations in hydrological regimes (Erwin, 2009; Mapeshoane, 2013; Berhanu et al., 2021). Regardless of the potentially profound impact caused by current and future climate change on wetlands, there is a lack of assessment of wetland degradation due to climate change in Africa. This indicates a significant and urgent need to develop methods for assessing potential changes in Africa's wetlands. The degradation of wetlands also can lead to an increase in the release of greenhouse gases (GHG) which further

exacerbate climate change (Limpert et al., 2020; Zou et al., 2022). However, one of the major threats is increased wetland fragmentation driven by rapid human population growth and associated land use changes across Africa (Kundu et al., 2022; Wu et al., 2022; Magure et al., 2022). The growing human population necessitates more land for various purposes, putting immense pressure on wetlands.

Studies show extensive wetland loss and conversion to agriculture as African populations expand and pressure intensifies for croplands (Bootsma et al., 2019). A good example is the Yala swamp of Kenya which suffers a lot of pressure due to high population, and this leads to uncontrolled exploitation of the wetland and its resources (Olusola et al., 2016). The swamps of this area have been subject to conversion since the 1960s, mostly for agricultural purposes, such as the growing of rice, groundnuts, cassava, yams and sugarcane (Mwita, 2013; Olusola et al., 2016).

Agricultural expansion is inextricably linked to population growth in Africa. As the population surges, the demand for food production rises. Wetlands, often characterized by fertile soils and abundant water resources, become prime targets for agricultural conversion (Mitsch and Gosselink, 2015). Draining wetlands for farming and diverting water has fragmented hydrologic connectivity (Magure et al., 2022). Population growth drives urbanization and infrastructure development, both of which contribute to wetland destruction and fragmentation (Klemas, 2013). The expansion of cities, the construction of roads, and the establishment of industrial zones frequently encroach upon wetlands. For example, a large area of the Makurdi

floodplain in Nigeria has been converted to a built-up area as a result of population expansion (Anule and Ujoh, 2017). Better understanding the relationship between population density and wetland fragmentation rates across Africa can help predict future impacts and target conservation efforts.

The multifaceted threats to African wetlands are intricately connected to population dynamics, emphasizing the need to understand the population-wetland fragmentation relationship. By recognizing this connection, policy makers and conservationists can develop effective strategies to mitigate the threats and ensure the preservation of these invaluable ecosystems.

2.4 Remote sensing

Remote sensing technology allows for the observation, measurement, and analysis of the Earth's surface and atmosphere, often resulting in the generation of imagery and data that can be used for scientific research, environmental monitoring, and decision-making (Alshammari et al., 2018; Kovács et al., 2022). Data acquired through remote sensing instruments allows for efficient mapping and analysis of land cover over large areas. Several satellite systems have provided key data for land cover mapping in recent years. These remotely sensed products are available at different spatial, temporal, and spectral resolutions, by a range of spaceborne and airborne sensors from multispectral sensors and hyperspectral sensors. These sensors include widely used ones such as Landsat (Multispectral Scanner: MSS, Thematic Mapper: TM, Enhanced Thematic Mapper: ETM+, Operational Land Imager: OLI), Moderate Resolution Imaging Spectroradiometer (MODIS), as well as

Sentinel 2 and Sentinel 1 SAR. Medium resolution (10-30m) multispectral data from Landsat 8, Sentinel-2, and SPOT have been widely used for broad vegetation and land use classification (Maxwell and Warner, 2020). Hyperspectral sensors like EO-1 Hyperion produce narrow-band spectra ideal for crop type discrimination (Hirschmugl et al., 2017). SAR systems including Sentinel-1 and ALOS PALSAR provide all-weather observation (Steele-Dunne et al., 2017) while Lidar data increasingly provides 3D structure data (Anderson et al., 2010; Carless et al., 2019).

2.4.1 Remote Sensing of wetlands

The availability of remote sensing data offers an opportunity to map and monitor wetlands in a spatially explicit manner in different climatic regions, lacking monitoring systems (Gxokwe et al., 2020). However, accurately mapping wetlands is a challenging task when using satellite data alone (Mwita, 2013; Gallant, 2015; Jamali and Mahdianpari, 2022). While different wetland classes have distinctive characteristics, they also share underlying ecological similarities that confuse spectral and backscatter signatures (Kaplan and Avdan, 2018b). For example, flooded forests and swamp forests exhibit similar flooding in radar and vegetation patterns in optical data (Schmitt et al., 2014; Zhang et al., 2023). Transitions between wetlands and uplands can also be gradational without clear boundaries (McCarthy et al., 2018). Additionally, wetlands demonstrate significant spatiotemporal variability due to change hydrology and phenology (Dabboor et al., 2017; Battaglia et al., 2021). These factors make effectively discriminating diverse wetland ecosystems difficult through remote sensing approaches. Low to medium resolution data such as MODIS, Landsat and SPOT images have been widely and successfully used for

monitoring the wetland vegetation and detecting the presence and extent of floods (Bassi et al., 2014; Gumbricht et al., 2017; Wang et al., 2020; Wu et al., 2021). However, their resolution may limit the ability to accurately identify detailed wetland vegetation types. Powell et al. (2019) demonstrated the effectiveness of integrating Landsat TM and ETM+ data sets coupled with digital elevation and light detection and ranging (LIDAR) data sets to classify and map land-cover types in the semi-arid wetlands of the Barwon-Darling River system, using the stochastic gradient boosting algorithm and the fractional cover model. The study identified four land-cover classes which included tree-dominated woodlands, shrub lands, vegetated swamps and non-flood dependent terrestrial communities with an overall accuracy of 88%. However, the study failed to distinguish between certain types of wetlands located at the boundaries of the drier wetlands from the Landsat TM and ETM+ images used. Li et al. (2015) assessed the effectiveness of MODIS spectral indices in monitoring the hydrological dynamics of a small, seasonally flooded wetland (1364 ha) in semi-arid southern Spain. Their analysis revealed a strong positive linear relationship between the MODIS-inferred inundation area and field-measured water levels, with an R^2 value of 0.96, indicating the success of the MODIS dataset in tracking the hydrological dynamics of seasonal wetlands. However, the study focused on a single seasonal wetland with only varying soil characteristics and unable to identify other semi-arid and arid seasonal wetlands with diverging characteristics e.g., marshes with dense emergent vegetation are even smaller and cover only a few MODIS pixels. Chen et al. (2013) used a 250 m resolution MODIS dataset along with daily field water levels to assess the effectiveness of MODIS time series data for monitoring wetland cover dynamics. Four land-cover classes which were water,

mudflats, submerged and emergent vegetation were identified with the overall accuracy of 80.18% and Kappa coefficient of 0.734. There were, however, omission errors of about 30% where water was confused with other classes such as mudflats and emergent vegetation. Much of this water was located at the interface of mudflats and other classes. Landmann et al. (2010) also utilised MODIS coupled with topographical landform data set to map basic wetland classes in semi-arid Burkina Faso and Mali. The results showed low accuracy in the classification of mapped land cover types. Although the studies demonstrated the success of these freely available datasets in detecting and mapping different wetland cover classes, the fine detailed differentiation between the classes was a major challenge.

Advances in remote sensing technology have led to an increase in the availability of high spatial and spectral resolution imagery. Sentinel-2 Multispectral Instrument (MSI) launched by ESA in 2015, a new generation multispectral sensor, has been successfully used in land use/land cover research, because of its high spatio-temporal resolution, wide spatial coverage and broad spectrum. Furthermore, the three red-edge bands of Sentinel-2 images are particularly effective for vegetation monitoring (Kaplan et al., 2019). The study by Lefebvre et al. (2019) showed that Sentinel 2 provided the highest performance (90%) than Landsat 7 (85%) and Landsat 8 (86%) for monitoring the water dynamics of seasonal wetlands. According to Sánchez-Espinosa and Schröder (2019) the use of Sentinel-2 improved the accuracy of mapping Mediterranean wetland area compared to using Landsat 8 alone. However, optical satellite sensors are always vulnerable to cloudy and rainy weather, so it is difficult to acquire adequate and clear Sentinel-2 images especially

in the tropical and subtropical coastal areas. Indeed, optical imagery is crucial as it provides important information on reflectance, which indicates the presence or absence of vegetation, identifies vegetation types, and reveals soil moisture levels in areas with dense canopies.(Cardoso et al., 2014; Amani et al., 2018; Mahdavi et al., 2018).

Synthetic aperture radar (SAR) systems like Sentinel-1, RADARSAT, and ALOS-2 are frequently used for wetland mapping, flood detection, forest classification, crop identification, and biomass mapping due to SAR's all-weather capability and sensitivity to surface roughness, texture, and moisture content under vegetation canopies (Clewley et al., 2015; White et al., 2015; Hribljan et al., 2017; Rüetschi and Schaepman, 2018; Huang, 2019; LaRocque et al., 2020; Masoud Mahdianpari et al., 2020). The utilization of SAR relies on both polarization and frequency considerations, as highlighted by Mahdianpari et al. (2017). In line with the scatter mechanisms of ground targets observed through Polarimetric SAR, numerous studies have been undertaken to discern diverse land cover types based on distinct shapes, structures, roughness, and permittivity. For instance, dual-polarization (vertical transmit-vertical receive (VV) / vertical transmit-horizontal receive (VH)) data have been used for the identification of the water body and vegetation(Evans and Costa, 2013; Mahdianpari et al., 2017; Kaplan and Avdan, 2018a) . Another parameter in SAR, known as frequency or wavelength, is associated with the penetration depths into ground targets, providing insights into the land surface structure. Longer wavelengths, such as those in the P- and L-band, possess greater penetration ability, allowing for the detection of the vegetation canopy and the

quantification of soil moisture. Conversely, shorter wavelengths, like those in the C- and X-band, exhibit better performance in classifying land cover in open areas, such as open wetlands. Consequently, multi-frequency and multi-source SAR data have been integrally exploited for wetland monitoring and achieved successful results (Mahdianpari et al., 2017; DeLancey et al., 2019; Amani et al., 2021). However, the high cost and challenges in acquisition often limit the feasibility of using multi-frequency and multi-source Polarimetric SAR data, particularly in time series analysis. Sentinel-1 satellites with a C-band and dual-polarization (VV/VH) sensor provides a promising opportunity for time-series wetland land cover analysis at low cost. Polarimetric features, such as backscatter coefficient interferometry data, the degree of polarization and linear polarization ratio, have been widely utilized to help identify wetland cover types (Guo et al., 2017; Mohammadimanesh et al., 2018).

Some studies reported that the backscatter coefficients in Sentinel-1 SAR time series have the greatest utility among SAR features in wetland cover classification and could obtain the highest classification accuracy (Li et al., 2020; Costa et al., 2021). However, the accuracy of land use/cover classification using SAR data is typically lower than that achieved with optical multispectral data at the same spatial resolution. Combining optical and SAR data for land cover and vegetation mapping brings accuracy higher than that of using only either optical or SAR images (Gao et al., 2017; Mahdianpari et al., 2018; LaRocque et al., 2020; Sahour et al., 2022). With the launch of many long-term observation missions, the volume and accessibility of optical and SAR remote sensing images enable the accuracy improvement in landcover research using remote sensing (Mahdianpari et al., 2020; Mahdianpari et

al., 2018). However, limited studies on wetland monitoring have utilized dense time series of optical and SAR images. Only recently, the time-series Sentinel-1 and Sentinel-2 images were combined to improve the land surface monitoring accuracy (Estupinan-Suarez et al., 2015; Slagter et al., 2020). Therefore, combining Sentinel-1 and Sentinel-2 data could be very useful for large scale wetland mapping at high resolution and has significant advantages in wetland mapping at regional or global level (Mahdianpari et al., 2018; Slagter et al., 2020).

Several remote sensing techniques have been used for mapping different types of wetlands (Ritchie and Das, 2015; Nhamo et al., 2017; Amani et al., 2019; Jamali et al., 2021). These techniques are use either use for mapping and identification of wetlands and different land covers. For example, an unsupervised classification technique known as iterative self-organizing data analysis (ISODATA) has been commonly used to map and classify wetland cover type (Mwita, 2013; Chen et al., 2014). This classification technique requires no training data and there is no expensive training phase in the classification process, only an analyst's time is required to classify the clusters. However, it is possible that this method may not produce spectral groupings that match the classes of interest resulting in misclassification error (Ritchie and Das, 2015). Supervised classification techniques such as Maximum Likelihood (ML), , Support Vector Machine (SVM), Artificial Neural Network (ANN), K-Nearest-Neighbors (K-NN), Decision Tree (DT), and Random Forest (RF) has been widely used for to classify wetland cover (Anule and Ujoh, 2017; Moser et al., 2016; Nhamo et al., 2017). These techniques may require training data for the classification but do not require much of the analyst's time. These

techniques also allow for the creation of classes matching those of interest (Ritchie and Das, 2015; Dang et al., 2021) In terms of accuracy and commonly used supervised classifiers for wetland mapping, RF is generally characterized by the highest mean classification accuracy, followed by the SVM classifier and the DT classifier, whereas those of NN and MLC are relatively lower (Gómez et al., 2016; Ma et al., 2017; Mahdianpari et al., 2018; Jamali et al., 2021).

2.5 Change detection techniques

Change detection involves the process of identifying variations in the state of an object or phenomenon by observing it at different times (Scharsich et al., 2017; Qu et al., 2022). Generally, change detection involves the application of multi-temporal datasets to quantitatively analyse the temporal effects of the phenomenon. Each change detection algorithm has their strength over the other depending on the area of application. Change detection algorithm can be into seven categories (Lu et al., 2004): (1) algebra, (2) transformation, (3) classification, (4) advanced models, (5) Geographical Information System (GIS) approaches, (6) visual analysis, and (7) other approaches.

Change detection algebra methods include image differencing, image regression, image ratioing, vegetation index differencing, change vector analysis (CVA) and background subtraction. A common characteristic of these algorithms is the selection of thresholds to identify areas of change. These methods (excluding CVA) are relatively simple, straightforward, easy to implement and interpret, but cannot provide complete matrices of change information. CVA is essentially an extension of

image differencing, capable of detecting all changes that exceed specified thresholds and offering detailed information about those changes. CVA can measure change in more than two spectral bands, giving it an advantage when mapping rapidly changing and highly diverse wetlands (Klemas, 2013; Gemechu et al., 2022). It produces robust results for detecting wetland changes due its sensitivity to variations in class reflectance caused by high intra-class variability influenced by landscape heterogeneity (Landmann et al., 2013; Liu et al., 2020). Landmann et al. (2013) used a MODIS CVA-approach to map wetland dynamics in the Linyanti wetland from 2001-2010. The result showed the high potential of the CVA to detect interannual wetland dynamics and trends over such a time period. The transformation category includes PCA, KT, Gramm–Schmidt (GS), and Chi-square transformations. One advantage of these methods is in reducing data redundancy between bands and emphasizing different information in derived components (Hussain et al., 2013; Hussaini et al., 2020). These methods can decrease the high correlation between the spectral bands providing independent information on change pixels of the wetland cover (Connell, 2012; Dronova et al., 2015; Chatziantoniou et al., 2017). However, they cannot provide detailed change matrices and require selection of thresholds to identify changed areas. Another drawback is the challenge of interpreting and labelling change information on the transformed images.

The classification type of change detection includes post-classification comparison (PCC), spectral–temporal combined analysis, expectation–maximization algorithm (EM) change detection, unsupervised change detection, hybrid change detection,

and Artificial Neural Networks (ANN) (Ojaghi et al., 2017). The major advantage of these methods is their capability of providing a matrix of change information and reducing external impact from atmospheric and environmental differences between the multi-temporal images (Hussain et al., 2013). However, selecting high-quality and sufficiently numerous training sample sets for image classification is often difficult, for historical image data classification. The time-consuming and difficult task of producing highly accurate classifications often leads to unsatisfactory change detection results, especially when high-quality training sample data are not available (Mwita, 2010; Hussain et al., 2013). In a study by Sica et al. (2016) PCC produced high accuracy for mapping and quantification of wetland changes in the Lower Paraná River Delta, Argentina. Dadaser-Celik and Cengi, (2013) successfully employed an ANN model to simulate and predict water levels in the Sultan Marshes. Debanshi and Pal (2020) demonstrated the potential of ANN for delineation and monitoring of wetlands in the Ganges delta revealing details on the shrinkage of the wetland area.

The advanced model-based change detection category includes the Li–Strahler reflectance model, spectral mixture models (SMM), and biophysical parameter estimation models. In these methods, the image reflectance values are often converted to physically based parameters or fractions through linear or nonlinear models (Guo et al., 2017). The transformed parameters are more intuitive to interpret and better to extract wetland vegetation information than are spectral signatures (Guo et al., 2017). For example, Halabisky et al. (2016) assessed the condition of wetland changes and trends using a spectral mixture method but the disadvantage

of these methods is the time-consuming and difficult process of developing suitable models for converting image reflectance values into biophysical parameters.

The visual analysis category includes visual interpretation of multi-temporal image composite and on-screen digitizing of changed areas. This method allows analysts to fully leverage their expertise and knowledge. Key elements such as texture, shape, size, and patterns in the images are essential for accurately identifying land use and land cover (LULC) changes through visual interpretation. The disadvantage of this method is the time consumed for a large area change detection application and it is difficult to update the change detection results in a timely manner. It is also difficult to provide detailed change trajectories.

The choice of particular change detection methods depends on their abilities to detect specific changes in land use/landcover. PCC, for example, specifies changes from a particular class to another, while CVA shows magnitude and the direction of change (D. Liu et al., 2020), and ANN works better with small areas and is very effective in also identifying areas with significant changes (Dadaser-Celik and Cengiz, 2013; Debanshi and Pal, 2020). The selection of a suitable method to implement accurate change detection for a specific research purpose or study area is still difficult even though a variety of change detection techniques have been developed. Post-classification comparison is the most common technique used in wetland studies to quantify total wetland change and locate specific areas where change has occurred (Tewkesbury et al., 2015; Ye et al., 2016). It involves independently classifying images from different years and then comparing the results

to detect change. However, conducting separate classifications introduces errors into each map that are then compounded when the maps are compare (Baker et al., 2007; Salih et al., 2017). This significantly impacts studies where most of the area is unchanged which result to vast unchanged to be classified multiple times, each time with new errors. This increases the overall error in the change analysis. In contrast, change vector analysis (CVA) can detect subtle differences in class reflectance resulting from high intra-class variability caused by landscape heterogeneity (Rahman and Mesev, 2019). By analyzing the intensity and direction of change vectors, CVA avoids the compounding of classification errors that often occurs when comparing independent classifications from two time points (Landmann et al., 2013; D. Liu et al., 2020). Additionally, CVA reduces the need for collecting training and reference data for historical images. Since unchanged areas can be used as reference data, this avoids errors introduced by collecting separate training data for each image date (Landmann et al., 2013; Salih et al., 2017).

For the purpose of this study I propose the use of change vector analysis to accurately quantify the changes between individual wetland class and other non-wetland categories.

2.6 Summary

Some wetlands vary seasonally and over years in their appearance and size, and they are sometimes highly dynamic. Others are fairly stable over long periods unless degraded by human action, at which point degradation can be rapid. Since ancient times wetlands have suffered from human disturbance, but over the past 200 years

these disturbances have rapidly accelerated. The current wetland mapping products on a global scale such as Global Lakes and Wetlands Database (GLWD) and the Ramsar site database cannot match either the need for global wetland dynamic monitoring or the need for understanding their internal processes due to their coarse spatial resolution. Many of these global wetland maps rely on data that can be decades old and, particularly in developing countries, with very limited ground truth data. It is therefore important to improve maps of these ecosystems, using a range of techniques, to get a complete picture of wetland area and to establish the range and extent of different wetland types and their fragmentation. Comprehensive wetland maps and an understanding of the nature of their fragmentation are needed to build economic assessments of wetland ecosystem service provision and to support decision-making by regional and international bodies seeking to protect wetland systems as well as for inclusion in coupled land-surface—climatic models. The latter is crucial since wetlands are important for land–atmosphere carbon dynamics, greenhouse gas exchange, and the water cycle.

A high-resolution continental view about the types and distribution of wetlands in Africa is lacking. Most of the studies on wetlands in Africa have been conducted at a local scale and given the vastness of the continent, there is a dearth of studies of wetland fragmentation which means that an overall assessment of the state and condition of African wetlands is currently very challenging. There is potential for remote sensing techniques to help with the assessment of the status and extent of African wetlands.

Chapter 3
Methodology

3.1 Overview

I used high resolution (10m) optical and radar imagery to map wetlands, their distribution and fragmentation, and to estimate the current extent of wetland area, the potential carbon flux from wetland degradation, and the relationship between population and highly fragmented wetland regions (Chapters 4 and 5). Following the identification of the spatial distribution wetland types and their fragmentation in Africa, a more focused change detection approach was conducted to analyse the trend of wetland changes in one of the most important transboundary wetland regions in Africa (Chapter 6).

To begin with, I produced an updated high resolution (10m) wetland map of Southern Nigeria (Chapter 4) leveraging the computational power of Google Earth Engine (GEE) and the availability of advanced remote sensing data collected by Copernicus Sentinels and other earth observation data. The whole study involves the integration of indices from both optical and radar imagery and classification of imagery using the Random Forest (RF) algorithm supported by compiled reference points containing information about the location and characteristics of wetlands from multiple sources.

I then scaled this approach up to map wetland areas across the wider African continent, adapting my methods to apply to different climatic zones (Chapter 5). The

next step was to develop an index to model the distribution of wetland fragments in relation to population, called Wetland Fragmentation and Population Index (WFPI) (see Chapter 5). This aimed to identify the association of wetland fragmentation with human population. To model the WFPI, the population datasets from the Gridded Population of the World database (GPW V4), was combined with my new high resolution wetland map. I used a fuzzy logic approach to create a membership rank for the fragmentation grid and population grid layer. The gridded fragmentation membership layer was overlayed with the gridded population membership layer to quantify the coincidence of wetland fragments and human population. In addition, I estimated the total carbon stocks stored in African wetlands and calculated the potential carbon emissions from different wetland types for two wetland degradation states in each of the five climate zones of Africa using the new wetland map.

In this chapter I outline the methods that underlie the work in the following chapters, namely: (1) selection and preparation of satellite imagery, (2) identification and collation of ground control points and (3) justification and ethos of the classification method.

3.2 Data collection and preprocessing

3.2.1 Selection and preparation of satellite imagery

In this study, I used three remote sensing image datasets (Landsat, Sentinel-1 and Sentinel-2, Table 3.1) accessed through the GEE Data Catalogue. For the 10m resolution wetland mapping, Sentinel-1 radar images and Sentinel-2 optical images were used, while Landsat images were acquired for the long-term wetland change

detection. I selected 345 and 13596 images of Sentinel-2 Top of Atmosphere reflectance data with 16 spectral bands for Southern Nigeria and the entire African continent respectively. Due to cloud coverage affecting a large number of Sentinel-2 observations in my study area, especially during rainy seasons, I used an initial selection criterion of cloud fraction <20%. Then I applied a cloud mask to remove cloud and cirrus-cover using the quality assurance bands available through GEE (Hird et al., 2017; Mahdianpari et al., 2018; Gulácsi and Kovács, 2020) before formation of a composite image. Surface reflectance data for two Landsat data products (Landsat 7 ETM+ and 8 OLI) from 2000 to 2022 were collected for the change detection analysis. While the Landsat archive contains remotely sensed imagery continuously acquired since 1972, frequent cloud cover creates substantial data gaps over certain regions, especially wetland areas or during wet seasons. To achieve my objectives, I created cloud-free image composites using scenes with minimal cloud cover. Notably, after the 2003 failure of the scan line corrector (SLC) on Landsat 7's ETM+ sensor, approximately 22% of pixels in its images contain data gaps. To fill these SLC-off gaps, I utilized a common gap filling technique to interpolate pixel values across the stripes of missing data (Chen et al., 2011). This allowed me to reconstruct the full images needed for continuous wetland mapping. For Sentinel-1 I used a total of 6112 Ground Range Detected interferometric wide-swath images collected in ascending orbit, which are projected onto a regular 10 m grid with dual VV/VH polarisation imagery available at an average acquisition interval of 12 days within the study area. Similar preprocessing steps implemented in the ESA SNAP Sentinel-1 toolbox including updating orbit metadata, thermal noise removal, terrain correction, GRD border removal and radiometric calibration were

applied. I then corrected for incidence angle (Hird et al., 2017) and reduced radar speckle using an adaptive sigma Lee filter on the GEE platform.

Table 3.1 A description of image data and features extracted.

Image data	*Sensor type*	*Bands*	*Feature extracted*
Landsat ETM+		450–12500nm	spectral bands 1 (blue), 2 (green), 3 (red) 4 (NIR) 5 and 7 (SWIR), the normalized difference vegetation index (NDVI, normalized difference water index (NDWI), modified normalized differential water Indices (MNDWI), and tasseled cap wetness index (TCWI).
Landsat	OLI	430–12500nm	
Sentinel-2	MSI	490–2190 nm	spectral bands 2 (blue), 3 (green), 4 (red) 8 (NIR) 11 and 12 (SWIR), the normalized difference vegetation index (NDVI, normalized difference water index (NDWI), modified normalized differential water Indices (MNDWI), and tasseled cap wetness index (TCWI).
Sentinel-1	SAR	VV-VH	vertically transmitted, vertically received SAR backscattering coefficient $\sigma^0 VV$. vertically transmitted, horizontally received SAR backscattering coefficient $\sigma^0 VH$. the ratio polarized index $\frac{VV}{VH}$, normalized polarized ratio $\frac{VH-VV}{VH+VV}$.

3.2.2 Image compositing and feature extraction

In this study two different types of image composites were generated: seasonal and yearly composites (Table 3.2). Since Sentinel-1 SAR backscatter is unaffected by cloud cover, I incorporated information from both dry and wet seasons to create two

seasonal composites to capture explicit phenological information appropriate for wetland mapping. However, it is only possible to produce a yearly composite for Sentinel-2 and Landsat data due to the high number of cloudy images which makes it impossible to collect sufficient cloud free image to generate full coverage seasonal composites. For the southern Nigeria region, each composite was constructed from the mean value for each pixel, per band basis, to obtain observations for the available dates at a point in a single representative pixel, hence preserving relationships between bands. To map the wetlands in different climate regions across Africa, individual composites for each climate zone were constructed to capture the semantic information of wetland classes within the different climate zones. I created a composite using the maximum pixel value for the Arid and Semi-arid climate zone to enhance wetland features within this drier region. The composites for Tropical Wet (TW), Tropical Wet and Dry and Mediterranean subtropical climate (MED) zones were constructed from the median pixel value of the stacked images. or this study, I utilized blue, green, red, near-infrared, and short-wave infrared bands from optical imagery. In addition to these optical bands, I calculated several indices: Normalized Difference Vegetation Index (NDVI), Normalized Difference Water Index (NDWI), Modified Normalized Difference Water Index (MNDWI), and the Tasseled Cap Wetness Index (TCWI). SAR features included backscatter from VV and VH, as well as the normalized difference (Ndiff = (VH-VV)/(VH+VV)) and ratio indices (Nratio = VV/VH) for both wet and dry seasons. The VH backscatter, which is vertically transmitted and horizontally received, is sensitive to volume scattering within the vegetation canopy and is highly responsive to vegetation structure (Steele-Dunne et al., 2017). On the other hand, VV, which is

vertically transmitted and received, is more sensitive to surface roughness and soil moisture, helping to distinguish flooded from non-flooded vegetation (Mahdianpari et al., 2018). VV also provides distinctive returns for herbaceous wetlands and areas with sparse or low vegetation, particularly during the early growth stages before canopy closure (Baghdadi et al., 2010).

Table 3.2 Composites and input variables for each region. The shaded box indicates the selected variables of highest importance used as input for final classification in each region.

Study region	***Composites***											
	Date	***value***	***B8***	***B12***	***NDVI***	***NDWI***	***MNDWI***	***TCWI***	***VV***	***VH***	$\frac{VV}{VH}$	$\frac{VH-VV}{VH+VV}$
Southern Nigeria	Jan - Nov 2019 Jan - March 2019 (dry) April – Oct 2019 (wet)	Mean					■	■	■	■	■	■
Tropical wet	Jan - Dec 2021	Mean					■	■	■	■	■	■
Tropical wet and dry	Jan - Dec 2021	Mean			■	■	■	■	■	■	■	■
Mediterranean/Humid subtropical	Jan - Dec 2021	Mean			■		■	■	■	■	■	■
Semi-arid	Jan - April 2021 (wet)	Maximum	■		■	■		■	■		■	■
Arid/desert	Jan - April 2021 (wet)	Maximum		■		■	■	■	■		■	

3.2.3 Identification and collation of ground control points

The reference data for training were obtained from the Food and Agriculture Organization (FAO) global dryland assessment (Bastin et al., 2017), Ramsar Sites database (2019), Global Peatland Database (GPD), other organization reports, journals, and academic theses (both PhD and MSc). The FAO datasets (7580 points (87% of control points in this study) were generated through augmented visual interpretation through Collect Earth (Bey et al., 2016) of VHR images available from Google Earth. The reference points were collected from a squared cell centered at a sample plot of 70 by 70 meters. The two imagery Sentinel 1 GRD (Interferometric Wide swath mode (IW) has a pixel spacing of 10m and Sentinel 2 imagery has a 10 m resolution which are stack together to correctly train each individual pixel. Each sample plot of training point closely aligned to 7x7 pixels of my Sentinel images which provides high accuracy validation on several Sentinel pixels. Training points from the Ramsar Sites database (2019) (415 points, 5% of ground control points), Global Peatland Database (GPD) (352 points, 4% of control points), other organization reports (54 points, 0.6%), journals (294 points, 3%), and academic theses (both PhD and MSc) (165 points, 2%) originated from field surveys of the different wetland sites across our study area. I checked and verified all the reference points by visual interpretation of Digital Globe very high spatial resolution images (< 1 m pixels) made available for visualization through Google Earth. The verification was performed to check for i) inconsistencies in wetland type among the references point in each wetland region, ii) isolated and mislabelled reference points. To check for inconsistencies, I compared the different reference points to make sure that all

points matched the same wetland type in each climate zone. A total of 173 reference points from different wetland regions were rejected due to inconsistency with the wetland type between our data sources. Isolated and mislabelled reference points were also excluded. The reference points were sorted into different climate zones to accurately map wetland types according to their features within that zone. These points were then grouped into training and validation points using random sampling within each zone (Figure 3.1). To avoid bias in our classification, both our training and validation points were uniformly distributed among the different wetland classes.

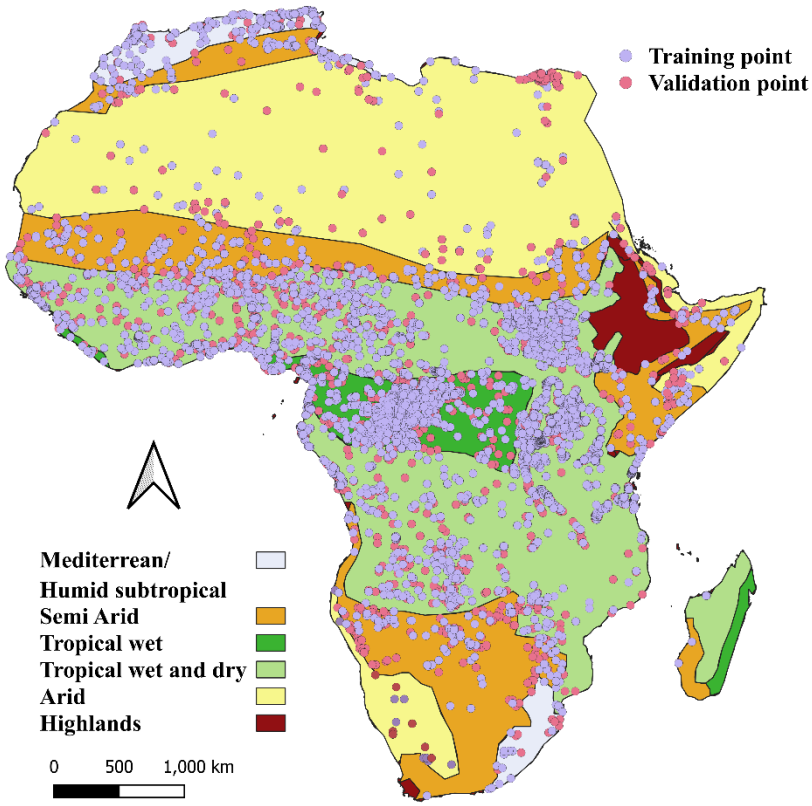

Figure 3.1 Distribution of training and validation across the different climate zones in Africa. Tropical wet (3,218 points), Tropical wet and dry (2,550 points), Semi-arid (1,144 points), Arid (536) and Mediterranean/humid subtropical (846 points).

3.3 Justification and ethos of classification method

The choice of a classification technique is based on three parameters - the accuracy, complexity, and processing time. I used pixel by pixel classification because it is a simpler and faster method when compared with object-based classification. In terms of accuracy, several studies have demonstrated the high accuracy performance of pixel-based classification (Moser et al., 2016; Acharya et al., 2017; Zhang et al., 2023) and, in some cases, it produced higher accuracies than object-based methods (Ardha Aryaguna and Danoedoro, 2016). Object-based classification has computational limitations for large-scale mapping and is therefore less suitable for continental-scale studies (e.g., Chapter 5). I considered supervised classification to be appropriate for my goals because I was able to source sufficient training data to allow image classification. These methods also allow for the creation of classes matching those of interest (Ritchie and Das, 2015). For my pixel-based analysis, the Random Forest (RF) machine learning algorithm was selected. The RF classification is a relatively well-known supervised machine learning algorithm that produces an ensemble of multiple decision trees iteratively using randomly selected subset of the training dataset (Figure 3.2). RF is particularly suitable for handling variation within land cover classes and reducing noise in the data and does not require prior knowledge of the data distribution, unlike other classifiers (Slagter et al., 2020).

RF is a non-parametric classifier made up of a group of tree classifiers, capable of handling high-dimensional remote sensing data (Belgiu and Dra, 2016). It uses bootstrap aggregating (bagging) to produce an ensemble of decision trees by using a random sample from the given training data and determines the best splitting of

the nodes by minimizing the correlation between trees. Assigning a label to each pixel is based on the majority vote of trees (Figure 3.2). The 'trees' are built at each node by randomly selecting a subset of input variables for splitting, which helps reduce overfitting and results in a more robust classification compared to other classifiers. (Breiman, 2001). In the RF algorithm, certain parameters must be defined to generate the forest trees: the number of decision trees to create (Ntree) and the number of variables to be selected and tested for the best split during tree growth (Mtry). The parameter Ntree was evaluated for values between 100 and 600, with a value of 500 chosen, as the error rates for all classification models remained constant beyond this threshold. I assessed the significance of sixteen variables (Band 2, Band 3, Band 4, Band 6, Band 7, Band 8, Band 11, Band 12, NDWI, NDVI, MNDWI, TCWI, (VH-VV)/(VH+VV), VV/(VH) (wet and dry)) as input channels for the RF classification across each climate zone. After running the variable importance algorithm for ten-fold, i then selected variables that were most important for classification accuracy as input for our final classification. Although RF is an effective and powerful machine learning algorithm, there are some drawbacks to consider when using it. RF can overfit noisy datasets or data with outliers, particularly when the number of trees is high. It is also susceptible to bias if there is imbalance in the training sample, thereby having poor performance on minority class. In addition RF is not suitable for real time analysis due to computational complexity.

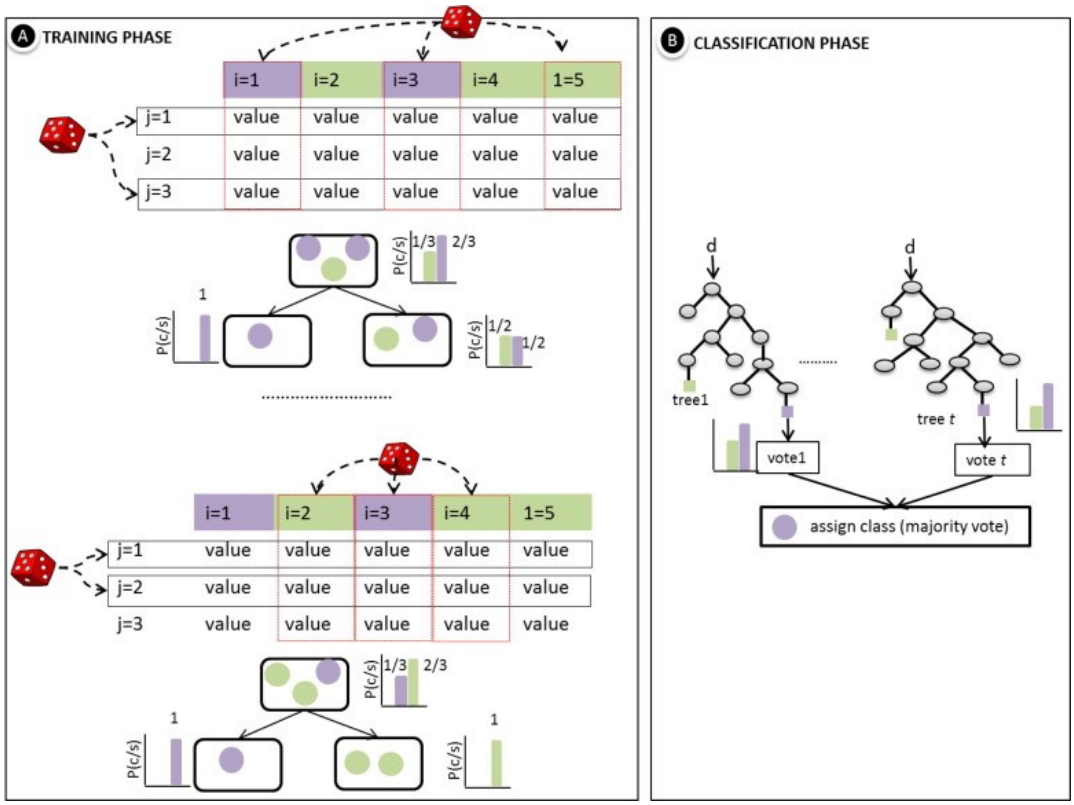

Figure 3.2 Training and classification phases of Random Forest classifier: *i* = samples, *j* = variables, *p* = probability, c = class, s = data, *t* = number of trees, d = new data to be classified, and value = the different values that the variable *j* can have (reproduced from Belgiu and Dra, 2016)

Chapter 4

Wetland mapping at 10 m resolution reveals fragmentation in southern Nigeria

Abstract

Wetland ecosystems play key roles in global biogeochemical cycling, but their spatial extent and connectivity is often not well known. Here, i detect the spatial coverage and type of wetlands at 10 m resolution across southern Nigeria (total area: 147,094 km²), thought to be one of the most wetland-rich areas of Africa. I use Sentinel-1 and Sentinel-2 imagery supported by 1500 control points for algorithm training and validation. I estimate that the swamps, marshes, mangroves, and shallow water wetlands of southern Nigeria cover 29,924 km² with 2% uncertainty of 460 km². I found larger mangrove and smaller marsh extent than suggested by earlier, coarser spatial resolution studies. Average continuous wetland patch areas were 120 km², 11 km², 55 km² and 13 km² for mangrove, marsh, swamp, and shallow water respectively. My final map with 10 m pixels captures small patches of wetland which may not have been observed in earlier mapping exercises, with 20% of wetland patches being <1 km^2; these were clustered around urban centres, suggesting anthropogenic wetland fragmentation. My approach fills a knowledge gap between very local (<400 km²) studies reliant on field studies and aerial photos, and low resolution (>250 m pixel dimensions) global wetland datasets and provides data critical for both improving land-surface climate models and for wetland conservation.

4.1 Introduction

Wetlands are one of the world's most important and productive ecosystem types, playing a vital role in climate change mitigation (Hassan et al., 2014), hydrological and biogeochemical cycles (Junk et al., 2013) and maintaining livelihoods (Hu et al., 2017; Wilen & Bates, 1995). The southern part of Nigeria contains many wetlands which are thought to consist mainly of marshes, mangroves and freshwater swamps (Ayanlade & Proske, 2016; Olalekan et al., 2014). However, great environmental pressure has been exerted on these ecosystems as result of land reclamation for agriculture and industrialization (e.g. Niger delta; Chidumeje et al., 2015), urbanization (e.g. Lekki lagoon of Lagos; Obiefuna et al., 2013) and contamination from pollution (e.g. oil spills; Igu & Marchant, 2017; Ohimain, 1996). The regional extent of existing wetlands that need protecting, and the extent of wetland loss and degradation, has thus far only been quantified at coarse resolution. Although there are some global wetland maps, such as Global Land Cover GLC250-2010 (250 m pixels) and the Global Lakes and Wetlands Database (GLWD-3, 1 km pixels), studies by Gumbricht et al., (2017), Hu et al., (2017) and Xu et al., (2018) show inconsistencies between them due to differences in methods, data sources, and validation. Many global wetland maps rely on data that can be decades old and, particularly in developing countries, with very limited ground truth data. It is therefore important to improve maps of these ecosystems, using a range of techniques, to get a complete picture of wetland area and to establish the range and extent of different wetland types and their fragmentation. Comprehensive wetland maps and an understanding of the nature of their fragmentation are needed to build economic assessments of wetland ecosystem service provision and to support decision-

making by regional and international bodies seeking to protect wetland systems as well as for inclusion in coupled land-surface - climatic models (e.g. JULES / QUEST: Clark et al., 2011; Dadson et al., 2010). The latter is crucial since wetlands are important for land-atmosphere carbon dynamics, greenhouse gas exchange, and the water cycle.

Southern Nigeria is a low-lying region covering ~ 147,094 km² (between 4° 00` and 7° 00`N, and 3° 00` and 9° 00`E, Figure 4.1) and is thought to have the most extensive wetlands in west Africa (Gumbricht et al., 2017; Uloacha, 2004). However, this area is undergoing huge population expansion and development and so the wetlands may be at risk. The only wetland maps that currently span all of southern Nigeria are from global projects (e.g., GLWD-3) and have relatively low resolution (1 km). However, there are some small-scale studies that have mapped a few small areas of wetland in the region using satellite imagery (e.g. Ayanlade & Proske, 2016; Obiefuna et al., 2013; Taiwo & Areola, 2009; locations shown in Figure 4.1. The accuracy of these small-scale studies has yet to be assessed due to absence of suitable ground truthing data. Furthermore, the techniques used in these studies are not suitable for larger region or country-scale wetland mapping.

Satellite images have been used successfully to identify and map different wetland types around the world (Fei et al., 2011; Guo et al., 2017; Klemas, 2011; Kuenzer et al., 2011; Mahdianpari et al., 2018). Interpretation of multi-temporal imagery in particular can aid classification of dynamic wetlands and their separation from other ecosystems (Mahdianpari et al., 2018, Ozesmi & Bauer, 2002). Many wetlands have

seasonal characteristics based on changes in water level and vegetation that can assist their detection using remote sensing. For example, marshes experience drying of vegetation and a decrease in water level during the dry season or low tide periods (Hudson et al., 2006). This can be observed using optical images from a decrease in the reflectivity in the near infrared and a slight increase in reflectivity to the red band due to suspended particles settling out at low water levels (Hudson et al., 2015).

The increasing availability of open access satellite data, and the growth of advanced machine learning tools integrated with robust cloud computing resources has recently made multi-temporal datasets more accessible (Mahdianpari et al., 2018). The majority of previous studies have used multi-temporal Landsat imagery to classify wetlands both with unsupervised classification algorithms (e.g. K-means and ISODATA; Mwita et al., 2012; Ramsey & Laine, 1997) and with supervised classification schemes (Bwangoy et al., 2010; Wright & Gallant, 2007), However, it is now possible to supplement this with Synthetic Aperture Radar (SAR) C-band multi polarization radar to discriminate between wetland types (Baghdadi et al., 2010), with cross polarization (HV, VH) providing better discrimination between some wetland classes. Combining multiple optical and SAR indices to classify different wetland types has great potential for wetland classification (Kaplan, et al., 2019; Mahdavi et al., 2018; Salehi et al., 2018), however, such approaches have not yet been applied to the wetlands of southern Nigeria. As the only wetland maps that currently span this entire globally important region have pixel sizes of 250 m and 1 km (Lehner and Döll, 2004; Gumbricht et al., 2017), there is a need for updated

datasets that can be met by the combination of optical and radar satellite data. There are limited attempts to map wetlands using remote sensing across certain parts of Africa. Amongst the few studies i include that of Landmann et al. (2010) were wetlands in western Burkina Faso and southern Mali (in West Africa) were mapped using spectral indices from MODIS and topographic features from SRTM. Mwita et al. (2012) map small scale wetlands in Tanzania and Kenya (in East Africa) using both optical and microwave data employing the decision tree classification techniques.

Here, i map for the first time, the extent of wetlands and categorize the different wetland types for the whole of southern Nigeria (147,094 km^2) at a 10 m resolution, leveraging the open access SAR and optical images acquired from Sentinel-1 and Sentinel-2 and exploiting cloud computing through Google Earth Engine (GEE). My primary aim is to provide knowledge of wetland extent and character that is needed to support both conservation efforts and land surface climate models. I anticipated that higher resolution wetland mapping would capture smaller patches of wetland than previously documented in regional or global datasets and that this would be dominantly associated with areas near major cities.

4.2 Materials and methods

My approach to mapping the wetlands of southern Nigeria involves the integration of indices from both optical and radar imagery and classification of imagery using the implementation of the Random Forest (RF) algorithm in Google Earth Engine (Gorelick et al., 2017). I use seasonal composite images in order to (a) maximise the

number of cloud-free pixels and (b) incorporate the seasonal variations in wetland characteristics into my classification (Section 4.3.1). I selected the most effective variables for classification in southern Nigeria using an estimation of relative importance (Section 4.3.3). This required the compilation of a new dataset of 1500 wetland and non-wetland control points for training and validation (Section 4.3.2, Supplementary Information Appendix A).

4.3 Class definitions

Wetlands can be classified on the basis of hydrology, soil type and vegetation. They include marshes (freshwater or saline waterlogged land areas that are periodically flooded, dominated by herbaceous plants), swamps (mineral soil wetlands dominated by trees with seasonal flooding), bogs (rain-fed peatlands, which can be with or without trees) and fens (groundwater-fed peatlands, which can be with or without trees) ((Mitsch and Gosselink, 2015). In this study, i consider swamps, marshes, shallow water (including human-made wetlands and lakes) and the swamp subtype of mangroves (coastal, characterised by salt-tolerant trees and shrubs), and attempt to distinguish between these categories in my mapping. The presence of peatlands (fens) across the southern region of Nigeria has been suggested by other mapping studies (e.g. CIFOR, 2016). The Nigerian government, however, suggested that the areas mapped by CIFOR as peatland are more likely to be mangrove/swamps (FREL, 2019). One potential source of confusion is that tropical ‘peat swamps’ are often referred to in the literature as there is a lack of an agreed tropical peatland classification system. Some swamps can have organic peat deposits while others may have a mineral substrate. To avoid confusion, i strictly

classify swamps for my control points as tree-dominated mineral soil wetland systems which may have minimal peat cover. Given this definition, peatland and swamp may in some cases still have similar Earth Observation signatures but would not be confused if ground truthed.

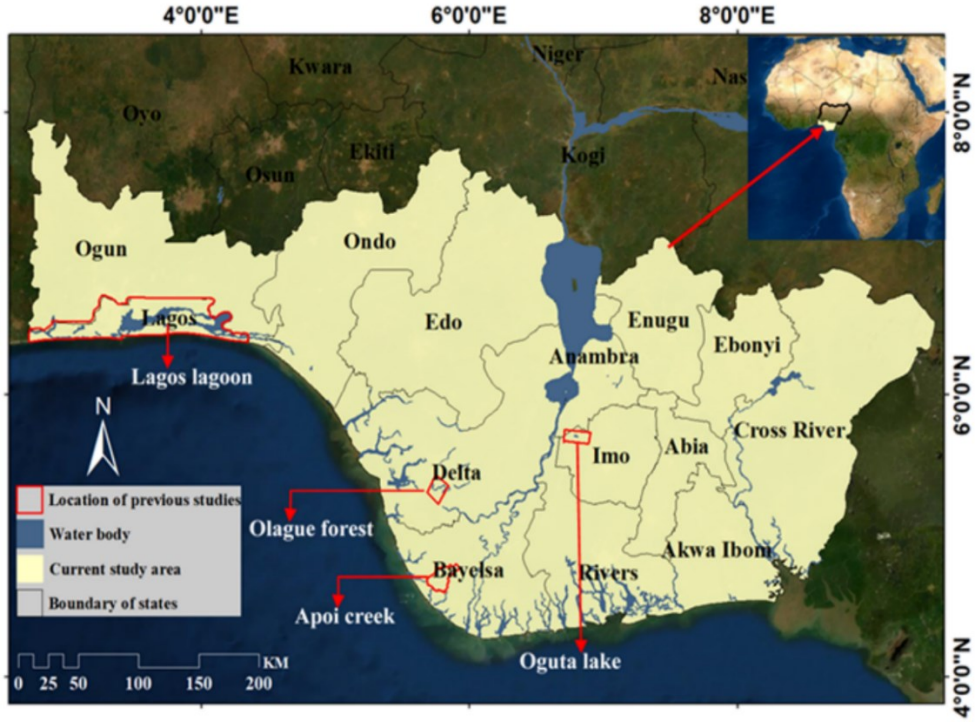

Figure 4.1 The study region: (a) Location of the study area using the standard government classification of southern Nigeria, and the locations used in previous studies referred to in the main text: Lagos lagoon (Taiwo and Areola, 2009), Olague forest, Apoi creek and Oguta lake (Ayanlade and Proske, 2016).

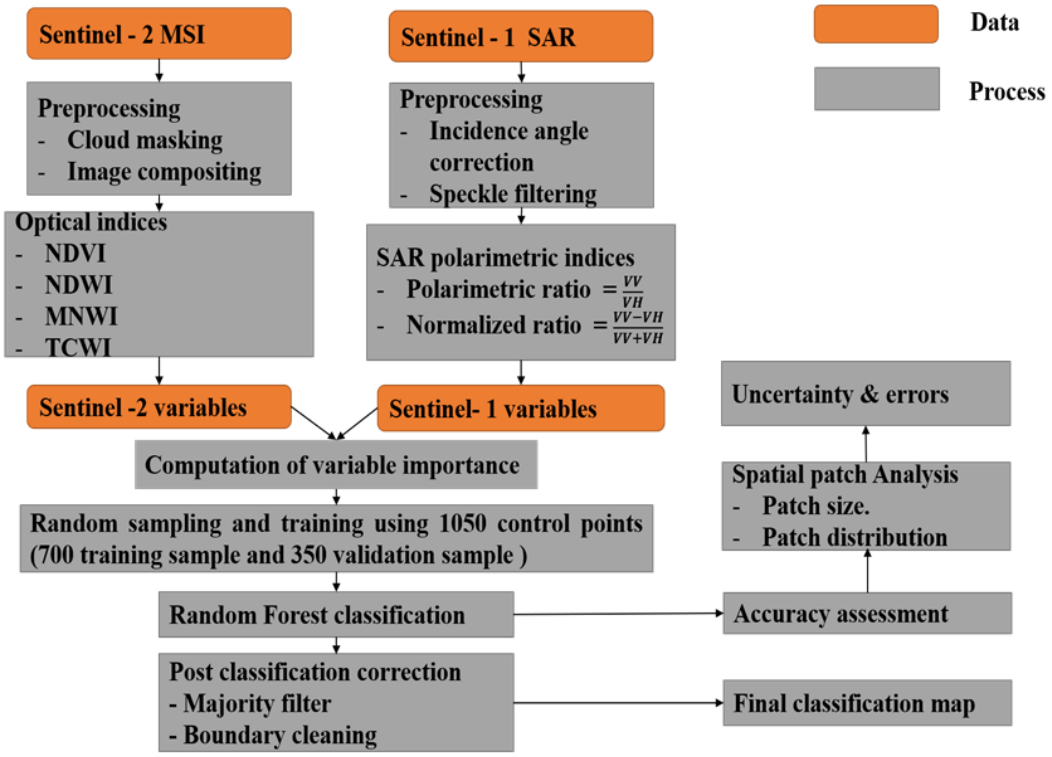

Figure 4.2 Methodological approach for mapping and characterization of southern Nigerian wetlands. The technique used a seasonal composite from Sentinel-2 optical imagery and Sentinel-1 radar for 2018.

4.3.1 Data selection

As the characteristics of wetland remote sensing signature varies between seasons, i use composite image for both optical and radar imagery. The southern part of Nigeria experiences a tropical climate with a well-defined wet and dry season. Southern Nigeria is covered by dense cloud during rainy seasons, so i use an initial selection criterion of cloud fraction <20% for each of 345 Sentinel-2 images from 2018 and apply a cloud mask to remove cloud and cirrus-cover (using the quality assurance bands available through GEE) before formation of a composite images (Figure 4.2). These are constructed from the median value for each pixel in 345 Sentinel-2 images acquired between January and November 2018 and are dominated by dry season (January to March) values. I use blue (0.496 µm, band 2),

green (0.560 μm band 3), red (0.665 μm, band 4), and near infrared (NIR, 0.835 μm, band 8), shortwave infrared 1 (SWIR1 1.613 μm, band 11) and short-wave infrared 2 (SWIR2 2.202 μm, band 12) bands to derive optical indices used for classification: Normalized Differential Vegetation Index (NDVI, Chatziantoniou et al., 2017; Dong et al., 2014; G. Kaplan & Avdan, 2017; Xing et al., 2018;Mahdianpari et al., 2018), Normalized Differential Water Index (NDWI, Chatziantoniou et al., 2017; Kaplan & Avdan, 2017; Mahdianpari et al., 2018; Xing et al., 2018), Modified Normalized Differential Water Indices (MNDWI , Ashraf & Nawaz, 2015; Chen et al., 2013; Ogilvie et al., 2015) and Tasseled Cap Wetness Index (TCWI , Tana, Letu, Cheng, & Tateishi, 2013; Xing et al., 2018) (Figure 4.3b-e).

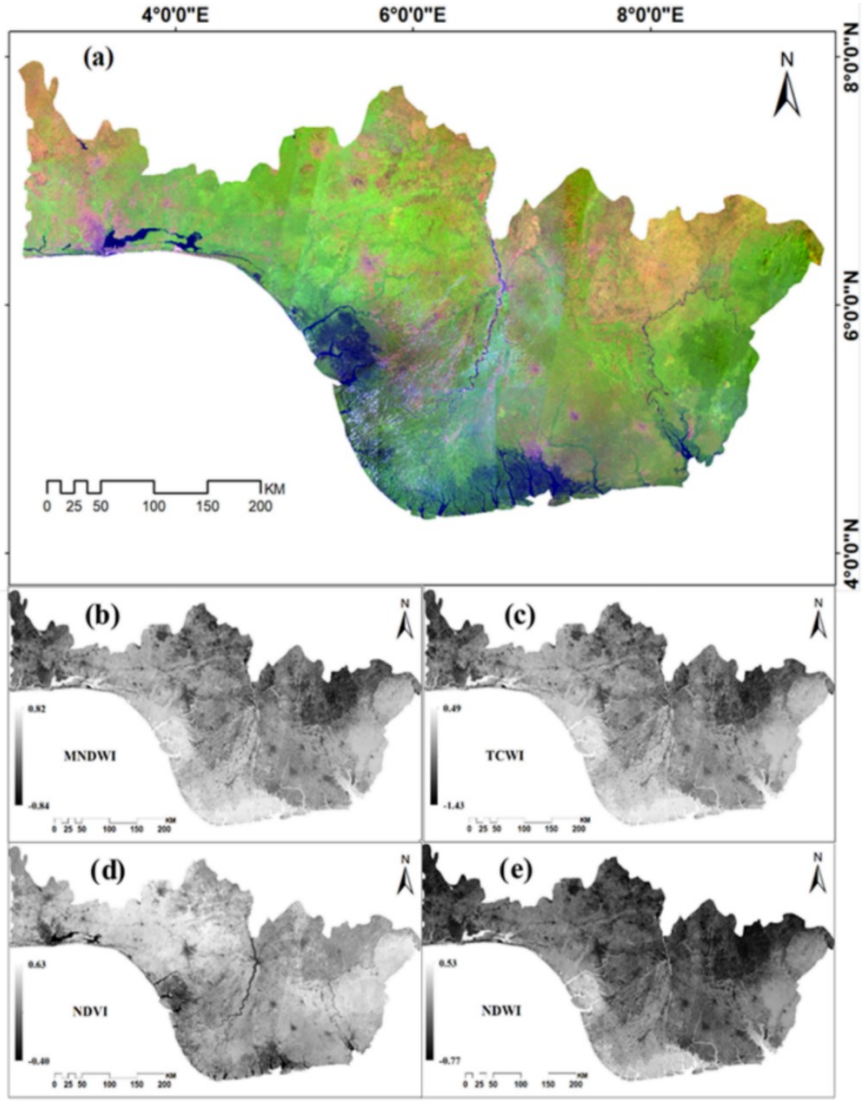

Figure 4.3 The Sentinel 2 composite and derived indices for Jan-Dec 2018 used for wetland classification in this study: (a) RGB composite images, red (band 11), blue (band 8), green (band 2), (b) MNDWI, (c) TCWI, (d) NDVI, (e) NDWI. The green shade in the RGB image results from reflection of vegetation, the dark blue shade represent reflection from water bodies, while urban settlement surfaces are shown in purple shade, and the lighter brown shade represents cultivated surfaces. For the indices (b-e) lighter gray shade indicates higher moisture and or vegetation value while a darker shade indicates lower values.

Since SAR backscatter is unaffected by cloud cover, I are able to incorporate information from dry (January-March) and wet seasons (April-July and September-November) into my classification scheme. Differences between flooded and unflooded periods are particularly strong since radar reflected by a water layer and backscattered by a double-bounce from ground and tree trunk creates contrast between the flooded and non-flooded terrain (Bwangoy et al, 2010b; Moser et al., 2016). I constructed dry and wet season composites that select the median backscatter value for each pixel, shown in Figure 4.2b and c as RGB images where dry season (January-March), wet season (April-July) and end of the wet season (Sept-Nov) are the red, blue and green channels, respectively.

I use the Ground Range Detected interferometric wide-swath Sentinel-1 images in ascending orbit from 2018 available through GEE, which are projected onto a regular 10 m grid. Dual VV/VH polarisation imagery was available at an average acquisition interval of 12 days over southern Nigeria. VV polarization (vertically transmitted, vertically received backscatter) is sensitive to surface roughness and soil moisture and can discriminate flooded from non-flooded vegetation (Mahdianpari et al., 2018). It also produces distinctive returns for herbaceous wetlands with low or sparsely vegetated areas especially in the early growth stages before canopy closure (Baghdadi et al., 2010). VH (vertically transmitted, horizontally received backscatter) known as cross polarization produces signals affected by volume scattering within the vegetation canopy and it is very sensitive to vegetation structures (Steele-Dunne et al., 2017). Icorrected for incidence angle (Hird et al., 2017) and reduced radar speckle using an adaptive sigma Lee filter on the GEE platform.. I calculated the

normalized difference and ratio features for each image as: Ndiff = $\frac{VH-VV}{VH+VV}$ and Nratio = $\frac{VV}{VH}$, where VH is a vertically transmitted, horizontally received SAR backscatter σ0 from the Sentinel-1 sensor, while VV is vertically transmitted and received SAR backscatter signal (Hird et al., 2017).

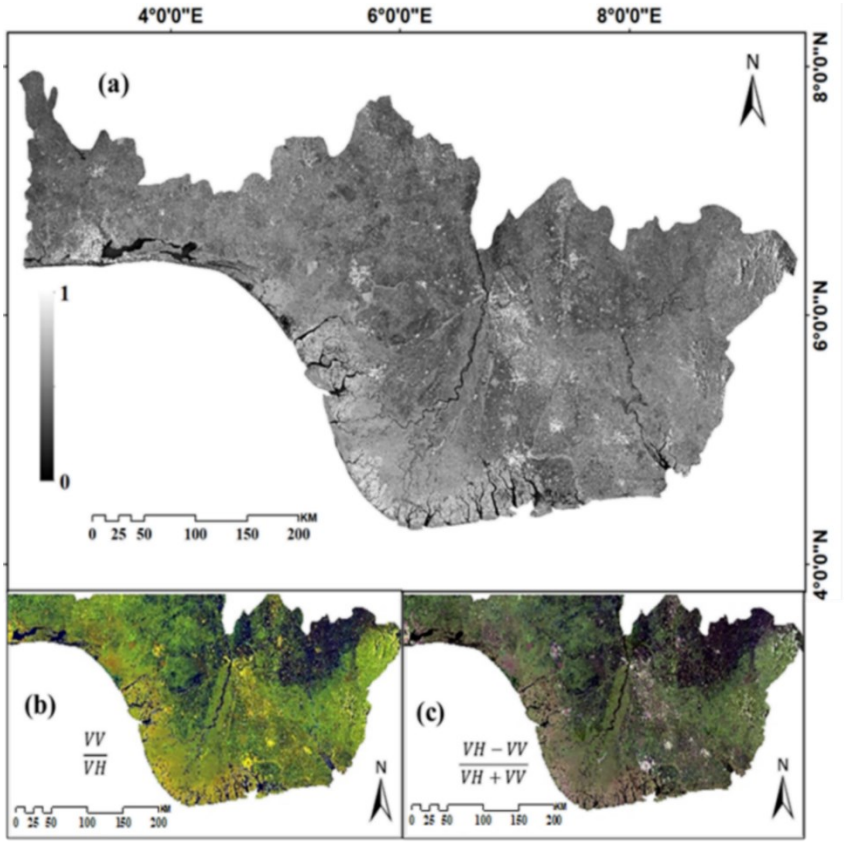

Figure 4.4 Extracted features from Sentinel 1 composite: (a) annual composite of VV and VH polarization; (b) seasonal composite images for Jan-Dec 2018 producing a ratio polarized image; (c) seasonal composite images for Jan-Dec 2018 producing a normalized polarized ratio image. The dry season (January-March), wet season (April-July) and end of wet season (September-November) composites were inserted into the red, green and blue channels respectively. The bright yellow shade in (b) and bright white in (c) shows high backscatter from urban areas in the red and green channels. The dark blue and black shade are the result of low backscatter from cultivated areas and water features.

4.3.2 Compilation of control point data

I compiled information about the location and characteristics of wetlands in southern Nigeria from multiple sources. My reference data were obtained from the Food and Agriculture Organization (FAO) global dryland assessment (Bastin et al., 2017), Ramsar Sites database (2019), other organization reports, journals, and academic theses (both PhD and MSc) (see Supplementary Information). The FAO reference points were compared with control sites from Ramsar and other studies, then verified by visual interpretation of Digital Globe very high spatial resolution images (< 1 m pixels) made available for visualization through Google Earth. My database comprises a total of 1500 sample points for wetland and non-wetland locations. The reference data were grouped into four wetland types which include swamp (205 points), mangrove (214 points), marsh (121 points), shallow water (184 points) and four non-wetland types grouped into deep water (194 points), urban/bareland (206 points), cultivated land (180 points), and forest (196 points) categories. The photo-interpreted database consists of both wetland and non-wetland cover classes with many subtypes, while only wetland control points were acquired from other studies.

4.3.3 Random Forest classification and feature selection

RF is a non-parametric classifier (i.e. it does not make strong assumptions about the form of the mapping function), comprised of a collection of tree classifiers, and can handle high dimensional remote sensing data (Belgiu and Dra, 2016). RF classification involves assigning a label to each pixel based on the majority vote of ‘trees’. The ‘trees’ are grown a node which is spilt using a random selection of the subset input variables, which reduces overfitting and yields a more robust

classification than other classifiers (Breiman, 2001). In the RF algorithm, i need to specify the parameters in order to produce the forest trees: the number of decision trees to be generated (Ntree); and the number of variables to be selected and tested for the best split when growing the trees (Mtry). The parameter Ntree was assessed for the values of 100 – 600: a value of 500 was selected as error rates for all classification models were constant beyond this point. I tested the importance of sixteen variables (Band 2, Band 3, Band 4, Band 6, Band 7, Band 8, Band 11, Band 12, NDWI, NDVI, MNDWI, TCWI, $\frac{VH-VV}{VH+VV}$, $\frac{VV}{VH}$ (wet and dry)), as input channels for the RF classification. I then selected six input variables that were most important for classification accuracy (see Section 4.3.3). A total of 900 training points spanning different landcover classes were used to train the RF classifier on the GEE platform. All classifications were based on the same training data. The remaining 600 control points were held back for validation (e.g., Liu et al., 2018). I divided the control points between training and validation data to ensure a spread between landcover classes, and otherwise to make their spatial distribution as even as possible across southern Nigeria. The classification was carried out with each index separately, before selecting the best combination to produce a final wetland map. I classified eight different landcover classes: mangrove, swamp, marsh, shallow water, forest, cultivated land, deep water, built-up/bare land. When selecting input variables used for my final RF classification, I assessed each of the optical and SAR indices for (1) the predictive power of each individual variable (Figure 4.5) and (2) the ability to distinguish between wetland classes.

I examine the significance of each input variable by calculating variable importance after training the RF classifier. The importance of a variable in this RF model is assessed using the total decrease in impurity across all trees in the forest for a specific choice of variable to split a node, where impurity refers to the probability of a classification being wrong if it were assigned according only to the distribution of classes in the data. The numerical values for importance assigned to each variable is the sum of the reduction in error of the splitting variable accumulated over the entire tree. Higher variable importance means that the variable played a significant role in the classification, while a low importance means only limited added value by that variable. Figure 4.5 illustrates the input variables and their corresponding importance for discriminating wetland classes.

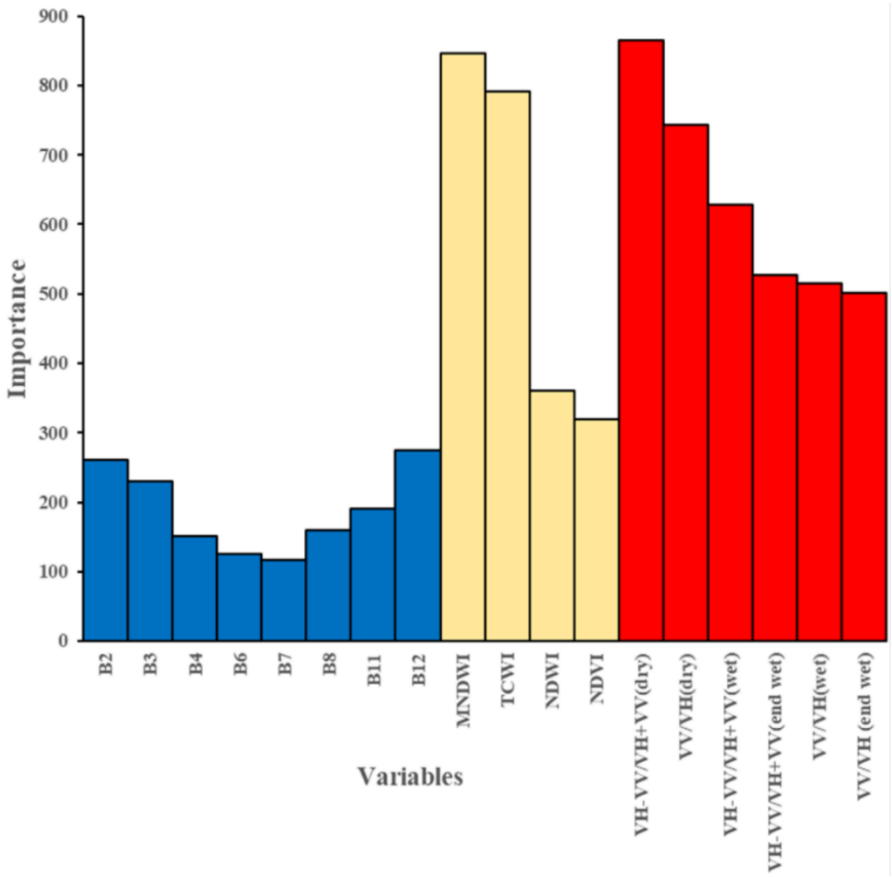

Figure 4.5 The importance of each extracted Sentinel-1 and Sentinel-2 features using the training dataset for Random Forest classification. The importance of the variable is the sum of decrease impurity each time the variable is selected to be split at the node for the entire trees in the forest and is unitless. The blue bars illustrate the importance of the optical bands, the light yellow shows optical indices and SAR polarimetric indices is represented by red bars.

As shown above, all the extracted variables from the Sentinel-1 seasonal composite appear to have higher predictive power than the optical indices except for the MNDWI and TCWI. With regards to variables extracted from the Sentinel-2 composite, the optical indices tend to possess higher significance when compared with the individual bands. Among the indices, MNDWI and TCWI have more information available for wetland cover prediction. The most important variables

(MNDWI, TCWI, ($\frac{VH-VV}{VH+VV}$, $\frac{VV}{VH}$ (wet and dry)) from Sentinel-1 and Sentinel-2 were selected for my final classification. However, each variable may have different strength in identifying a particular landcover class regardless of their relative importance. I further perform classification on individual variable to optimize my selection of combined model for the final classification map.

4.3.4 Wetland patch analysis

I calculate the number of patches and their individual sizes for each wetland class. The average continuous patch size for each wetland class was also calculated using the total count of connected pixels for continuous patches, which i define as pixels that share face boundaries. Here, i consider patches where the number of pixels is greater than 1000 (patch size> 1000 pixel) as continuous patches. The area of each individual patch was calculated by multiplying each patch size with the pixel area ($10m^{2)}$. The patch size is equivalent to the total number pixels in a patch while the patch area is the patch size x pixel area ($10m^2$). I use:

$$Pch_{avg} = \sum_{j}^{n} \frac{Pch_{cont}}{Pch_n} \qquad \text{Equation 4.1}$$

where Pch_{avg} is the average continuous patch for each wetland class in a particular climate zone, Pch_{cont} is the sum of the pixels of continuous patches (for patch size > 1000 pixel) in each class, whereas P_{chn} is the total number of continuous patches for each wetland class.

4.4 Results

My final map (Figure 4.6) has a pixel size of 10 m and shows how wetlands are distributed in southern Nigeria, broadly consistent with global datasets at low resolution, but quite different when studied in detail at high resolution. I capture wetlands of <1 km^2 that were omitted from global datasets and therefore provide much needed additional data on wetland coverage. The result of my classification shows high accuracy with 2% uncertainty. I have most confidence in my classification of swamp and shallow water, relative to mangrove or marsh.

4.4.1 Classification validation

The results of RF classifications for each index and for my preferred combination of indices (MNDWI, TCWI, ($\frac{VH-VV}{VH+VV}$, $\frac{VV}{VH}$ (wet and dry)) were evaluated using one third (600) of the total control points spatially selected from each class on a random basis. The overall accuracy describes the effectiveness of the overall classification, which can be determined by dividing the sum of correctly classified sample by the total referenced sample (Table 4.1). The producer's accuracy shows how well the referenced sample is represented in the classified map, while the user`s accuracy indicates the chances that a classified pixel of an individual landcover actually represent the same category on ground (Table 4.2). The agreement, beyond chance, of a classification and the real land cover can be described by the Kappa coefficient (e.g., Ayanlade, 2014). The Kappa coefficient is more useful than the overall accuracy as it provides a measure of how the classification performs in comparison to the probability of randomly assigning pixels to their correct categories. With the exception of NDVI, the classification results using spectral indices from optical

imagery were more accurate than those from SAR imagery alone (Table 4.1). However, the integration of the SAR normalized difference and ratio images with MNDWI and TCWI yield the highest accuracy. I attribute this to the improvement in accuracy of the identification of marsh, swamp and mangrove classes due to the information about vegetation structure captured by SAR imagery (Figure 4.4b &c).

Table 4.1 Overall accuracies and Kappa coefficients obtained from classification of wetland versus non-wetland in this study. Perfect classification of control points would yield a Kappa value of 1. S1+S2 represents my preferred combination of MNDWI and TCWI with the SAR polarimetric indices.

Indices	Overall accuracy (%)	Kappa coefficient
NDVI	73.10	0.68
NDWI	77.16	0.72
MNDWI	83.78	0.82
TCWI	83.74	0.79
$\frac{VH-VV}{VH+VV}$ (wet and dry)	85.14	0.83
$\frac{VV}{VH}$ (wet and dry)	74.30	0.72
MNDWI+TCWI+$\frac{VH-VV}{VH+VV}$ +$\frac{VV}{VH}$	88.40	0.85

For all landcover classes, classification using a combination of optical and radar data resulted in a higher accuracy than using any of the individual indices in isolation. My preferred classification (MNDWI+TCWI+$\frac{VH-VV}{VH+VV}$+$\frac{VV}{VH}$ in Table 4.1) performs as well as any other index in its classification of mangroves (214 control sites) and swamps (205 control sites), and better than any other index for classification of marsh (121

control sites). All classes have higher producer`s and user`s accuracies except the marsh with lower users accuracy, which was often misidentified as shallow water or swamp (Table 4.2). Overall, the classification of wetland classes was less accurate than for non-wetland classes. The combined use of optical indices (MNDWI and TCWI) and SAR features ($\frac{VH-VV}{VH+VV}$, $\frac{VV}{VH}$ (wet and dry)) resulted in greater accuracy for all the wetland classes than the use of either Sentinel-1 or Sentinel-2 imagery in isolation, and so this combination was used to produce my final wetland map.

Table 4.2 Confusion matrix using the set aside validation data (40% of control points). The rows are the classification results and the columns are the true class. MNG = Mangrove, SWP= Swamp, FRST= Forest, SHW= Shallow Water BTU= Built-up, DPW= Deep water, CTL = Cultivated land.

CLASS	MNG	SWP	FRST	MSH	SHW	BTU	DPW	CTL	Total	User Accuracy
MNG	75	8	1	1	0	0	0	1	86	0.87
SWP	9	69	2	1	0	0	0	1	82	0.84
FRST	1	2	61	2	2	0	0	10	78	0.78
MSH	4	1	0	34	4	0	0	5	48	0.70
SHW	0	0	0	2	67	0	5	0	74	0.90
BTU	0	0	0	0	0	78	0	4	82	0.95
DPW	0	0	0	0	2	0	76	0	78	0.97
CTL	0	0	0	2	0	1	0	69	72	0.95
Total	89	80	64	42	75	79	81	90	600	
Producer Accuracy	0.84	0.86	0.95	0.80	0.89	0.98	0.93	0.76		0.88

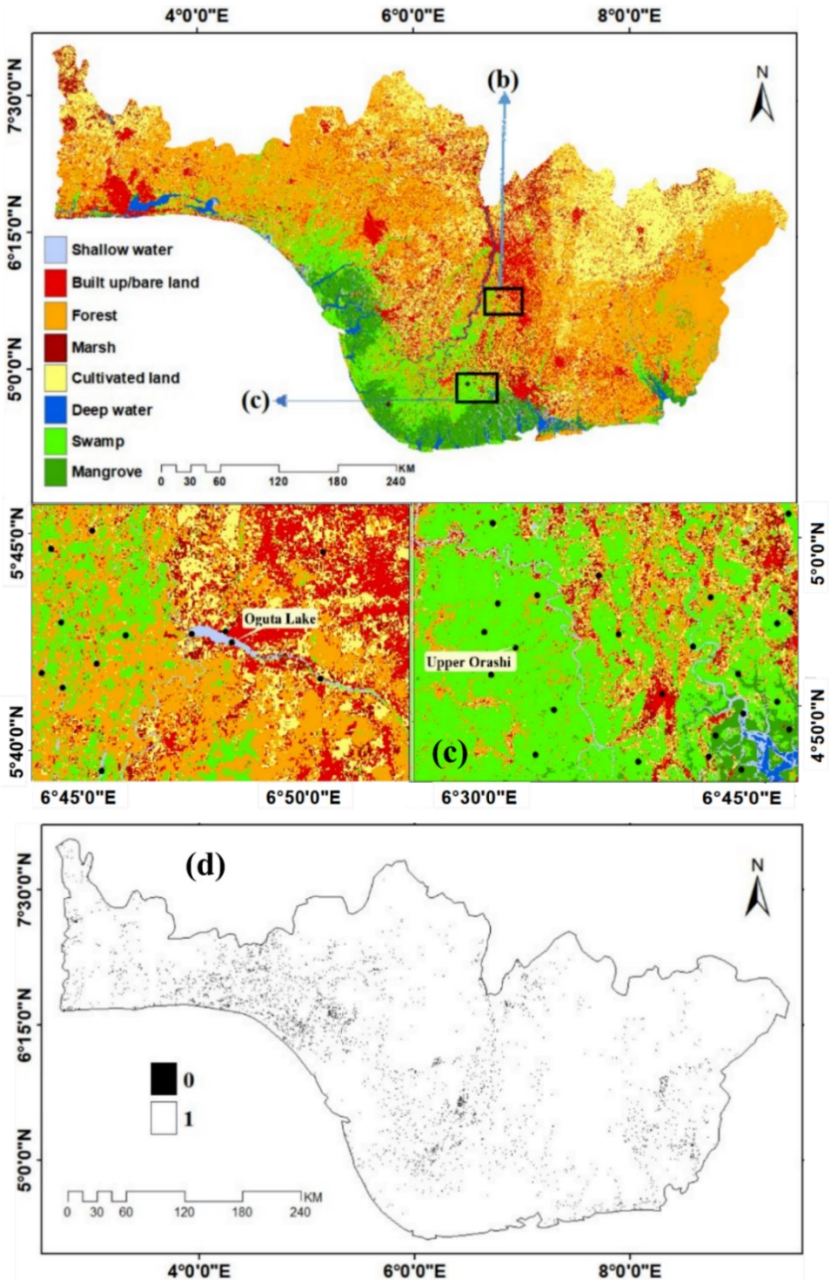

Figure 4.6 Final land cover map of southern Nigeria for 2018 obtained from RF classification of indices derived from Sentinel-2 optical data and Sentinel-1 SAR data (a), with inset (b) showing Oguta Lake and inset (c) showing Upper Orashi forest, both being examples of Ramsar wetlands while (d) displays the spatial distribution of uncertainty where the value 1 in white shade shows matching landcover class and the value 0 in black shade indicates a mismatch class from the comparison of a map produced using the entire control point dataset with a map produced from a randomly selected subset (70%) of control points.

My final wetland cover map (Figure 4.6a) shows the distribution of all land-cover classes, at 10 m resolution, across the extensive area of southern Nigeria. Both the wetland and non-wetland cover are well delineated with an estimated mapping accuracy of 88%. The detailed inset in Figure 4.6b & c shows how shallow water (e.g., Oguta lake, Figure 4.6b) and swamp (e.g., Upper Orashi swamp forest) are correctly distinguished from other landcover classes at two Ramsar wetland locations. I make an assessment of the spatial distribution of uncertainty in my wetland map by comparing it to a map produced from a randomly selected subset (70%) of control points with the map produced using the entire dataset (Figure 4.6d). In Figure 4.6d i show locations where land cover classifications agree for the two maps a value of 1 (white), and those that disagree a value of zero (black). I found that mismatches mostly lie on swamp and marsh landcover classes (Figure 4.6d), with fewer found to lie on mangrove and shallow water.

4.4.2 Wetland spatial extent

I estimate that the wetlands of southern Nigeria cover a total area of 29,924 km² which is over one fifth of the area of the whole region. The dominant wetland type is swamp which made up 44% of the total wetland area followed by mangrove (31%), marsh (20%) and shallow lakes (5%) (Figure 4.7a). The vast majority of these wetlands are located in the coastal region of the Niger delta and Lagos. My estimate of total wetland cover is less than the estimate by Center for International Forestry Research (CIFOR) (31,829 km²) but larger than GLWD (24,408 km²) (Figure 4.7a), mainly resulting from my larger mapped area of mangrove and my identification of

fewer marsh wetlands. While the maps look similar when viewed at low resolution, they are quite different in detail (Figure 4.7b-c).

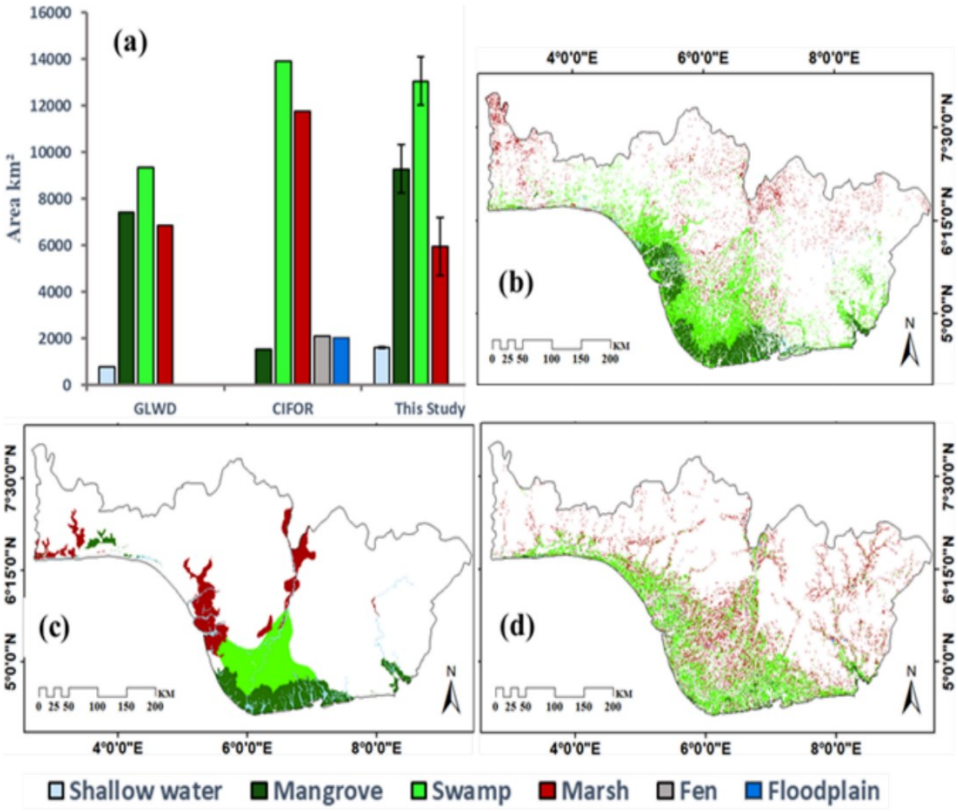

Figure 4.7 A comparison of wetland map products for southern Nigeria: (a) areas of different wetland classes in southern Nigeria - error bars show misclassification levels based accuracy achieved for each wetland type in my study; (b) map of southern Nigeria covered by wetlands identified in my study showing only the wetland classes; (c) the Global Lakes and Wetlands Database (GLWD) by Lehner & Döll,(2004) and (d) the global wetland database by the Center for International Forestry Research (CIFOR).

4.5 Discussion

4.5.1 Wetland extent and fragmentation

I calculated the average continuous patch size for each wetland class using the total pixel count of connected pixels for continuous patches, which i define as pixels that share face boundaries. I found mean continuous wetland patches of 120 km^2, 11 km^2, 55 km^2 and 13 km^2 for mangrove, marsh, swamp, and shallow water respectively. The maximum patch size was 2740 km^2, 1530 km^2, 160 km^2 and 50 km^2 with a standard deviation of 660 km^2, 765 km^2, 25 km^2 and 26 km^2 for these wetland types respectively. Larger patches of wetland are found along the coastal areas while smaller fragments are mostly located around urban areas suggesting a role for anthropogenic fragmentation of wetlands. Mangroves tended to be located in zones with lower population density. There were a large number of small wetland fragments, mostly of single pixel patches, especially for the marsh class. These smaller patches were distributed across the map but had higher uncertainty relative to larger patches. Understanding wetland fragmentation and its impacts on biodiversity and ecosystem services, and the role of both larger and smaller wetland patches in landscapes requires further work, but my dataset provides a starting point for enhanced modelling of such effects**.**

The extent of wetland in southern Nigeria was found to be larger in this study when compared to some previous studies but was smaller than the estimate by CIFOR (Figure 4.7a). This discrepancy could be due to a combination of factors including differences in wetland land cover class definitions (e.g. in CIFOR's global wetland database https://www.cifor.org/global-wetlands/ swamps and bogs are classed as

one type of wetland, while many floodplain wetlands appear to be swamps in this wetland map), classification methodology, timeframe (e.g. wetland loss or creation between different studies), data resolution and time of acquisition. For example, more conservative methods used by previous studies based on combining existing maps with other data sources may have resulted in exclusion of a large proportion of the swamp and mangrove that i identify here. Another major difference is my use of satellite imagery with higher resolution (10 m pixel size, relative to 1 km for GLWD) which improves my ability to identify small-scale wetlands (see Figure 4.9) and aids in discriminating wetland and non-wetland features. Some areas where wetlands have not previously been reported (e.g., around Akampka in Cross Rivers) have been mapped in this study. Some studies have suggested that the GLWD may underestimate wetland extent because of low resolution input data (Gumbricht et al., 2017), so wetlands much smaller than 1 km^2 are missed. About 20% of the wetlands that I identified in my new map have spatial extents of <1 km^2 (100 pixels). A series of small wetlands may be very important at a landscape scale in terms of water, nutrient and carbon cycling dynamics (Page et al., 2011) and so my work indicates how higher resolution wetland mapping may be important for improving regional and global environmental models.

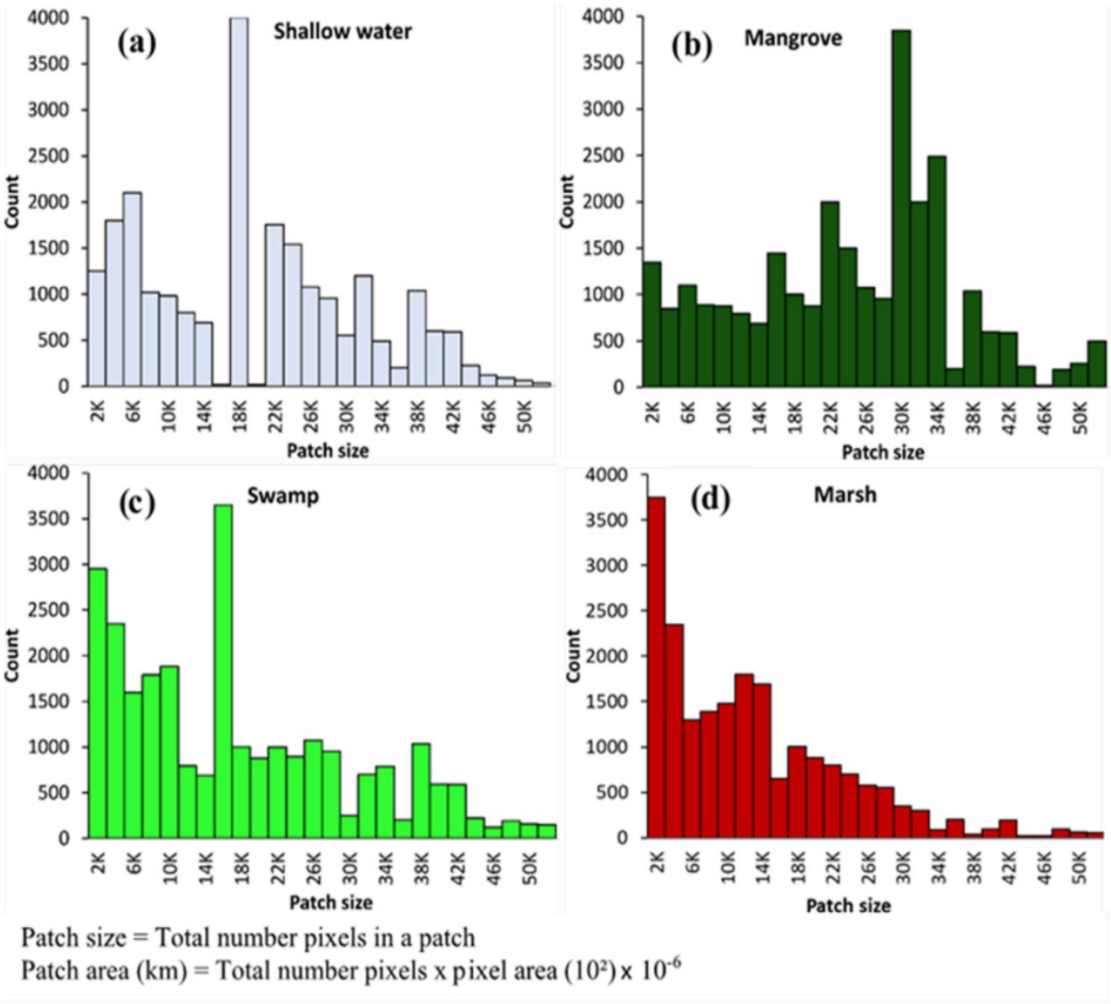

Figure 4.8 Distribution of patch size for different wetland classes: (a) shallow water; (b) mangrove; (c) swamp; (d) marsh. The patch size is defined as the number of pixels within a patch, the count is the frequency of patches with number of pixels in each category.

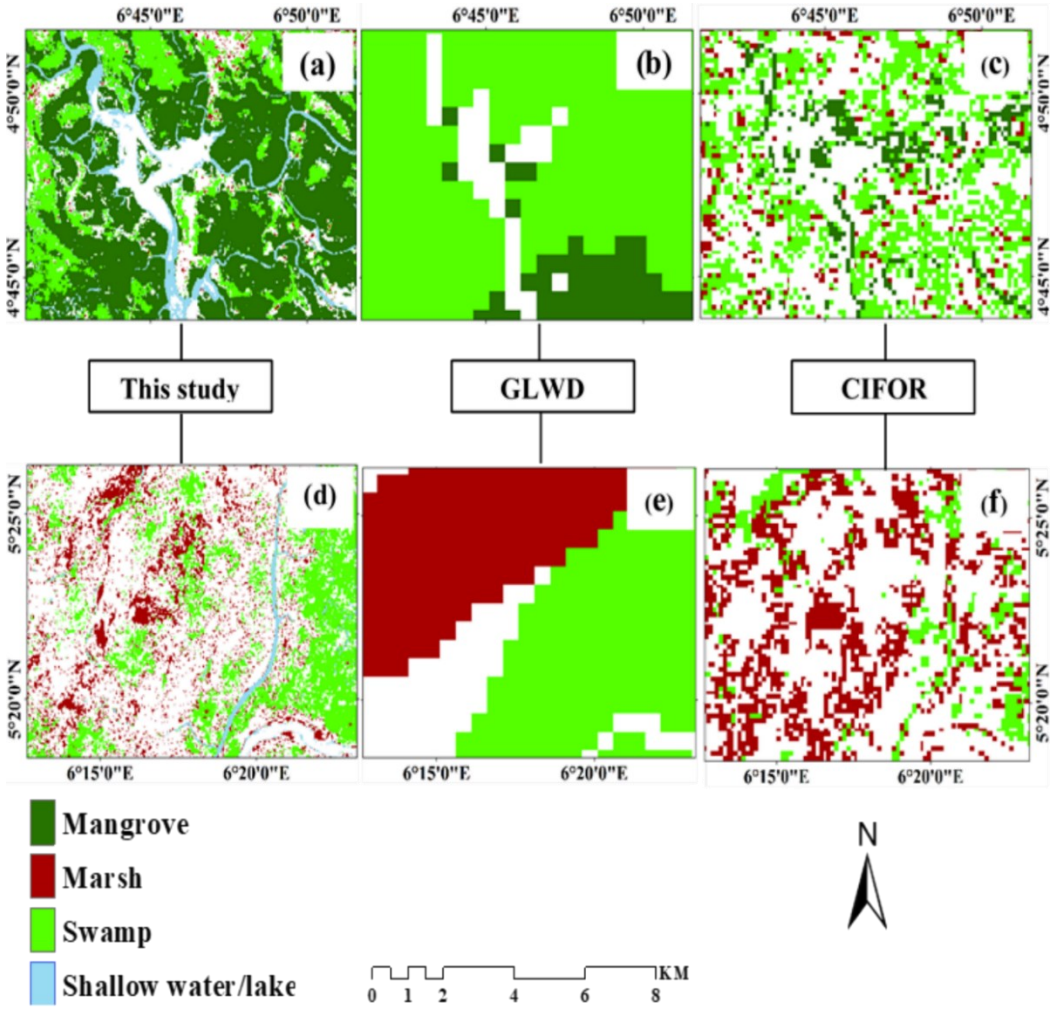

Figure 4.9 Comparison, for the same geographical area, between delineated wetland cover in two example locations (first location shown in top row a-c, second location shown as bottom row d-e): (a) and (d) this study using high resolution Sentinel data (full map shown in Figure 4.6 (a), (b) and (e) GLWD from a combination of low-resolution data, (c) and (f) the global wetland database by the Center for International Forestry Research (CIFOR).

4.5.2 Sources of uncertainty

The most important sources of uncertainty in this study come from (1) the subtlety of the differences in remote sensing signals between some wetland classes, and (2) the distribution and characteristics of the control sites used as the reference for

different land-cover types. Specifically, i expect uncertainties to be introduced by both a lower number of control sites for marshes and similarities in the remote sensing expression of marshes vs. mangroves, especially at 1610 nm and 2190 nm. I assess the uncertainties by comparing classifications made using the entire control point dataset with those produced using only a subset of control points selected at random for each wetland class (see Figure 4.6d). The mismatched pixels from each class were multiplied with the pixel area to obtain the mismatched area for each class. Swamp, with a total area of 13,000 km^2 had the highest uncertainty of 250 km^2 followed by marsh (area of 6,000 km^2) with uncertainty of 123 km^2. Lower uncertainty was estimated for mangrove (9,000 km^2) at 72 km^2 and shallow water (1,616 km^2) with 14 km^2. While this approach gives some indication of the uncertainties associated with this classification accuracy and limitations in the number of control points, it does not include systematic uncertainties associated with my choice of landcover classes. However, more than 98% of the control points accurately matched the classified land-cover class. Based on control point accuracy values for each wetland type (Table 4.2) there was a higher error with marshes due to their misinterpretation as mangroves and bare land / settlement features. A higher uncertainty occurred in areas around Ovia (south-west Edo state), northern parts of Ogun state and around Ndokwa in eastern Delta state due to the number of smaller patches of marsh. There were no control points for fen peatlands. However, my analysis suggests that areas mapped by other studies as peatlands (e.g., around Apoi creek forest) (refer to Figure 4.1**)** in southern Nigeria are swamps (with total of 149 control points), for which i had a high confidence in their classification.

4.5.3 Data limitations

Despite the high accuracy obtained from the classification model, there are some limitations in the dataset that may lead to bias in the model. Using training data from existing wetland locations is affected by ambiguity in definitions of wetland class and variation in the landscape. The basic assumption that training data represent a particular class may not always be absolutely correct as individual training points may belong to other wetland classes. To address this, i characterize the training data based on the class composition and internal variability. I then identify the possible outliers from the distribution of each wetland class and filter them out from the training data. Training data for ephemeral forested wetlands and peatlands such as bogs, fens are missing from my dataset which would have improved the classification.

The imbalance in the size of my training data for the wetland classes may bias classification accuracy, because the model is sensitive to wetland class with larger numbers of training points (in my case [mangrove]). This results in higher accuracy than for wetland classes with small amounts of training data (e.g., marsh).

Users of this wetland map should also consider (1) the limitations of the class definitions appropriate for use with satellite imagery and (2) the differences in accuracy of classification for different classes due to different numbers and spatial distribution of training points. For example, my EO-based classification of [swamps] comprises wetland with a range of characteristics in terms of vegetation type, water depth and soil composition.

4.5.4 Applicability to different settings

My novel study adds to a small number of locations around the world where wetlands have been mapped using combined SAR and optical Sentinel 1 and 2 data (e.g. Hird et al., 2017; Mahdianpari et al., 2018; Slagter et al., 2020). However, here i have covered a much larger area at high resolution. The wetlands of southern Nigeria are thought to represent about 19% of west African wetland and 3% of the total wetlands in sub Saharan Africa (Rebelo et al., 2010). Nigerian wetland ecosystems are similar to those in the rest of west Africa, so I expect that similar classification approaches could be adopted for this region. My methodological approach could be expanded to explore wetland areas across the wider African continent as well as globally. Furthermore, my technique can be used to globally detect changes and connectivity/fragmentation of wetland ecosystem in response to human action such as urbanization. Using data from different seasons is important for mapping and distinguishing between different types of wetland extents. For example, seasonal data has played an important role in identification of shallow water and marshes (Figure 4.6a). Seasonal data will be essential for mapping the wetlands in the arid regions of Africa, where wetlands exhibit dramatic seasonal cycles (e.g. the Sebkhel el Kelbia of Tunisia). Challenges of producing high-resolution datasets over large spatial areas can be minimized by employing the SAR polarimetric feature and optical indices which help to distinguish between types of vegetation. Wetland types such as peatlands which were not covered in this study should be mapped using suitable control points to aid classification. There is also a need to incorporate elevation/topographic data and a diverse range of multi-temporal datasets in order to improve the identification of wetlands across different terrain, such as valley

bottom wetlands. This will help to capture the hydro geomorphological properties of the wetlands.

4.6 Conclusions

This study combined optical indices and SAR polarimetric features to map four wetland types at 10 m resolution across southern Nigeria, filling a gap between existing low spatial resolution global maps and a few very local studies at higher resolution. Using freely available global satellite datasets (Sentinel-1 and 2), i achieve a mapping accuracy of 88% by integrating optical indices and SAR polarimetric features from different seasons using Random Forest classification. I estimate that in 2018 southern Nigeria contained 29,924 km² of wetlands with an uncertainty of 460 km², covering 20% of the region. I found a large number of small wetland patches, particularly around urban areas, consistent with human action enhancing wetland fragmentation in Southern Nigeria. Given the rapid expansion of population in Nigeria, it is now critical that wetland protection organizations undertake more adequate change detection at high resolution and take action, while modellers can utilise my high resolution land surface data.

Chapter 5
Wetland fragmentation associated with large populations across Africa

5.1 Introduction

African wetlands are among the most productive ecosystems in the world (Langan et al., 2018), providing a wide range of services that contribute to human wellbeing, such as provision of water, food, dry season grazing, and fuel wood. They can support flora and fauna and serve as an important carbon pool sequestrating large amounts of carbon from the atmosphere, thereby regulating climate (Saunders et al., 2012). Depending on topographic context, wetlands can also play a significant function in flood attenuation and shoreline protection (Junk et al., 2013; Acreman and Holden, 2013; Hu et al., 2017) and also play a key role in the hydrological cycle (Acreman and Bullock, 2003).

Wetlands in Africa are experiencing immense pressure from human activities, the most important being direct drainage and conversion to farmland, diversion of water away from wetlands for agricultural irrigation, population growth and urban expansion into wetland areas, pollution, overgrazing, and hydropower development; there has often been excessive exploitation by local communities (Schuijt, 2002; François et al., 2005; Mitchell, 2013). A large number of African wetlands are thought to have been heavily modified by overexploitation (e.g. the Yala swamp and Kingwal wetland in Kenya and Nakivubo swamps in Uganda) (Schuyt, 2005; Saunders et al., 2012) and upstream developments altering the quality and flow of water feeding

wetlands (e.g. Hadejia Jam`are floodplain in Nigeria (Schuijt, 2002)). Many African wetlands have been lost due to agricultural conversion such as the Ga-mampa swamp in South Africa (Rebelo et al., 2015). However, the current extent of wetland across Africa, at high resolution, is not known and most continental datasets are very coarse estimates (e.g. 250 m to 1 km resolution) (Schuyt, 2005; Landmann et al., 2013; Hu, Niu and Chen, 2017; Gumbricht, 2018; Y. Liu et al., 2020; Zhang et al., 2023). Small-scale wetlands may have been omitted or overestimated in previous continental mapping studies due to coarse resolution datasets, lack of ground control points and validation (Bwangoy et al., 2010; Moser et al., 2014; Leemhuis et al., 2016; Gumbricht et al., 2017; Mahdianpari et al., 2018). It is therefore not known whether the cumulative coverage of small wetlands is significant and there is a need to ensure appropriate representation of African wetlands for sustainable management and for modelling climate mitigation and biogeochemical cycles. The lack of high-resolution data hinders the estimates of the total amount of carbon stored by these wetlands and estimates of the potential for net carbon uptake or loss from African wetlands at a continental scale. Much wetland carbon is belowground, yet potentially fragile and susceptible to rapid loss with wetland degradation (Poulter et al., 2021). Wetlands can become divided or separated into smaller, isolated patches or fragments due to both human activities and natural processes, including urbanization, agriculture, infrastructure development, and changes in hydrology. Wetland fragmentation poses a serious threat to the health and functionality of wetland ecosystems, highlighting the need for conservation efforts focused on preserving and restoring these valuable habitats.

In this study, I used high resolution satellite datasets in combination with 8204 ground control points to systematically map the spatial distribution of wetland types across Africa. I verify the classification of each wetland control point by visual interpretation of Digital Globe very high spatial resolution images (< 1 m pixels) through Google Earth and spanning 2018 -2021. My independent sources of data for control points wetland types include papers, reports, and academic theses from various dates spanning 2015 - 2019, so i consider verification with the more recent Digital Globe imagery (2018 - 2021) a necessary step for classification of the 2020-2021 Sentinel 1 and 2 imageries.

I grouped the control points into five wetland types including marsh (2202), mangrove (1477), swamps (1891), peatland (1580) and seasonal wetland (1054). Here i classify swamps as mineral soil wetlands, while peatlands include fen and bog systems with or without trees (these include what are sometimes referred to as peat swamps). These classes capture critical differences in wetland vegetation, soils and water levels (see Appendix B Table B.3-B.7) and importantly are separable using optical and radar-derived indices from freely available satellite datasets. Fragmented wetlands are vulnerable to human development; thus, presence of human population indicate potential threat to these wetlands. I analysed the relationship between wetland patchiness derived from my map and population data from Gridded Population of the World database (GPW V4) and test the hypothesis that highly fragmented wetlands are associated with large populations. I used a 10 km grid for fragmentation analysis based on my previous studies that suggested that average continuous wetland patches cover an area of 10-11 km^2 (Chapter 4).

I calculated total carbon stocks for each wetland type by multiplying the total area of the wetland with typical values of carbon stock per hectare estimated by previous studies (IPCC Task Force on National Greenhouse Gas Inventories, 2014; Adame et al., 2015; Foerster et al., 2015; Samer Elshehawi et al., 2019; Ouyang and Lee, 2020; Csillik et al., 2022; Young et al., 2023). I then estimated the carbon emissions from different wetland types for two wetland degradation states (pristine and drained condition) in each climate zone.

5.2 Methods

5.2.1 Datasets

5.2.1.1 Ground control points

I collated data on the location and characteristics of wetlands across Africa from reliable sources, including the Food and Agriculture Organization (FAO) global dryland assessment database, Global Peatland Database (GPD), research journals, academic and NGO reports. I verified each data point and screened them to exclude any coordinates that were inaccurate, mislabelled or inconsistent by using visual interpretation of very high spatial resolution digital globe images (>1m pixel) made available for visualization through Google Earth. The final dataset used 8204 control points for different wetland types in Africa. I sorted the control points based on the climate zones in Africa and assigned to either training or validation points. Thus, I grouped the control points into an equal number of training and testing points to ensure robust accuracy assessment.

5.2.1.2 Satellite data

Sentinel-1 and -2 satellite images covering the entire study area for the period of January 2021 to December 2021 were available through the Google Earth Engine platform (GEE) at 10 m resolution. I use the Ground Range Detected interferometric wide-swath Sentinel-1 images acquired in dual-polarization (VV/VH) and pre-processed as a Level-1 data product, with an average acquisition interval of 12 days. A total of 5728 Sentinel-1 images in ascending order were collected for the study area. Sentinel-2 Top of Atmosphere reflectance data with 16 spectral bands were obtained through the GEE. Sentinel-2 images with cloud cover of <20% were selected from January 2020 to January 2021 which resulted in a total of 13596 images.

5.2.1.3 Population data

I obtained information about population distribution from the Gridded Population of the World database (GPW V4) provided by Center for International Earth Science Information Network (https://sedac.ciesin.columbia.edu). The GPW dataset has an approximate resolution of 30 arcsec, equivalent to 1 km at the Equator, that contains global population counts, density, urban/ rural status, age and gender structures with more than 12,500,000 input units maintained by NASA's Socio-Economic Data and Applications Center (SEDAC). The population input data are collected at the finest resolution available from the '2010' round of censuses, which occurred between 2005 and 2014.

The data were used to produce population estimates for the years 2000, 2005, 2010, 2015, and 2020 (https://earthdata.nasa.gov/data/catalog?keyword=gpw-v4/methods). I selected the population estimates for 2020 for our analysis.

5.2.2 Mapping of wetland extent

To accurately delineate the wetlands of Africa I classified the continent into different major zones according to the climatic and ecological features. These zones include tropical wet, tropical wet and dry or grassland, semiarid and desert or arid. I also grouped the control points for each wetland type based on these climate zones. I processed the images collected from Sentinel-1 and -2 images for the period of 2020-2021 to develop optical and radar indices for each climate zone. The optical variables used include spectral bands 2 (blue), 3 (green), 4 (red), 8 (NIR), 11 and 12 (SWIR), the normalized difference vegetation index (NDVI), normalized difference water index (NDWI), modified normalized differential water Indices (MNDWI), and tasseled cap wetness index (TCWI). SAR variables included vertically transmitted, vertically received SAR backscattering coefficient ($\sigma^0 VV$), vertically transmitted, horizontally received SAR backscattering coefficient ($\sigma^0 VH$), and the normalized difference (Ndiff= $\frac{VH-VV}{VH+VV}$) and ratio indices (Nratio= $\frac{VV}{VH}$) for the wet and dry season. I then undertook a variable importance analysis (Kim et al., 2012; Van Beijma et al., 2014; Suiter, 2015; Zabala, 2017; Na et al., 2018; Mohammadimanesh et al., 2018; Jamali and Mahdianpari, 2022; Csillik et al., 2022) for each climate zone to select the most important variables to input into the final classification. For all images in the arid and semi-arid region I extracted the maximum pixel values while a median value was used for other regions to enhance identification (Maxwell and Sylvester, 2012).

Finally, I applied a Random Forest algorithm (RF) to classify and validate wetland types in each climate zone.

RF is an ensemble classifier that produces multiple decision trees, using randomly selected training samples and variables (Belgiu and Dra, 2016). RF is more robust compared to other classification algorithms, solving the problems of over-fitting with other decision trees. The RF is particularly suitable for handling variation within land cover classes and reducing noise in the data. It does not require prior knowledge of the data distribution compared to other classifiers. It involves assigning weight to each pixel based on the number of votes received in each tree. The final result is obtained after some level of correlation in fitting and majority voting (Breiman, 2001). To produce the forest tree in RF we need to identify the two important parameters: the number of decision trees to be generated (Ntree); and the number of variables to be selected and tested for the best split when growing the trees (Mtry). The parameter Ntree was assessed for the values of 100 – 600: a value of 500 was selected as error rates for all classification models were constant beyond this point. In this study I used the combined SAR and Optical indices as input variables.

5.2.3 Classification map accuracy and uncertainties

I undertook classification of wetlands according to each climate zone using the RF classifier. The control points for different wetland types were compiled for each climate region separately to classify the input variables developed for each region. To accurately classify the wetland types based on their distinctive features in a particular region, the input variables were extracted from composite images

constructed from different pixel values over a particular period of the year. In the arid and semi-arid region, seasonality is often a key property of wetlands. I therefore used the variables extracted from seasonal composites of maximum pixel value to train the RF classifier (Chapter 3 Table 3.2). I identified seasonal wetlands using the maximum value from my seasonal composites. For the Tropical Wet (TW), Tropical Wet and Dry (TWD) and Mediterranean subtropical climate (MED) zones, the variables constructed from the mean pixel value composites were used to train the RF classifier (Chapter 3, Table 3.2).

I assessed the accuracy of RF classifications for each climate zone using cross validation by splitting the control points into two halves (50% training and 50% testing points), spatially selected for each climate zone from each class on a random basis. My accuracy estimation matrix includes the overall accuracy (OA), Kappa coefficient, producer accuracy, and user accuracy. Overall accuracy determines how well the classification algorithm performed, which can be measured by dividing the total number of correctly identified sample point by the total number of the testing points (Table B.3-B.7 Appendix B). I evaluated the uncertainties by comparing classifications made using the entire control point dataset with those produced using only a subset of control points selected at random for each wetland class in each climate zone. The uncertainties are associated with my classification accuracy, high confusion between wetland classes (e.g., swamps and peatlands) and limitations in the number of control points. Common issue with the gridded population data is misallocation of population to areas outside the urban areas. These errors were

minimized by down sampling the 1 km grid population taking the average population within 10 km grid.

5.2.4 Carbon loss estimation

I used the CO_2 emission factor provided by the IPCC Wetland Supplement guidance (IPCC Task Force on National Greenhouse Gas Inventories, 2014) to estimate the amount of carbon loss from each wetland type for different climate zones in Africa. An emission/removal factor is a coefficient that quantifies the emissions or removals of a gas per unit area. It is calculated using a sample of measurement data, averaged to determine a representative emission rate for a specific activity level under defined operating conditions. I multiplied the total area of each wetland type with its corresponding emission/removal factor across the different climate zones for two assumptions: 1) the wetlands are in pristine condition; 2) wetlands are drained. The $CO_{2\ equivalent}$ emission was calculated by:

$$CO_{2\ emission\ i} = \sum_{i,c,y}(EF * Area) \qquad \text{Equation 5.1}$$

where $CO_{2\ equivalent}$ emission is the annual net carbon emission/uptake from a wetland type in tonnes $CO_2\ yr^{-1}$, area is the land area of drained land cover category in climate domain c, in ha, and *EF* is the emission factor for drained organic soils, by climate domain c, in tonnes C $ha^{-1}\ yr^{-1}$.

I also adopted the empirical function of Zou et al. (2022) to estimate the wetland carbon flux using water level as function of carbon emission. Equation 5-2 was used to calculate the carbon flux from selected wetland types under different moisture regimes in different climate zones:

$\text{Emission}_y = \sum(Efs_{ijk} \times Area_{ijy})$ Equation 5.2

where *Efs* is emission factors, i is the climate zone, j is the water-table level (coded -3 to 2), y is the year and k is the wetland type.

5.2.5 Carbon stock estimation

The total amount of carbon stored by each wetland type in Africa was evaluated using the acquired data of carbon stock per hectare from the studies by (IPCC 2014: Adame et al., 2015; Boone and Bhomia, 2017; Dargie et al., 2017; Samer Elshehawi et al., 2019; Ouyang and Lee, 2020). To calculate the total amount of carbon stored by each wetland I multiplied the total area of the wetland with the value of carbon stock per hectare:

Wetland carbon = Total wetland area (hectare) * Carbon stock (t C ha^{-l})

Equation 5.3

5.2.6 Wetland fragmentation and population index (WFPI)

I compared the distribution of wetland fragments and population at the same cell size across 10 km grid areas. For my analysis I used only the count of wetland fragments estimated at a resolution of 10 km to allow comparison to the gridded population data at 10 km resolution. This resolution was selected because it was found to be the mean dimension of wetland fragments from my earlier study (Chapter 4).

I aimed to identify the association of wetland fragmentation with human population. I used a fuzzy logic approach to create a membership rank for the fragmentation grid and population grid (ranging from 0-1), with 0 representing lowest membership and

1 the highest membership in increasing order. Lower membership indicates grid cells with less fragments or which are sparsely populated, while grid cells with a large number of wetland fragments or which are densely populated are assigned to a higher membership group. Finally, I overlayed the gridded fragmentation membership layer with the gridded population membership layer to quantify the coincidence of wetland fragments and human population. Higher WFPI indicates interaction of dense population with wetlands resulting to patchiness within the grid cells.

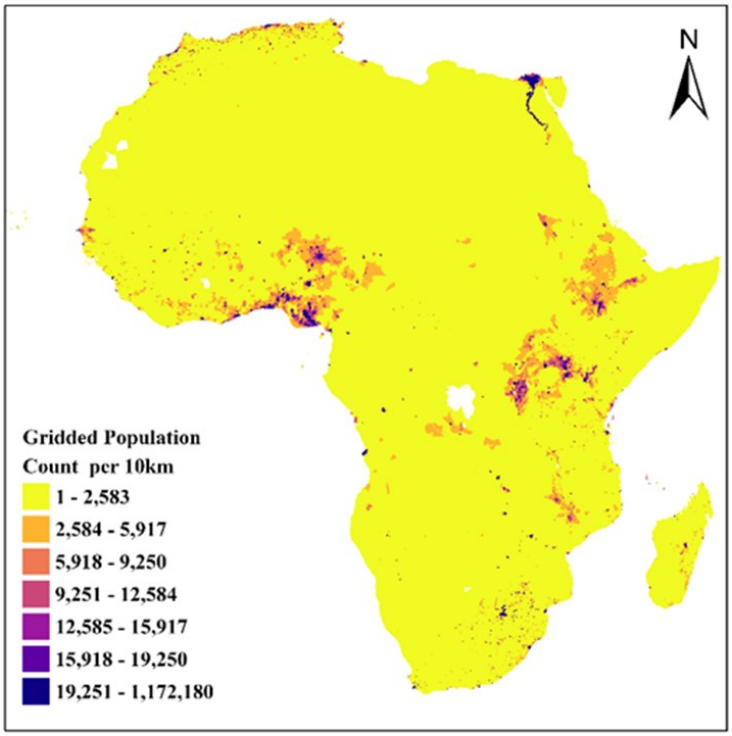

Figure 5.1. The 10-kilometer square gridded layer of population count of Africa. The yellow regions indicate grids with lowest population count (maximum count of 2,583 persons per 10 km^2), while the ultra blue colored region represents grids with a population count greater than 19,250 persons per 10 km^2. White patches have no data.

5.2.6.1 Population grid

The population grid was created by transforming population data obtained from GPW V4 data using 10 km grid reference cells across the continent of Africa. I classified the cells in different class ranges from lowest to highest based on the population count in each grid cell (Figure 5.1). Most of the grids with dense population are located near major city centres, or close to river networks. I used this grid as an input for the for fuzzy membership transformation.

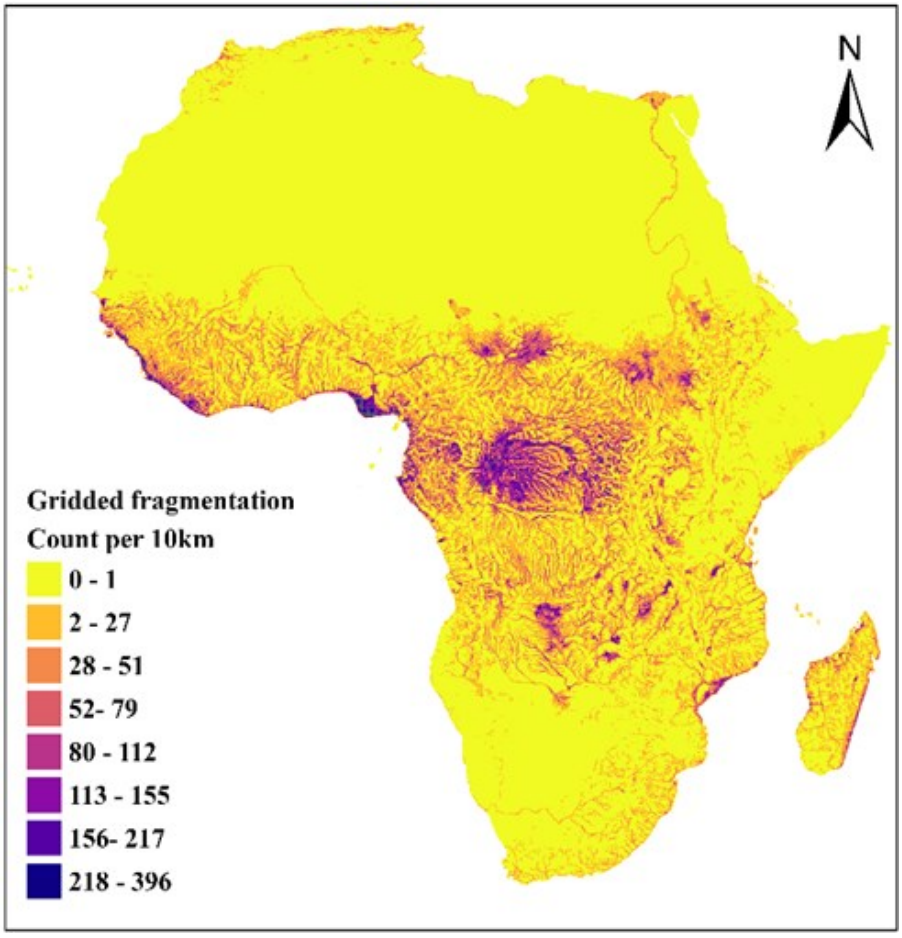

Figure 5.2. The 10-kilometer square gridded layer of wetland fragmentation in Africa. The yellow regions indicate a non fragmented grid (fragment <=1), while the ultra blue represents a highly fragmented grid.

5.2.6.2 Fragmentation grid

To create the fragmentation grid, I converted the classified wetland raster to polygons using the conversion tool in ArcGIS pro. I used an algorithm similar to spatial aggregation by overlaying 10 km x 10 km grid on the original 10m resolution fragmentation map. For every 10m cell within a 10 km grid, the number of unique wetland fragments is calculated. I then identified and labelled distinct fragments within each grid. The fragment count within each 10 km grid cell is computed to derive a metrics of the total number of fragments. The total number of fragments per grid cell was used to group the cells into eight groups from low to highly fragmented (Figure 5.2). The total fragment in each cell was calculated by:

$$Frag_{grid} = \sum_{i}^{n} Grid_i \qquad \text{Equation 5.4}$$

where $Frag_{grid}$ is the fragmentation grid (10 km), n is the number of fragments in grid cell i, and i is the code of the grid cell.

5.2.6.3 Fuzzy membership

I transformed the population and fragmentation grid into a fuzzy membership layer scaled from 0 to 1. 0 indicates grid cells that are not members of any set while 1 is assigned to grid cells with full membership. I use the fuzzy linear membership function to transform the input values linearly on the 0 to 1 scale, with 0 being assigned to the lowest input value and 1 to the largest input value (Figure 5.3). All of the values in between receive some membership value based on a linear scale, with the larger input values being assigned a greater possibility, or closer to 1.

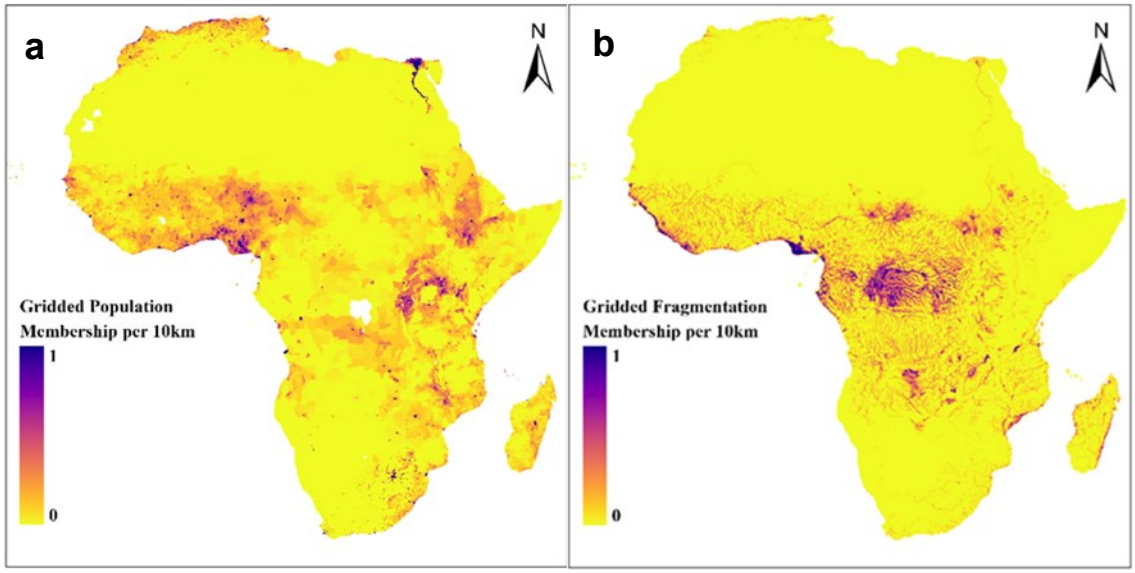

Figure 5.3 Fuzzy membership showing the distribution from lowest to highest members: (a) population grid, (b) fragmentation grid. From 0 to 1 in an increasing order. 0 label represents the lowest membership which indicates sparsely populated grids, while the label 1 indicates densely populated grids assigned to the highest membership group.

5.2.6.4 Fuzzy overlay

The Fuzzy Overlay tool is used to evaluate the probability of a phenomenon belonging to several sets in a multicriteria overlay analysis. It determines whether a phenomenon is a possible member of a particular set and analyzes the relationships between the membership of the multiple sets. I used the “fuzzy And” function to find the relationship between the population and fragmentation membership layer. I overlayed the population grid with the fragmentation grid using a fuzzy overlay tool (Raines et al., 2010). This allowed me to analysed the relationship between the multiple members set from each grid layer. Stronger relationships are found between higher membership sets while lower membership sets showed weak relationships. Coincidence of a dense population grid (higher population membership grid) with a

highly fragmented grid (higher fragmentation membership grid) result in the highest WFPI region.

5.3 Results

5.3.1 The current extent of African wetland

My high-resolution continental study reveals that wetlands cover ~947,750 km^2 of Africa (excluding deep water bodies) which constitutes ~3% of the total land area. Marshes and swamps are the most dominant wetland covering 436,743 km^2 (46% of total wetlands) and 231,776 km^2 (24%) respectively. Peatlands cover 208,842 km^2 (22%), while seasonal wetlands (5%) and mangroves (3%) have the least coverage. Most of these wetlands are concentrated in western and central parts of Africa (Figure 5.4a), where there is a high amount of rainfall throughout the year. However, some important wetland complexes are situated in North Africa such as in the Nile region. The largest wetland complex is located in the Congo region of central Africa covering about 278,450 km^2, which contains the most extensive peatland area (165,250 km^2) in the entire continent (Figure 5.4e). Other important wetland complexes are situated in southern Sudan (the Sudd) (67,150 km^2) (Figure 5.4d), the Zambia (43,170 km^2), Angola (46,072 km^2) and Nigeria (47,130 km^2).

5.3.2 Distribution of wetland across African climate zones

I examined the spatial distribution of different wetland types according to the five main climatic regions in Africa: Tropical Wet (TW), Tropical Wet and Dry (TWD), Semi-Arid (SARD), Arid or Desert (ARD) and Mediterranean subtropical climate (MED). TW has the most extensive wetland, hosting 57% (~448,210 km^2) (Figure

5.5b) of the total wetland area in Africa. Peatlands (37%) and swamps (34%) are the most dominant wetland types of TW which cover 165,950 km^2 and 153,580 km^2 respectively. Mangroves (2%) and seasonal wetlands (0.5%) are the least common wetland types in TW covering only about 14,000 km^2.

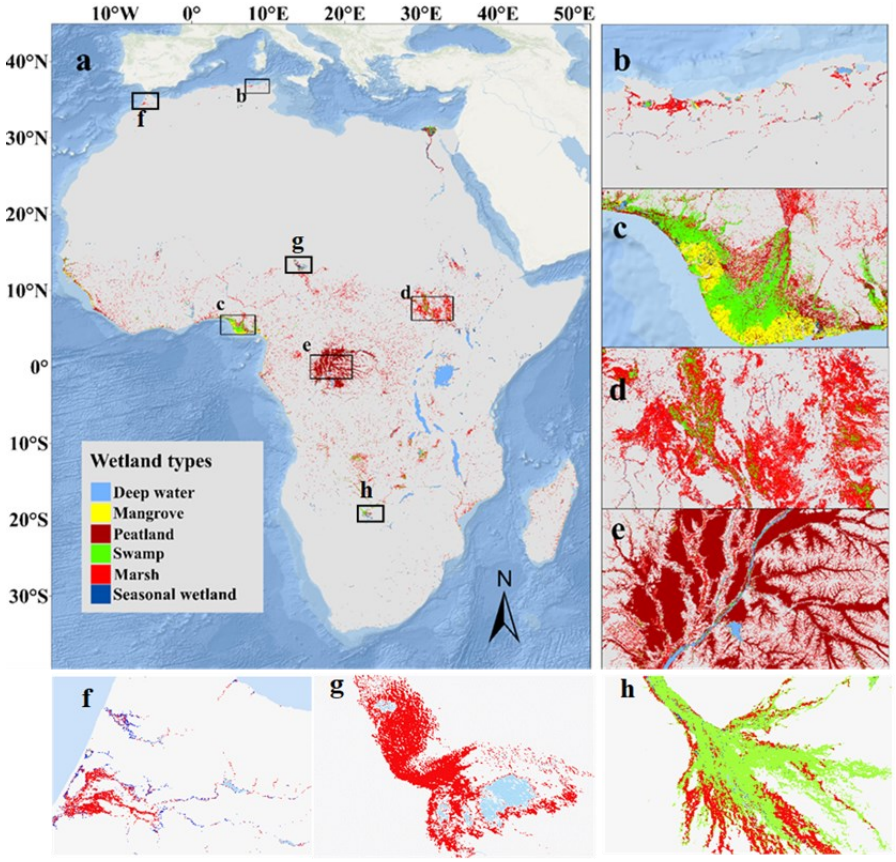

Figure 5.4 The distribution of wetland in Africa, at 10 m resolution, derived from classification of a combination of Sentinel-1 and Sentinel-2 composites between January 2020 and January 2021 showing extensive wetland complexes in (b) northern Algeria and Tunisia, (c) Nigeria, (d) South Sudan, (e) part of the Congo basin, (f) Morocco, (g) Chad, (h) Botswana.

The largest climate region is the TWD, covering up to 38% of the total area of Africa. Wetlands in this region constitute only 3.2% (~362,980 km^2) (Table B.1 Appendix B) of the total area with 52% being marshes (Figure 5.5a). This region has a distinct

climatic feature with alternating wet and dry periods throughout the year, which plays a significant role in the formation of different wetland conditions and variability across the season. Thus, TWD has a higher amount seasonal wetland cover relative to other climate zones (Figure 5.5). SARD is characterized by little rainfall throughout the year, covering 6,700,000 km^2 (22%) of Africa. Only about 1.4% of SARD is covered by wetland, of which seasonal wetlands are the most dominant type. ARD is the second largest climatic region in Africa extending up to about 9,000,000km^2 and has the lowest wetland coverage (0.4%).

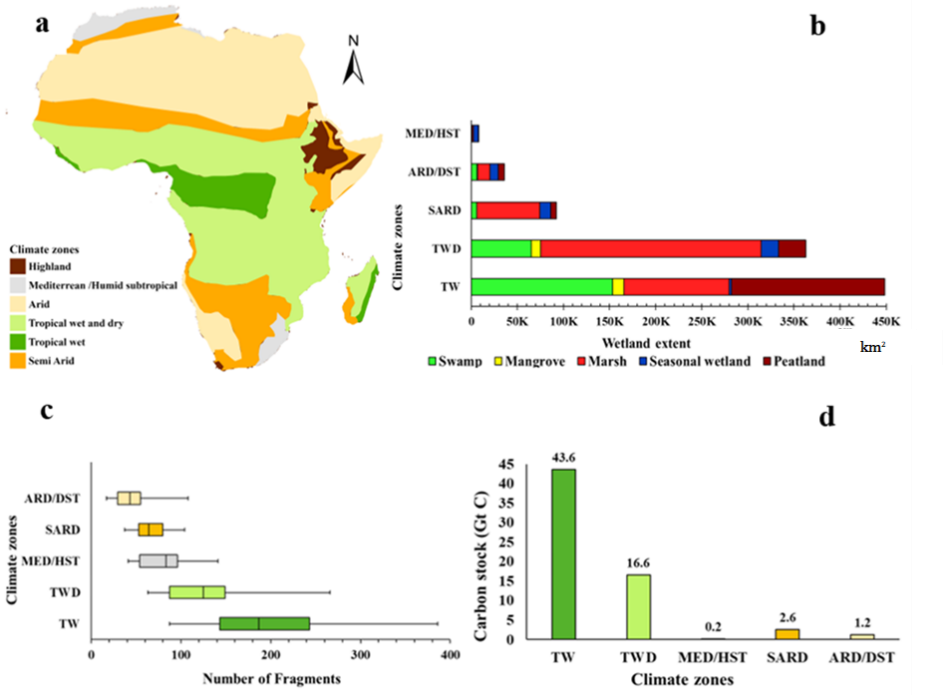

Figure 5.5 Distribution of wetland types in different climatic zones showing: (a) division of Africa into different climate regions, (b) estimate of areal extent of wetland types in each climate zone (c) the intensity of wetland fragmentation in each zone per 10 km grid, (d) carbon stock in wetlands for each climate zone.

5.3.3 Wetland fragmentation and human population

I developed a wetland fragmentation and population index (WFPI) by overlaying the gridded population layer with the gridded wetland fragmentation layer using the fuzzy overlay method (section 5.2.4.4). The fragmentation index is an indicator of regions with high wetland patches per 10 km grid and the population index is a count of persons per kilometer grid indicating areas of high concentrations of population. My WFPI shows areas where fragmentation is coincident with humans (Figure 5.6) using 10 km grid cells across Africa.

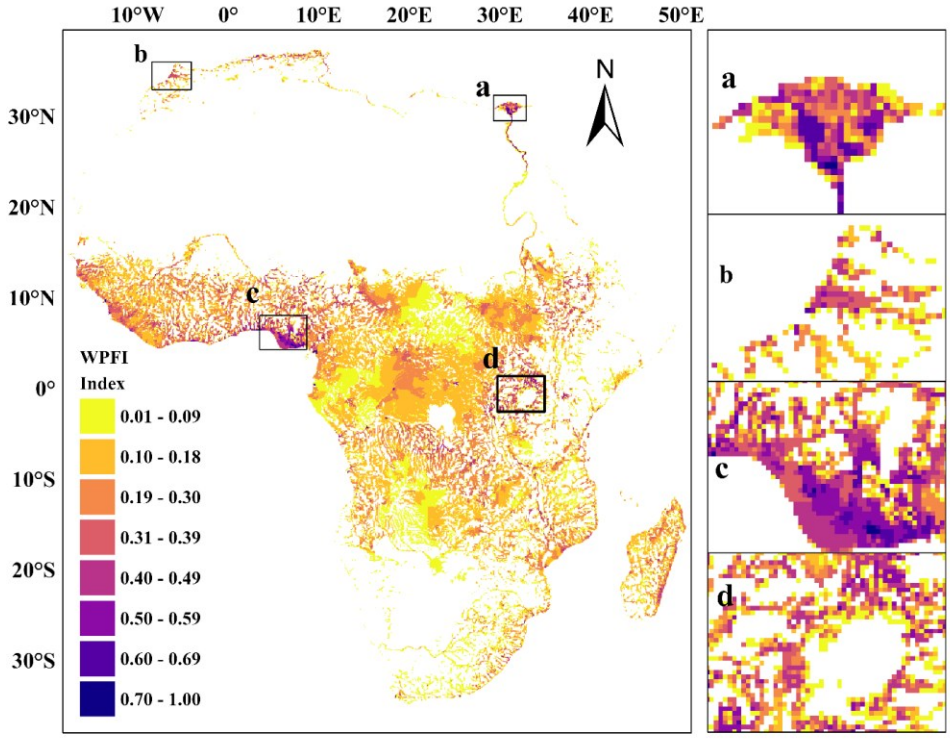

Figure 5.6 Gridded wetland fragmentation and population index for 10 km cells across Africa showing areas where fragmentation is associated with population (values closer to 1). The insert map a-d shows areas of high WFPI value.

I identified nine regions with a WFPI value indicating highly fragmented grid cells (80-226 wetland fragments per 10 km^2) related to large population size (40,000-300,000 persons per 10 km^2). Six of these regions are in west Africa (Nigeria, Liberia, Gabon, Guinea and Cameroon), two in north Africa (Egypt and Algeria) and one in east Africa (Kenya). In west Africa, areas such as Rivers State and Lagos in Nigeria, and Monrovia in Liberia, have highest WFPIs of 0.89, 0.76 and 0.83 respectively (Table 5.1). These areas are characterized by high population growth associated with urban expansion, thereby increasing pressure on nearby wetlands, mainly coastal mangroves and swamps. Other areas with high WFPI include Conakry in Guinea (0.68), Alexandra in Egypt (0.66), Algiers in Algeria (0.61) and Murang'a in Kenya (0.59) often associated with agriculture encroaching on wetlands in these regions (Kariyasa and Dewi, 2011; Hedjal et al., 2018; Maina and Mwangi, 2023). The index indicates that a total of 13,021 km^2 of wetlands may be heavily threatened by human activity within Africa (WFPI.>0.5) and about 28,724 km^2 of wetland occurs in populated areas that suggest a moderate at risk of human interactions (WFPI 0.3-0.5). However, large wetland complexes with a high concentration of fragments (for example the Congo basin wetlands) that are far away from settlements or sparsely populated show little or no relation between fragmentation and human populations (Figure 5.6). The high concentration of fragments in the Congo basin are thought to be geomorphologically and climatologically controlled rather than driven by human activities (Young et al., 2023), though these peatlands could be highly sensitive to human-induced fragmentation in the future.

Table 5.1 The location, number of fragments and population of high WFPI 10 km^2 grid cells across Africa.

Location	Country	Population per grid cell	Fragmentation per grid cell	WFPI
Rivers State	Nigeria	130698	209	0.89
Lagos	Nigeria	303143	107	0.76
Greater Monrovia	Liberia	136475	185	0.83
Alexandra	Egypt	168943	94	0.66
Algiers	Algeria	220546	76	0.61
Muranga	Kenya	72349	61	0.59
Conakry	Guinea	98844	174	0.68
Littoral	Cameroon	67846	173	0.57
Estuarie	Gabon	41947	226	0.55

5.3.4 Carbon stock in African wetlands

Healthy wetlands can store large amounts of carbon, but the quantity of carbon stored varies among different wetland types (Adame et al., 2015; Poulter et al., 2021). Among these wetland types, peatlands are thought to have the highest carbon stock followed by mangroves, swamps and marshes (Adame et al., 2015; Boone and Bhomia, 2017; Ouyang and Lee, 2020; Sjögersten et al., 2021). I use the IPCC mean carbon stock for each wetland type to estimate the total carbon stored in four wetland types of Africa. My new continental map indicates that African wetland contains 54 ±11 Gt of carbon which is around 5% to 9% of wetland soil carbon stored globally (520 - 710 Gt C) (Poulter et al., 2021), and higher than that of European wetlands (12-31 Gt) (Malak et al., 2021). Peatlands store about 41% of

this African wetland carbon, while 28% is stored in marshes, 27% in swamps and 3% in mangroves.

5.3.5 Net carbon uptake or loss from African wetlands

I estimated the contribution of African wetlands to the global carbon budget across each climatic region using empirically derived emission rates for selected wetland types for which data are available (see Method). I used two approaches. First, I used the default emission factor from the IPCC emission factor database to calculate total carbon emissions from wetlands under two conditions (drained or natural). Using my new map of wetlands in Africa, i calculated that drained peatland, mangrove and marsh are capable of emitting 260Mt C yr^{-1} (936Mt CO_2 yr^{-1} equivalents) which is equivalent to 2.4% of global net annual CO_2 emissions (Friedlingstein et al., 2022) and almost ten times the mean net annual uptake under natural conditions of 27Mt C yr^{-1} (98Mt CO_2 equivalents yr^{-1}) by these wetlands. Wetlands within high WFPI areas, under drained conditions, could release 10.3Mt C yr^{-1} (37Mt CO_2 equivalents yr^{-1}).

The net wetland carbon flux varies according to water level (Evans et al., 2021; Zou et al., 2022). Therefore, in my second approach, i used the emission factor for different wetland types at various water levels obtained from Zou et al. (2022) to estimate the carbon flux for peatlands, marshes and swamps. The six categories of water level range from -3 to 2 (WTL-3 ≤ -70 cm; -70 cm < WTL-2 ≤ -50 cm; -50cm < WTL-1 ≤ -30 cm; -30 cm < WTL0 ≤ -5 cm; -5 cm < WTL1 ≤ 40cm; and 40 cm < WTL2), where negative values indicate depth below the surface, while positive

values indicate ponding. At water level -3 i estimated that African wetlands will have a net release of 310Mt $CO_{2\ equivalent}$ yr^{-1}, while for water level -2 they will emit 115Mt CO_2 yr^{-1} and 46Mt CO_2 yr^{-1} for water level -1, while 91Mt CO_2 yr^{-1} will be taken up by African wetlands when the water level is at level 1.

5.4 Discussion

My estimate of wetlands in Africa (947,750 km^2) is larger than that of the coarser global wetland dataset by CIFOR (859,278 km^2) and that of GLWD (934,481 km^2). The biggest difference occurs in the classification of marsh followed by swamp and mangrove. This variation may be due to the coarse resolution dataset used to produce previous global wetland maps which may result in misclassification and omission of small-scale wetlands. This inconsistency highlights the importance of using high-resolution data to improve the estimation of wetlands, which in turn can be used to develop policy and monitoring to protect wetlands. This study shows close similarities with smaller geographical scale studies, such as the peatland map of Angolan highlands constructed by Lourenco et al. 2022 (Figure 5.7)

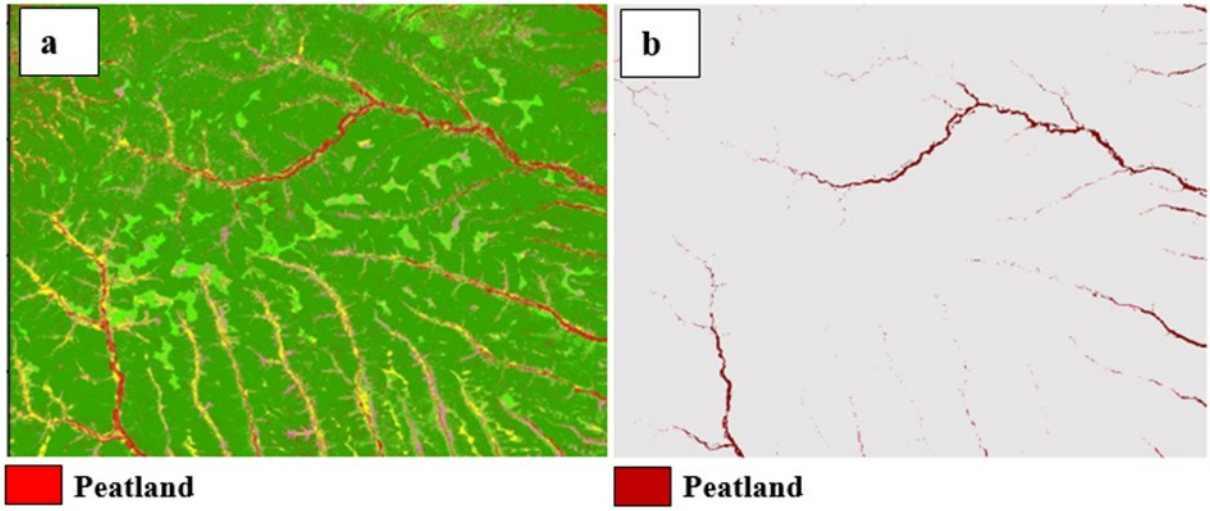

Figure 5.7 The Map of Angolan highlands peatlands by (a) Lourenco et al. 2022, (b) This study.

The overall accuracy of the trained algorithm compared to validation ground control data was higher for wetlands in the TWD region (89%) with mangrove and marsh well distinguished from other wetland classes with producer's accuracies exceeding 80% (Table B.3-B.7 Appendix B). There was high confusion in discriminating mineral soil swamps and peatlands especially in the TW region with user`s and producer`s accuracy below 70% and 80% respectively. There is also a common confusion amongst other wetland classes such as swamps and mangrove, marsh, and seasonal wetlands due to similarities in their visual and spectral signatures. The low accuracy in the Arid region was a result of confusion in discriminating swamp and peatlands along the Nile area, due to the presence of a peat deposit within the swamps. Similar confusion occurs in TW and TWD due peat deposits in the swamp and my method did not perform well in discriminating between non-peatland swamps and peatland.

The WFPI analysis generally identifies sites where the presence of human population poses a threat to nearby fragmented wetlands. My new map can be used as a baseline to monitor and assess wetland changes over time at a fine scale (10m resolution). It should also be noted that my method can now be used to generate timeseries observations for analyzing human-driven and natural wetland changes as well as their fragmentation, supporting future remotely sensed observations on the success of different wetland protection policies. My future work will be concentrated on gathering more and better-quality ground control data to support some future timeseries analyses.

I explored the possible impact of African wetlands on global climate through net carbon uptake/loss under natural and a range of drained conditions. I found that the three selected wetland types (peatland, mangrove and marsh) under drained conditions could contribute up to 3% of global net annual carbon loss, a value which might be much higher if data for emissions from other wetlands become available and included in the estimation. Human activities have been widely reported to be a key driver of wetland degradation (Van Asselen et al., 2013; Dixon et al., 2016; Davidson, 2017). The degradation of wetland is often related to deeper water-tables which leads to increased decomposition and release of carbon to the atmosphere (Laine et al., 1996; Limpert et al., 2020). I found that wetlands which are currently highly fragmented in heavily populated areas of Africa have the potential to release CO_2 equivalent to 0.6 % of total global annual emissions. Hence, protection of African wetlands, particularly in Tropical wet (TW), Tropical wet and dry (TWD) regions and most areas with high WFPI where the largest carbon stocks and greatest

net C emission potential is to be found, will be important for managing future land-based emissions.

My analysis of African wetlands provides a high-resolution insight as to their extent, condition and their potential contribution to the global carbon balance, providing data critical for both improving land-surface climate models and for wetland conservation.

Chapter 6
Detecting changes in wetland area of the Lake Chad region using change vector analysis

6.1 Introduction

Wetland ecosystems play an important role in society by offering richly resourced habitats and providing sustainable livelihood opportunities. These ecosystems help develop, grow, and sustain the natural environment. Depending on their topographic setting and local conditions, they can reduce flood impacts, enhance water quality by absorbing pollutants, and serve as important faunal habitats, among many other environmental, recreational, and economic advantages (Acreman and Holden, 2013; Junk et al., 2013; Mitsch and Gosselink, 2015). Within the context of climate change and resource exploitation, these ecosystems face significant threats from anthropogenic activities that may lead to their widespread loss. Changes in land use around wetlands may exacerbate the risks posed by climate change, potentially causing disastrous effects on surrounding populations by impacting water and food security (Lemoalle et al., 2012; Magrin, 2016; Pham-duc et al., 2020).

The Chad basin (2.5×106 km^2) contains one of the largest wetland complexes in Africa with Lake Chad as a key feature (Policelli et al., 2018). The wetland systems cut across three main African climate zones including arid, semi-arid and tropical wet and dry (Birkett, 2000; Lemoalle, 2005). The region comprises a complex of permanent freshwater marshes inundated as part of Lake Chad, rivers and their deltas, and the shallow lake itself (Lemoalle, 2005). The wetlands of this basin are

economically important, providing water, fish, and other resources to the surrounding populations (Lemoalle et al., 2012). However, I note that increasing rainfall variability and irregularity over the past four decades, combined with human impacts such as upstream dam construction, have led to the slow degradation of these wetlands (Leblanc et al., 2011; WWF, 2014). The prolonged drought episodes over the region from the 1970s to the 1990s and the lake retreat greatly modified natural resource availability in the basin and around the Lake Chad wetlands. Degradation was further escalated by human activities such as the damming of rivers, and abstracting water in upper reaches, for irrigation. Studies have shown that there has been a slight increase in the wetland extent around Lake Chad with a corresponding decrease in open water area especially in the northern pool of the lake, while the wetlands in the southern pool area of Lake Chad seem to be stable with the open water area slightly increasing after the late 20th Century drought period (e.g. Leblanc et al., 2011; Lemoalle et al., 2012; Pham-duc et al., 2020; Policelli et al., 2018). However, there is a lack of high temporal-resolution data to capture dynamic changes in wetland extent in this region.

Remote sensing has been used as an important tool for monitoring and identifying wetland changes (Chen et al., 2014; Ashraf and Nawaz, 2015; Jochems et al., 2021; Al-Nasrawi et al., 2021). Advancements in high spatial and spectral resolution imagery have allowed for improved remote sensing capabilities for wetland mapping (Klemas, 2011), which could be beneficial for long-term monitoring by detecting patterns within wetlands and landscapes (Kelly et al., 2011). In addition, the application of current remote sensing techniques not only helps quantify ecological

changes in wetlands over time, but such analysis can help to link environmental changes to anthropogenic drivers (Byrd et al., 2004). A variety of techniques have been developed for mapping landcover using remote sensing time series data (Xia et al., 2002; Zhao et al., 2009; Zhu and Woodcock, 2014; Estupinan-Suarez et al., 2015; Van Tricht et al., 2018). Time-series mapping based on phenological differences provides critical information on spatiotemporal patterns of land cover. However, applications of time-series remote sensing data to African wetland ecosystems remain limited, with most studies focused on semi-arid West Africa (Zhao et al., 2009; Kovács et al., 2022). The complex water dynamics, diverse wetland types, and spectral similarities between wetlands and other land cover classes complicate the ability to conduct detailed and long-term monitoring of wetland cover on a frequent basis (Ozesmi and Bauer, 2002; Niu et al., 2012).

Over the past decades, much literature on changes in the Lake Chad region has investigated the variability of the extent of open surface water using satellite data (Birkett, 2000; Leblanc et al., 2011; Lemoalle et al., 2012; Policelli et al., 2018). Zhu et al. (2017) investigated the variations of water level in the southern pool of Lake Chad for 25 years using satellite altimetry products and Landsat TM/ETM+ images. Policelli et al. (2018) estimated the total surface water area of Lake Chad using a combination of land surface temperature and radar remote sensing data. The study utilized thermal infrared data to analyze land surface temperature variations, identifying and delineating water bodies based on temperature differences between water and land. Mahamat et al. (2021) utilized satellite images from Landsat-MSS to Landsat-OLI of Lake Chad to explore alterations in the open water surface area

across the years 1973, 1987, 2001, 2013, and 2017. They showed a decrease in Lake Chad surface water area from 1973 to 2017. Despite these advances, I found that few studies account for changes in the surrounding wetlands interlocking with open water areas and other land cover types in Lake Chad. In a recent study by Hussaini et al. (2020), changes in Lake Chad landcover were evaluated during the preceding three decades by utilizing satellite imagery, encompassing OLI, ETM+, and TM sensors. Changes in five land cover types were analyzed across three epochs: 1985, 2000, and 2015. The findings revealed a significant growth in farmlands and gallery forest from 1985 to 2015, whereas a decrease in barren land, shrub, and water bodies was observed. However, the datasets and the approach used in these studies may not be robust for quantifying the changes within the wetland cover type in the Lake Chad basin due to lack of ground control points. Furthermore, most of these studies focused exclusively on assessing surface water dynamics and overlooked the changes in wetland systems within the Lake Chad region. Thus, I emphasize the importance of obtaining up-to-date, high-resolution information on wetland extents and changes in the Lake Chad area using advanced remote sensing techniques.

My previous studies have demonstrated the potential of advanced remote sensing techniques using machine learning with high resolution imagery to map wetlands of southern Nigeria (Garba et al., 2023) and the African continent as a whole (Chapter 5). In this study I used Change Vector Analysis approaches to map the types and quantify long-term dynamic changes of the wetlands of the Lake Chad area. CVA has been found to have several advantages over other change detection

applications (Karnieli et al., 2014). Firstly, it can concurrently process changes across all available spectral bands simultaneously, rather than handling each band separately. Secondly, by directly analyzing pixel vectors between dates, CVA avoids compounding spatial and spectral errors that often occur when classifying each date independently and comparing the classifications. Thirdly, CVA can detect not only conversions between discrete land cover classes, but also more gradual changes in the condition or state of a given cover type over time. Finally, CVA computes multi-dimensional change vectors containing rich information on the magnitude and direction of changes. These vectors can be separated into components representing different change processes and synthesized into change images that preserve this detailed change information to aid in interpretation and labelling of the changes observed. My aim is to use CVA to quantify wetland changes, analyze trends over the past two decades, and identify potential factors driving these changes in the Lake Chad Basin.

6.2 Study area

The Lake Chad area is an extensive shallow depression in the central part of the Sudano-Sahelian zone of Africa which lies between latitudes 12˚0'N and 14˚20'N and longitudes 13˚0'E and 15˚20'E. It is bounded within the area of four countries: Chad, Cameroon, Niger, and Nigeria (Leblanc et al., 2011; Mahamat et al., 2021). The area is characterized by variable climate conditions with an average rainfall of 320 mm which mainly occurs during June to October, which is considered as a wet season (Lemoalle, 2005; Lemoalle et al., 2012; Hussaini et al., 2020; Mahamat et al., 2021). The Lake Chad area has been variously categorised as a large inland

sea, a large lake with numerous islands, or a great marshy area (Sarch and Birkett, 2000; Leblanc et al., 2011; Ndayisaba et al., 2017). Historically, the surface area of the lake has varied as a result of rainfall fluctuations, but the extent of the lake surface also drastically decreased during the 1970s and 1980s (Lemoalle et al., 2012). The region is characterized by an alternation of desert and vegetated areas with hundreds of raised terrains in the middle of a desert environment. It is also covered by a succession of dunes of variable dimensions.

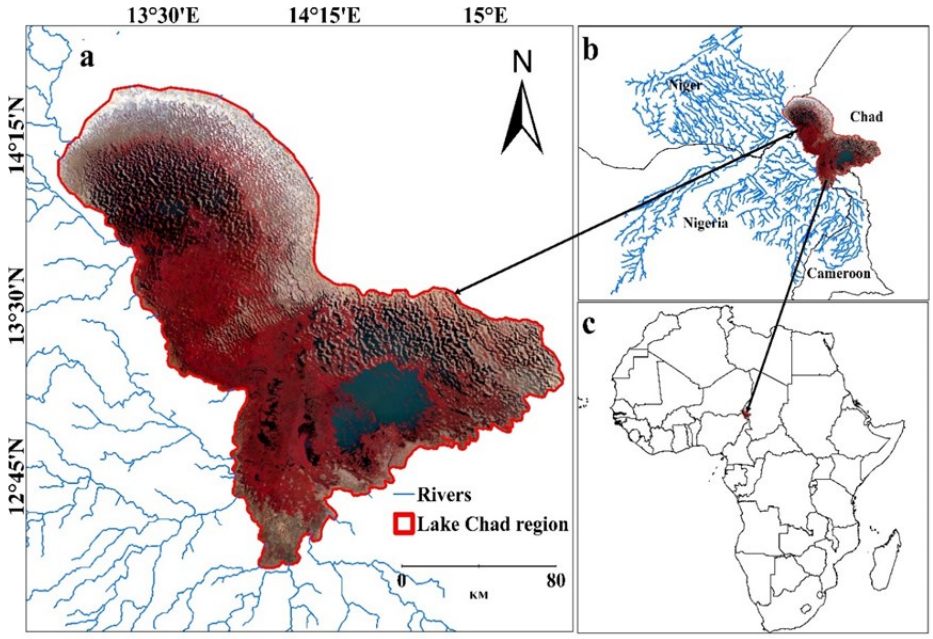

Figure 6.1 The study region, showing (a) the extent of the Lake Chad region with the major rivers and their tributaries, (b) transboundary location of the Lake Chad region and surrounding countries, (c) position of the Lake Chad region within Africa.

The region is rich in fauna and flora, characterized by many species of fish and migratory birds such as Fulvous Babbler, Marsh Warbler, River Prinia and Wattled Starling. It provides an important resource for most of the rural population, which is

growing very rapidly, because it provides for agricultural and pastoral lifestyles as well as fish farming.

6.3 Materials and methods

I calculated the Tasseled Cap Index (TCT) using Landsat bands as input into the CVA to identify changing pixels. I applied a machine learning random forest (RF) classification algorithm to classify wetlands at each time step. Using the CVA equation, I calculated the magnitude of spectral change among the three TC components. My aim was to identify areas of substantial change in TC response, regardless of the wetland areas' transitions, by focusing only on the magnitude of the change vector while ignoring its direction. I determined the change threshold value using areas with known wetland changes as a reference. I then classified only the potentially changed locations (i.e., high change threshold values) using the RF algorithm, utilizing my reference data. CVA allowed me to identify subtle differences in class reflectance due to high intra-class variability resulting from landscape heterogeneity. By interpreting the CVA magnitude and direction of change, I avoided the accumulated error often associated with class-to-class comparisons between two image dates. I implemented the overall methodology in Google Earth Engine (GEE), a cloud-based geospatial analysis platform that provides access to over two decades of imagery, making it feasible for analyzing landcover across large regions.

6.3.1 Selection of satellite imagery

I used atmospherically and terrain-corrected surface reflectance (SR) data from Landsat 7 Enhanced Thematic Mapper Plus (ETM+) and Landsat 8 Operational

Land Imager (OLI) Level-2 imagery, with a 30 m spatial resolution and a 16-day temporal resolution, accessed via the Google Earth Engine (GEE) platform. I acquired ETM+ data for the period 2000–2013 and OLI data for 2014–2020. To address the spectral differences between the Landsat sensors, I harmonized the ETM+ surface reflectance values to match the OLI range using OLS coefficients (Roy et al., 2016), producing an analysis-ready time series. I created a spatial subset of the region of interest from the spectrally calibrated series. Clouds and shadows were removed using supplementary pixel quality assessment flags.

6.3.2 Reference data

I obtained reference data from the Food and Agriculture Organization (FAO) global dryland assessment (Bastin et al., 2017). These datasets were generated by photointerpretation of images of less than <1 metre resolution. I collected a total of 805 ground sample points for wetland and non-wetland locations in the Lake Chad region. The reference data included wetland (401 points) and non-wetland types grouped into open water (143 points), urban/bare land (152 points), cultivated land (215 points), and grassland (194 points) categories. I randomly divided these points into training (50%) and validation (50%) datasets, ensuring even geographic coverage for classifier input (Chapter 4).

6.3.3 Creation of Image Composite

To achieve higher accuracy for identification and classification of my change landcover, I created a composite image for each year and classified each composite using a Random Forest (RF) classification algorithm. I created a multi-temporal

composite using the mean value from the composite after cloud masking. Several studies have shown that a yearly composite image captures explicit phenological information suitable for wetland mapping (Griffiths et al., 2013; Mahdianpari et al., 2018). I used the selected spectral bands and extracted indices (TCT) as an input variable for each year into the RF classifier. An RF classifier is more robust compared to the Decision Tree (DT) algorithm and easier to execute relative to a Support Vector Machine algorithm (Rodriguez-Galiano et al., 2012). It uses bootstrap aggregating (bagging) to produce an ensemble of decision trees by adopting a random sample from the given training data and finds the best splitting of the nodes by minimizing the correlation between trees (Breiman, 2001). About 400 training points for different landcover types were used to train my classifier. The rest of the sample points were set aside to validate the accuracy of the classification (Liu et al., 2018; Mahdianpari et al., 2018).

6.4 Change Detection Technique

6.4.1 Tasseled cap index

Tasseled Cap Transformation (TCT) was developed as a means of compressing and visualizing data obtained from the Landsat-1 Multispectral Scanner (MSS), with a specific focus on extracting information about agricultural landscapes. The TCT components were selected because they are scene independent and have been proven as highly effective for the interpretation, classification, and analysis of phenomena and processes related to the dynamic changes in land use/cover features (Rahman and Mesev, 2019; Stoyanov, 2022). I performed CVA for wetlands and other landcover areas using the first three TC components derived from the

Landsat images. These components measure brightness, greenness, and wetness, which account for more than 97% of the spectral variability observed in a standard scene (Baker et al., 2007). TC component brightness is a measure of image brightness derived from the responses of all bands except thermal Landsat bands. The greenness component is calculated primarily through differencing near infrared with visible bands. The wetness component is determined by comparing visible and near infrared responses with shortwave infrared responses. The brightness component is an indicator associated with bare soil or bare ground: increase in brightness signifies a shift towards bare soil, whereas a decrease in brightness indicates a shift away from bare soil (Rahman and Mesev, 2019). Greenness is directly related to chlorophyll presence and photosynthetic activity, and hence alterations in the measured greenness can be attributed to increase or decrease in vegetation (Baker et al., 2007; Thakkar et al., 2016; Poortinga et al., 2020). Wetness can be an indicator of vegetation density and soil moisture, and hence decrease in wetness indicates declining vegetation or soil moisture (Xu, 2006; Poortinga et al., 2020).

6.4.2 Change Vector Analysis

Change vector analysis (CVA) assesses the magnitude and direction of change between different dates within spectral space. Fundamentally, it applies a variation of the Pythagorean theorem to calculate the Euclidean distance between the digital values of a given pixel at Time 1 (T1) and that same pixel at Time 2 (T2). This Euclidean distance represents the magnitude of spectral change that occurred at that pixel location, while the direction of the change vector provides information

about the nature of the change (Rahman and Mesev, 2019). CVA offers flexibility in that it can be applied to diverse multispectral datasets enabling radiometric change detection useful for monitoring a variety of landscape processes and dynamics over time (Singh and Talwar, 2014). The CVA was conducted by computing the change vector (CV) between vectors **H** and **Q at dates t1, t2** given by **H =** (h_1, h_2, ….., h_n) and **Q** = (q_1, q_2, ..., q_n), respectively, and n is the number of bands, so that a change vector is defined as:

$$\Delta\mathbf{CV} = \mathbf{H} - \mathbf{Q} = \begin{pmatrix} h_1 & -q_1 \\ h_2 & -q_2 \\ h_3 & -q_3 \\ h_n & -q_n \end{pmatrix} \qquad \text{Equation 6.1}$$

The CVA method for magnitude was applied to three TC components using equation 6.2:

$$|\mathrm{M}| = \sqrt{(a_2 - a_1)^2 + (b_2 - b_1)^2 + (c_2 - c_1)^2} \qquad \text{Equation 6.2}$$

where $|\mathrm{M}|$ denotes the total changes between the vector of the three-components a, b and c corresponding to TC brightness, greenness, and wetness respectively at two different times.

The greater the $|\mathrm{M}|$ the higher the chances of change illustrated in Figure 6.2a. Magnitude values at or near zero identify areas with little or no change. However, pixels that remain unchanged fall within a certain range around the origin due to factors such as noise and imperfect normalization. This noise is removed by applying a threshold to the magnitude. A decision on whether a change has occurred is determined based on whether the change magnitude exceeds a predefined

threshold value. After a pixel is classified as having experienced change, further examination of the change direction is conducted to ascertain the specific type of change that took place. The type of change is often identified using the angle of the vector in two spectral dimensions, or sector codes if more than two spectral dimensions are involved (Figure 6.2b).

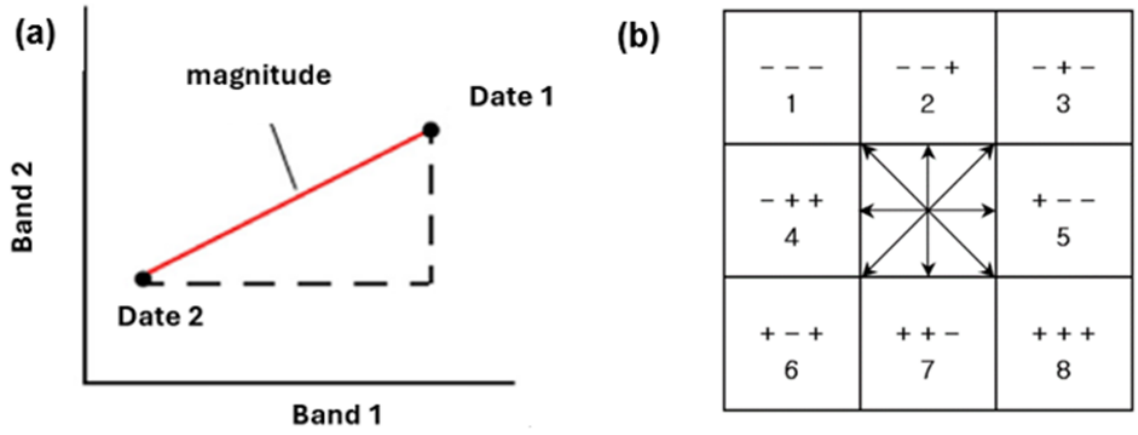

Figure 6.2 Representation of change vector measure (a) change magnitude for two input bands, (b) change direction sector code (after Yoon et al., 2003)

6.4.3 Determination of Optimal Threshold

Determining an appropriate threshold value to differentiate real changes from noise or insignificant fluctuations in the dataset was a critical step in my CVA process. I established the change threshold iteratively, selecting it based on training samples that represented all possible types of changes. My assumption was that these training samples adequately reflected the characteristics of the entire study area. The change detection threshold, therefore, was determined using the remote

sensing analyst's expert knowledge: a threshold leading to the maximum accuracy of change detection within the training samples is considered optimal for this study.

In this process, I first calculated the change magnitude image and selected representative change areas as training samples. A sensitive change magnitude value was then chosen to detect potential change pixels. As the threshold decreased, the number of identified change pixels increased, enhancing accuracy within the training samples. However, it is important to acknowledge that lowering the threshold also increases the likelihood of identifying no-change pixels outside the training samples as change pixels, consequently resulting in higher commission errors. I used the potentially changed sites to create a mask for each image pair, retaining only the changed pixels. The masked pixels (as shown in Table 6.1) were classified, while the remaining study area pixels were treated as unchanged.

6.4.4 Change type classification

The evaluation of change types is essential in change detection. In this study, change pixels are classified using the random forest algorithm. I used the collected reference data for five landcover types to train the model to build up relationships for different landcover categories. All training data were selected through random sampling from areas designated as unchanged to assure that high classification accuracies are achieved. The potentially changed pixels were also classified to identify wetland and non-wetland landcover classes. These classes were then compared to the same classes identified in the initial wetland classification from the unchanged pixels to determine if landcover had changed regarding wetland areas between the two image dates.

6.4.5 Change accuracy

To evaluate the performance of the CVA method, I estimated the accuracy of both "change/no-change" detection and "from-to change" detection levels. The sampling locations were randomly selected to include all possible change types. However, sampling pixels belonging to the no change area cover a larger proportion of the sampling compared to change pixels, due to the latter constituting a larger area of the study location. The error matrix of "change/no-change" detection constructed from 2,500 sample pixels for four change periods is illustrated in Table 6.2. For the "from-to change" detection level, the accuracy assessment was carried out based on the changed pixels belonging to the different landcover types for four change periods. The sampling pixels for the detected change area for each landcover type were randomly selected using the collected reference data. The accuracies and errors of detecting changes from wetland to other landcovers are shown in Table 6.3. Finally, I estimated the total area of wetland changed to different landcovers for each change period.

6.5 Results

6.5.1 CVA change detection

I calculated the change vector and magnitude using Equations 6.1 and 6.2 for four periods: 2000–2005, 2005–2010, 2010–2015, and 2015–2020. The spatial distribution of change vectors varied throughout these periods. Figure 6.3 shows the spatial distribution of change vectors for the TC components, ranging from -0.5 to 0.6. The analysis revealed a severe decline in wetness in the northeast basin of Lake Chad and at the western edge of the southern basin's archipelago between 2000

and 2005 (Figure 6.3a), with moderate changes spread across the north and southern parts of the basin. During 2005–2010, I observed widespread negative changes in wetness and greenness, along with an increase in brightness pixels, indicating expanded bare soil due to wetland decline (Figure 6.3a and b). For 2010–2015, the majority of change pixels showed increased wetness and greenness across the basin. However, for 2015–2020, all three components reversed, confirming drying conditions during this period (Figure 6.3d).

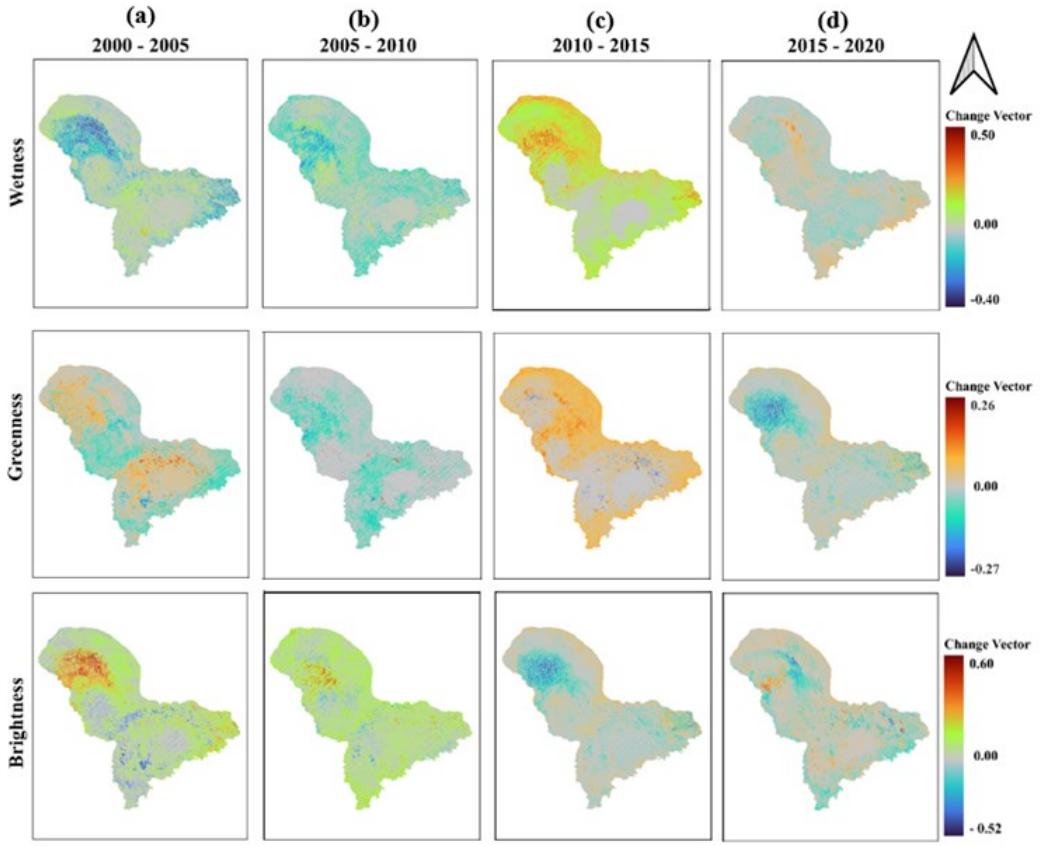

Figure 6.3 Change vector images of change vector analysis (CVA) in four periods: (a) between 2000 and 2005; (b) between 2005 and 2010; (c) between 2010 and 2015, (d) between 2015 and 2020. The legend palette ranges from -0.40 (deep blue) to 0.50 (dark red) for wetness, -0.27 (deep blue) to 0.26 (dark red) for greenness and -0.52 (deep blue) to 0.60 (dark red) for brightness. The negative sign indicates a decrease in pixel value while a positive sign shows an increase in pixel value within the period of change.

I analyzed the change vector magnitude, as shown in Figure 6.4, which illustrates spatial variations in change intensity ranging from 0 to 0.6 across four time intervals. Most change magnitudes were below 0.4. Higher-intensity changes were predominantly concentrated in the northern part of the basin, while moderate changes were dispersed throughout the region. The periods 2000–2005 (Figure 6.4a) and 2010–2015 (Figure 6.4c) exhibited more pixels with high-level changes compared to 2005–2010 and 2015–2020, which showed low-level changes, except for patches in the northern and eastern parts of the lake (Figure 6.4b and 6.4d).

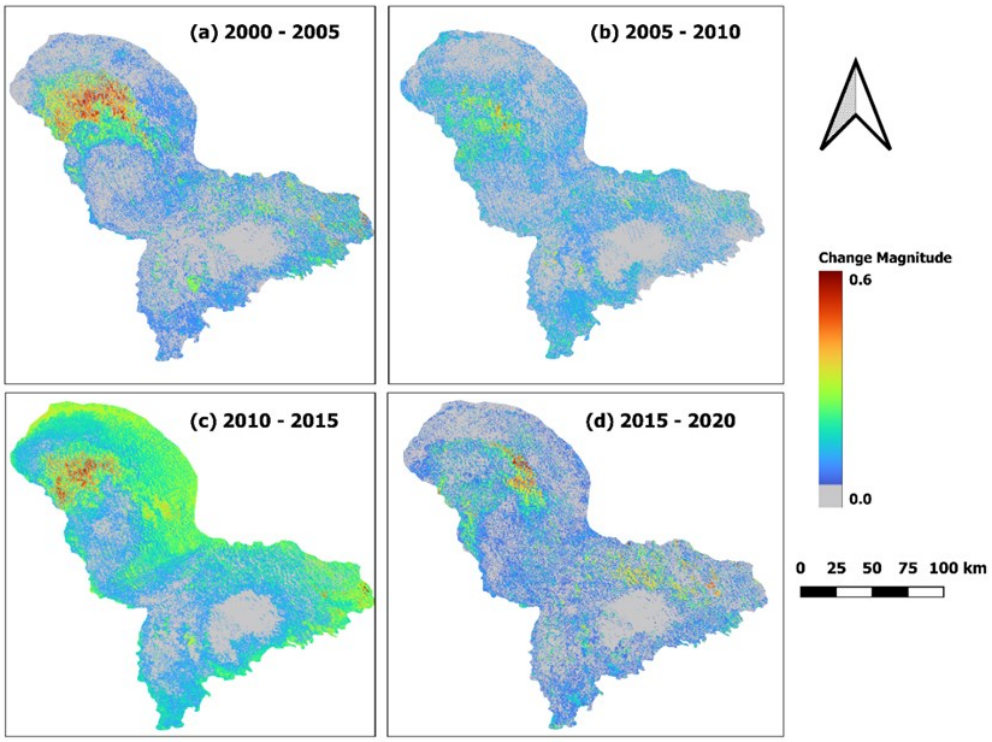

Figure 6.4 Change magnitude images of change vector analysis (CVA) in four periods: (a) between 2000 and 2005, (b) between 2005 and 2010, (c) between 2010 and 2015, (d) between 2015 and 2020. The magnitude value ranges from 0 (grey) to 0.6 (dark red)

I derived the change and no-change areas by thresholding the change magnitude maps. The optimal threshold was selected from five sample areas of known change

locations. For the periods 2000–2005, 2005–2010, and 2015–2020, I used a threshold of 0.16, while for 2010–2015, a threshold of 0.2 was more appropriate for distinguishing change/no-change areas. These thresholds captured 98% of the known change areas, which were also identified using visual interpretation of raw images.

Figure 6.6 illustrates the spatial pattern of changed pixels by applying the cut off thresholds. Most of the pixels are masked out as unchanged for all periods (77% - 90%) (Figure 6.7). The highest amount of changed pixels occurred in 2010 – 2015 as shown in Figure 6.6c, covering about 576 km^2 (Table 6.1), while the least masked change area was found in 2015 – 2020 (191 km^2, Table 6.1) corresponding to only about 7% of the total area. The threshold for 2000 – 2005 retained the largest proportion of the initial changed pixels (82%) as observed from the pixel counts and estimated area (Table 6.1), while about 50% – 60% of initial potential change pixels are detected in other periods by the threshold.

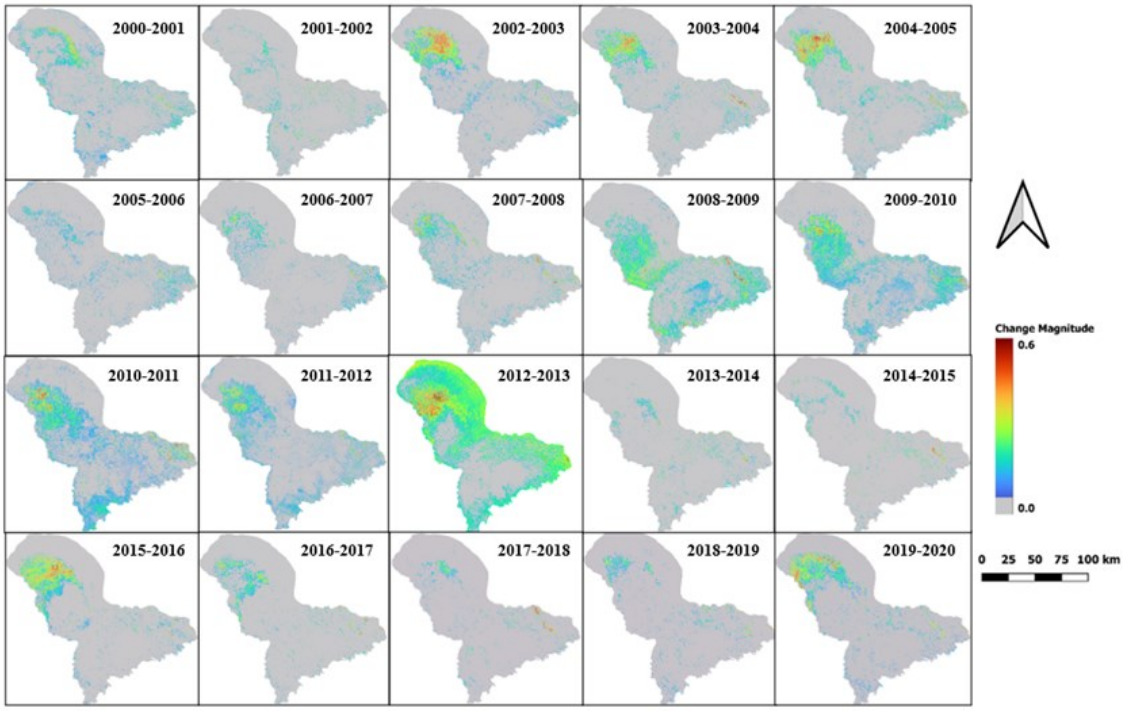

Figure 6.5 Time series change vector magnitude for yearly changes from 2000 to 2020.

Table 6.1 Estimate of mask change area using the suitable threshold for four change periods

Change period	Total change pixel count	Change pixel area (km^2)	Threshold pixel count	Threshold change area (km^2)
2000 - 2005	3805111	342.46	3128209	281.53
2005 - 2010	4514524	406.31	2193038	197.38
2010 - 2015	10023724	902.14	6400843	576.07
2015 - 2020	4102177	369.19	2122727	191.05

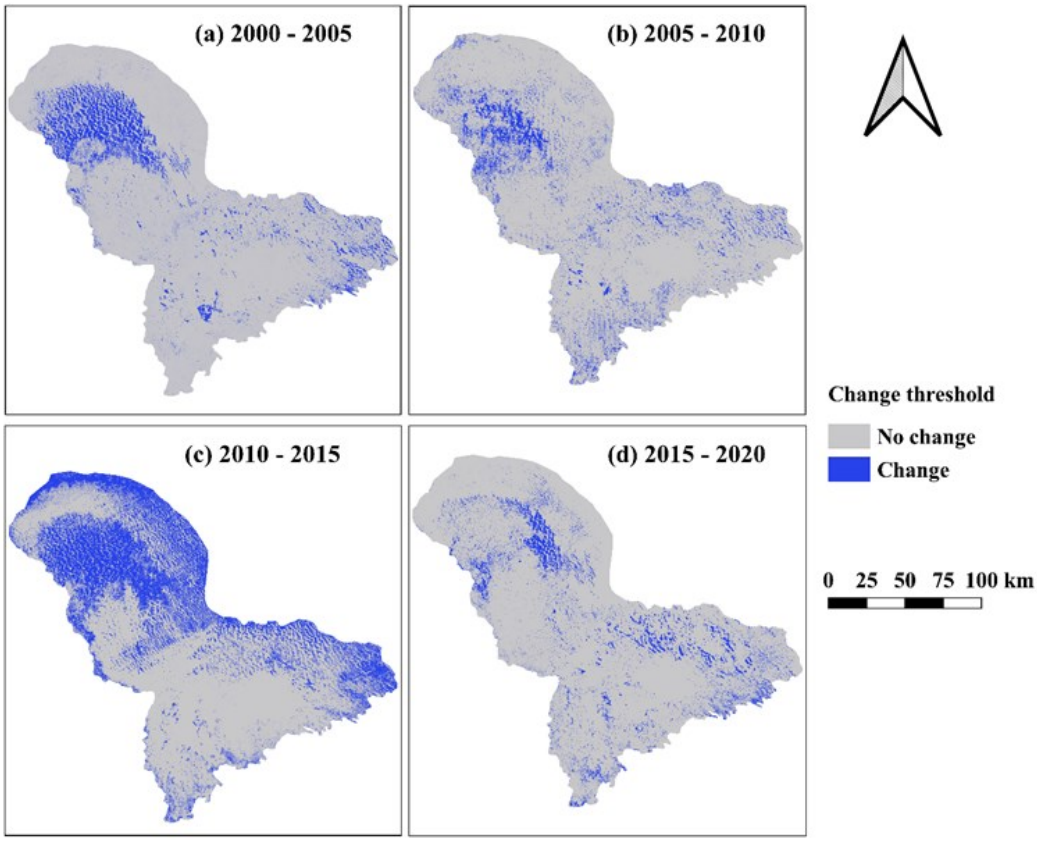

Figure 6.6 Change magnitude threshold image in four periods: (a) between 2000 and 2005, (b) between 2005 and 2010, (c) between 2010 and 2015, (d) between 2015 and 2020.

6.5.2 Accuracy assessment

The overall accuracies for both “change/no-change” detection and “from-to change” detection levels were high, as observed in Table 6.2 and Table 6.3, ranging from 93.11 to 97.88%. The change/no change for the period of 2010 – 2015 had a lower accuracy as compared to other periods largely due to large number of unchanged pixels (14.93%) wrongly identified as changed. The fewest errors were obtained in the 2005 – 2010 change classification, which means the change/ no change pixels were well distinguished with the highest accuracy (97.8%) (Table 6.2). In 2000 – 2005 and 2015 – 2020 a significant number of changed pixels were labelled as

unchanged resulting in higher omission error (Table 6.2). For assessment of changes from wetland to other landcovers, the highest confusion occurs in classifying change pixels between wetland versus open water and wetland versus forest vegetation for all four change periods (Table 6.3).

Table 6.2 Error matrix for "change/no change" from 2000 - 2020 at five-year interval. The omission error refers to the percentage of reference wetland change sites that were left out. Commission error refers to percentage of reference site change sites incorrectly classified as wetland change

Reference change		**2000 - 2005**			
		Change pixels	No Change pixel	Sum	Commission error
Classified change	Change Pixels	458	42	500	8.40%
	No Change Pixels	57	1943	2000	2.85%
	Sum	515	1985	2500	
	Omission Error	11.06%	1.60%		
	Overall Accuracy	96.29%			
		2005 - 2010			
	Change Pixels	415	35	450	7.71%
	No Change Pixels	18	2032	2050	0.87%
	Sum	433	1985	2500	
	Omission Error	4.15%	1.70%		
	Overall Accuracy	97.88%			
		2010 - 2015			
	Change Pixels	368	32	400	8.00%
	No Change Pixels	46	2054	2100	2.22%
	Sum	414	2086	2500	
	Omission Error	11.11%	1.53%		
	Overall Accuracy	96.88%			
2015 - 2020					
	Change Pixels	368	32	400	8.00%
	No Change Pixels	46	2054	2100	2.22%
	Sum	414	2086	2500	
	Omission Error	11.11%	1.53%		
	Overall Accuracy	96.88%			

In 2010 – 2015 and 2015 – 2020 the accuracy of mapping changes between wetland and cultivated lands were much lower than observed in other change periods with both commission and omission error greater than 8%. The smallest error was obtained with classifying changes from wetland to bare land where a high accuracy level of 95% -100% for all periods was achieved (Table 6.3). This was achieved because of the spectral distinction between wetland and bare land features.

Table 6.3 The accuracy assessment of "from-to" change detection for four change periods. The omission error refers to the percentage of reference wetland change sites that were left out. Commission error refers to percentage of reference site change sites incorrectly classified as wetland change.

Change period	**Errors %**	Wetland					**Overall accuracy (%)**
		Open water	Forest	Cultivated Land	Grassland	Bare Land	
2000 - 2005	Omission	14.81	10.25	4.79	6.08	0	95.41
	Commission	7.84	8.05	2.29	0	0	
2005 - 2010	Omission	8.16	6.45	4.51	3.43	0	96.27
	Commission	7.38	5.35	0	2.04	0	
2010 - 2015	Omission	7.57	9.25	9.05	4.04	3.03	93.11
	Commission	9.09	14.76	11.88	3.45	2.08	
2015 - 2020	Omission	2.08	5.45	9.25	5.09	2.38	94.48
	Commission	19.15	6.11	8.25	1.33	4.11	

6.5.3 Evaluation of wetland change

Using the high accuracy classified change, I estimated the area of wetland changes compared to other landcovers (Table 6.4). The overall result shows a net loss of wetland in all four periods. The highest wetland decline was estimated between 2000

– 2005 with a net loss of 277 km^2 (±12 km^2) converted to different landcover types. For this period, about 112 km^2 (±11 km^2) and 42 km^2 (±7 km^2) area of wetland was converted into forest, and open water (Table 6.4). However, there are patches of wetland expansion during the period especially around the middle barrier of the basin. High wetland loss of 116 km^2 (± 6 km^2) was also observed during the period of 2005 – 2010, where a large area of wetland (47 km^2) was converted to forest vegetation. The lowest wetland decline occurred during 2010 – 2015 which accounts for a total loss of 77 km^2 (±5 km^2).

Table 6.4 Estimation of wetland change area for four change periods. The negative value indicates the area of wetland loss (km^2) due to conversion to a given landcover type while the positive value indicates area of wetland gain during the change period interval.

Change period	Wetland net change				
	Open water	Forest	Cultivated Land	Grassland	Bare Land
2000-2005	-41.72	-111.99	-11.45	-35.52	-31.45
2005-2010	-15.49	-47.44	-14.43	-11.55	-22.69
2010-2015	-34.96	23.37	-27.84	0	-1.81
2015-2020	12.45	-30.35	-52.12	-28.33	12.71

6.6 Discussion

Lake Chad is an endorheic wetland ecosystem, where the source of water is mainly from precipitation and surrounding rivers, which means any fluctuation in the annual rainfall affects the basin directly. Several studies have highlighted the long-term effect of climatic changes which result in the variation of lake extent and water level

in the region (Lemoalle, 2005; Zhao et al., 2009; Lemoalle et al., 2012; Policelli et al., 2018; Hussaini et al., 2020). Data about the variability of mean annual precipitation obtained for my study periods from Climate Hazards Group InfraRed Precipitation (CHIRP) shows strong connection with wetland changes. Since rainfall is a key factor in the formation and succession of the wetland ecosystem, its dynamic changes have a large impact on the system dynamics. During 2000 – 2005, the mean annual precipitation dropped by about 42 mm from 302 mm to 260 mm (Figure 6.7). The mean annual precipitation further declined by 57 mm between 2005 - 2010 and was the lowest among the study periods, implying that climate variability was one of the causes of wetland change. Concurrently the rate of wetland decline was reduced with the increase in mean annual precipitation during 2010–2015 (reached up to 390 mm).

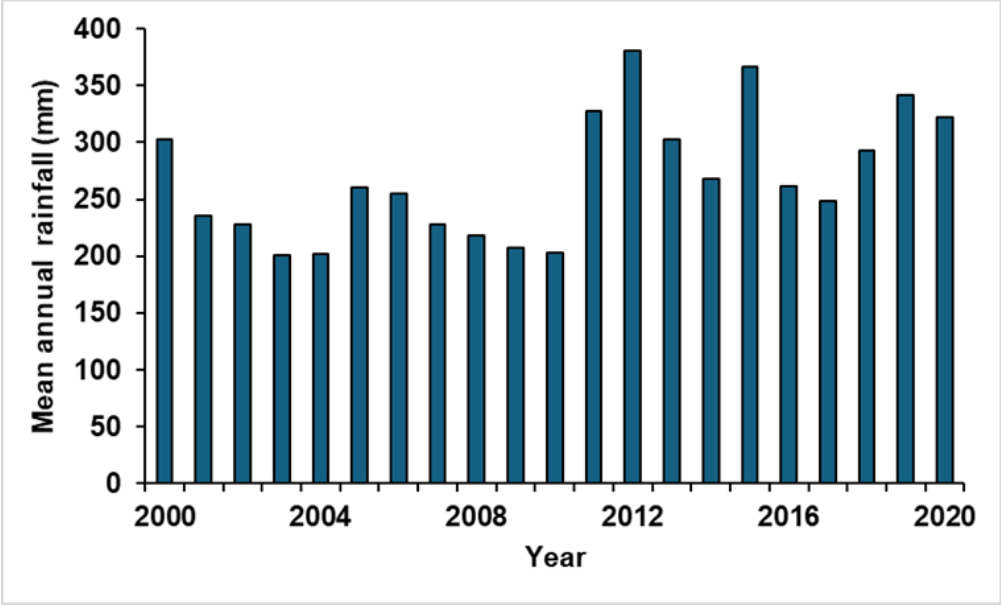

Figure 6.7 The mean annual precipitation of the changed area for 2000 – 2020.

Anthropogenic activities were also an important likely cause of wetland changes in the Lake Chad region. The shrinkage of the lake provides an increasing area of land rich in silt, and wet all year-round, compared to surrounding areas, which has in recent years been a pull factor for immigration into the region (Okpara et al., 2016). Lake Chad has therefore attracted many people who have lost their former livelihoods and have moved to practice fishing, cultivation and herding in the former lakebed (Lemoalle et al., 2012). Population around Lake Chad has soared in recent decades at a rate between 1.5% and 3.7% per year (IAEA, 2017). Increase in population implies an increase in demand for water and land resources for a variety of economic and livelihood activities. Zhu et al. (2019) reported that annual water loss as result of human activities at Lake Chad increased threefold between 1997 to 2013. However, the major change observed in wetlands is towards forest rather than agriculture, indicating that agriculture is not the sole driver of wetland change. This occurs because of receding water levels causing previously flooded areas to become exposed, allowing woody vegetation to establish and gradually convert wetland areas to forest (Lemoalle et al., 2012).

My study has revealed spatial changes in wetland within the Lake Chad area between 2000 and 2020. Wetland declined from 2000 to 2020 with a net loss of 511 km^2 (24%). During the 2000-2020 period much wetland area was changed to forest vegetation which accounts for a net loss of 237 km^2. In comparison with Hussaini et al. (2019) who estimated wetland loss to gallery forest to be about 11% between 2000 to 2015, I found a slightly larger area of wetland converted to forest (14%) (Figure 6.8). I also observed a large area of wetland had been changed to grassland

(125 km^2) and bare soil (82 km^2), and this conversion was found to be greatest between 2005-2010 (Table 6.4). This wetland loss likely occurred due to a decrease in water discharge from the supplying lakes within the Lake Chad basin (Magrin, 2016; Policelli et al., 2018). However, between 2010 – 2015 the CVA result shows that a net area of 136 km^2 (±15 km^2) wetland was restored due to increasing water supply to the basin mostly through rainfall from 2011 (see Figure 6.7). After 2015 the wetland area begins to decline again leading to a loss of about 97 km^2 (±5 km^2) by 2020, as a result of agricultural activities and to forest (Hussaini et al., 2020) with conversion of a significant proportion of wetland area into cultivated fields and grassland.

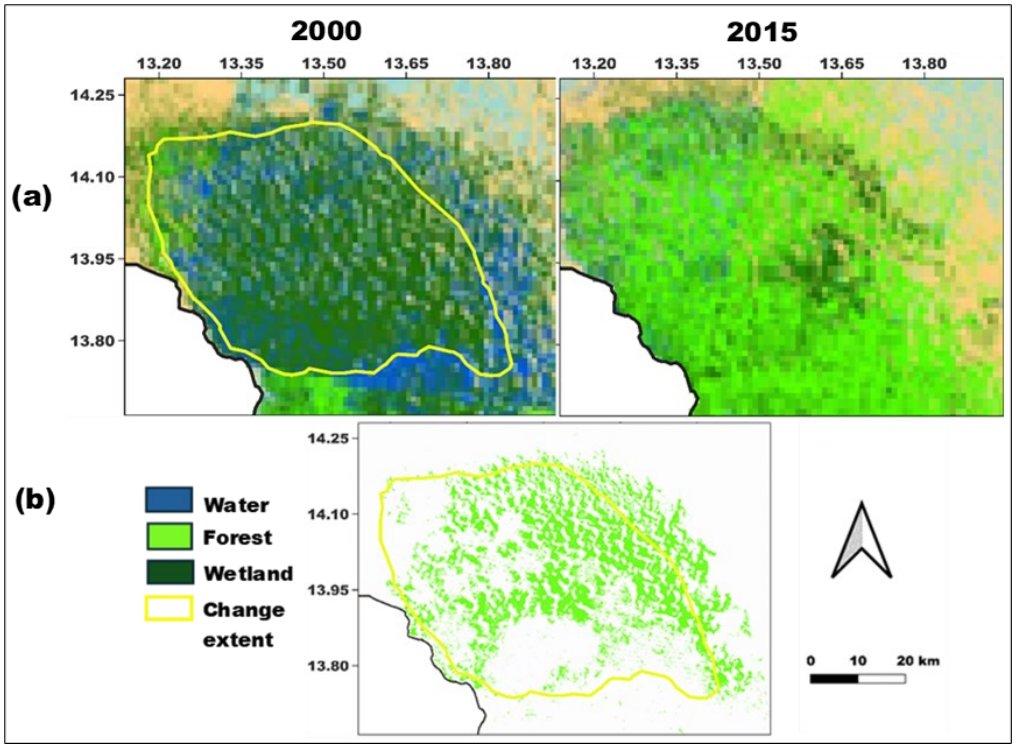

Figure 6.8 Comparison of wetland area conversion to forest from 2000 to 2015 in the northern pool between (a) Hussain et al., 2020 and (b) this study showing change vector classified as forest in 2015. The yellow polygon illustrates the extent of change area from Hussain et al.,2020.

Since many of the studies on changes to the Lake Chad area as described in section 6.1 are based on the analysis of surface water area covering different time spans, they cannot be directly compared to my results. However, it is worth noting that most studies (Birkett, 2000; Alfa et al., 2010; Lemoalle et al., 2012; Okpara et al., 2016; Onamuti et al., 2017; Policelli et al., 2018; Mahamat et al., 2021) show a large decline of the Lake Chad open water area. Hussaini et al., (2020) suggested there was a decline in wetland area and an increase in gallery forest from 2000 - 2015, which is consistent with a net loss of the wetland area during the same period of my research. The results of my study aligns with the findings of Pham-duc et al., (2020) who suggested that the northern pool shows higher variability (see Figure 6.5) with a descending trend of the surface water extent from 2002 reaching its minimum in 2010 before starting to slowly increase again in the following years. The impact of long-term rainfall variability the Lake Chad has been exceptional with an expansions during wet years and severe contractions during droughts due to combined effects of climatic and anthropogenic factors (Buma et al., 2018; Zhu et al., 2019; Gbetkom et al., 2023). However, there is the potential for other African wetlands to be impacted by rainfall dynamics: for example, the Sudd wetland has been significantly impacted by long periods of drought (Zeleke et al., 2024). My results showed that the wetlands in the Lake Chad region continued to decline for all periods, including the phase with increased rainfall, from 2000 to 2020 which means that this wetland has become fragile and susceptible to further changes. The rate of wetland loss to agriculture has also doubled by 2020 (Table 6.4). This confirms that more in-depth understanding and effective management plans are urgently needed in order to conserve and preserve the Lake Chad wetlands especially those around the northern pool of the

lake which seem to be more vulnerable (Lemoalle et al., 2012). The results of this study provide a basis on which the respective organizations such as the Lake Chad Basin Commission (LCBC) can incorporate wetland ecosystem protection in their management plans.

While policies can be implemented to protect these wetlands from changes in land use, findings from this study indicate that this wetland is highly sensitive to changes in precipitation. Therefore, it remains uncertain how this wetland will respond to future climate change. However, with the expectation of precipitation to generally increase by about 5%-15% by 2100 within the region under warmer global temperature scenarios (Schmitt and Simpson, 2018; Adeyeri et al., 2019; Sylvestre et al., 2024), it is likely to positively affect the functioning of this wetland depending on the nature of human interactions and land management. It is also important to note that the rise in lake level can be associated with wetland loss due to complete inundation.

An advantage of the relative change detection technique that I apply here between successive images is that it reduces errors in classification. Accuracy of change detection is therefore improved by 14% compared to previous studies of Lake Chad. However, there remain many challenges associated with detecting long-term changes in Lake Chad wetlands, among them is the seasonal variability of the rainfall that might affect the spectral signal. Another challenge is short-term changes, such as a rainy year followed by a drought year, which can introduce high uncertainty in different areas. To improve the accuracy of the change estimate I recommend long-

term analysis based explicitly on images of above-average rainy years and from the same phenological stage.

6.7 Conclusion

In this study, a change detection approach for monitoring wetland dynamics was developed using Tesseled cap indices and CVA. In this approach, wetness, greenness, and brightness components of wetlands were derived from the Tesseled cap index. Finally, the change magnitude and directions were calculated, which refers to the detailed wetland change information. I further estimated the area of wetland changes to other landcovers during four change periods in the Lake Chad basin. During 2000–2010, a severe wetland decline occurred in the northern pool of the lake, and marginal area of the southern pool of the lake, where the wetland was mostly converted to forest vegetation. Despite a rise in rainfall from 2010 to 2015, the wetland still faced a decline due to inundation from increase in lake levels. This study has presented a novel and up to date quantification of wetland depletion trend that occurred in the Lake Chad area over the past two decades (2000 – 2020). It provides a good estimation of wetland changes by differentiating wetland and other landcover classes using the CVA analysis. It is observed that the highest wetland conversion was associated with forest vegetation (39%) which is dominant in the northern pool, while the smallest wetland conversion was to cultivated land (9%). My study reveals an unexpected outcome of net wetland loss during wetter periods, which contrasts with assumptions from previous literature about wetland recovery during periods of increased rainfall. The wetland change information in this study was based on time-series remote sensing data; the results can offer guidance for

scientific monitoring and sustainable management of wetlands. This approach could be applied to wetland change studies in other areas.

Chapter 7
Discussion and Conclusion

7.1 Section outline

In this Chapter I summarise the project as a whole and discuss how the work contributed to answering the three underlying research questions:

1. What is the current extent of wetland area in southern Nigeria and how is this broken down into different wetland types?

2. What is the current extent of wetland area across Africa, how is this broken down into different wetland types and climate zones, what is its carbon store and potential for GHG forcing under different degradation scenarios, and what is the relationship between population and highly fragmented wetland regions?

3. What is the trend of change in Lake Chad region wetlands (as a regional case study) over the past two decades and can these changes be linked to clear human drivers of change?

The project findings are therefore discussed in the context of these questions and subsequent implications for ecosystem services outcomes and conservation goals. Areas in which the understanding or interpretation of past work has been extended or challenged are also considered. The relevance of the work to the wider international context and some of the project limitations are reflected upon. Finally, overall conclusions and resulting recommendations for wetland management, policy and future research directions are outlined.

7.2 Implication of the research findings

7.2.1 Large-scale wetland mapping at 10m spatial resolution

This research produced the first systematic and comprehensive map of wetlands at high spatial resolution (10 m) first for southern Nigeria and then for the whole of Africa (Chapter 4 and 5), which provides a detailed and up-to-date resource for numerous applications in conservation, wetland management, scientific research, and sustainable exploitation. Sustainable wetland development can help to alleviate poverty, enhance food security, and promote broader sustainable development in Africa (Gardner et al., 2015). Reliable maps of African wetlands are crucial for supporting livelihoods, reducing poverty, and advancing sustainable development (Gardner and Finlayson, 2018). Additionally, the relationship between climate change and wetlands is a key research focus, as African ecosystems are already experiencing significant impacts from climate change, with more expected in the future (Erwin, 2009; Field and Barros, 2014). Wetlands play a vital role in regulating global climate by absorbing and releasing large quantities of carbon, and controlling atmospheric concentrations of greenhouse gases like methane, carbon dioxide, and nitrous oxide, which contribute significantly to global warming (Meng et al., 2016). Maintaining the sustainability of African wetlands is critical for mitigating climate change, and the high-resolution wetland map helps in accurately determining wetland categories, estimating carbon stocks, and assessing greenhouse gas emissions, thereby improving the understanding of wetland-climate interactions. My wetland mapping using improved spatial resolution data captured a significant amount of wetlands missed by existing global maps (Chapter 4, Figure 4.9). Existing wetland mapping products on a global scale, such as the Ramsar site database,

contains only information on wetlands that have been classified as of ‘international importance’ and the Global Lake and Water Database (GLWD) has information that is two decades old and probably incomplete (Gumbricht et al., 2017; Hu, Niu and Chen, 2017; Steinbach et al., 2021). Recent mapping products such as PEATMAP (Xu et al., 2018) and global wetland map (Gumbricht et al., 2017) are typically based on secondary data of varying quality and age with a mix of spatial resolutions. This thesis produced the first regional (Chapter 4) and continental wetland map (Chapter 5) at high spatial resolution (10 m) which provides high quality and detailed information about the location, distribution, and extent of wetlands in Africa. This mapping product could be easily integrated into global ecosystem models, climate models, population models or hydrological models to investigate wetlands at a global scale. The codes used to create this mapping products will be made available online for other users. Analysis of the 10-metre wetland map suggests that in previous global assessments, wetlands in Africa have been underestimated due to coarser resolution investigation, resulting in misclassification and omission of small-scale wetlands. For example, in comparison with the CIFOR global wetland dataset, about 80,400 km^2 of small-scale wetlands in Africa were identified by my study, that were not included by CIFOR. This series of small wetlands contains a significant fraction of stored carbon and could be an important target for conservation. Hopefully, my study paves the way for further studies to assess the impact of human populations around wetland margins, monitor wetland changes over time, and explore the influence of climate change on dynamics of wetlands in Africa.

7.2.2 Wetland patchiness and relationship to human populations

My 10-metre resolution wetland map reveals fragmentation which has significant ecological, hydrological, socio-economic and policy implications. Fragmented wetlands threaten biodiversity by isolating habitats, disrupting hydrological processes essential for flood control and groundwater recharge, and diminishing carbon sequestration capacity, contributing to climate change (Adade et al., 2017; Kundu et al., 2022; Magure et al., 2022). For example, in Chapter 5 I found that wetlands which are currently highly fragmented could potentially emit CO_2 equivalent to 0.6 % of total global annual emissions. They also become more vulnerable to human encroachment from agriculture and urbanization, compromising ecosystem services such as water purification, nutrient cycling and flood mitigation, which local communities rely on. The map produced for my Nigerian study (Chapter 4), with 10 m pixels, captures small patches of wetland < 1 km^2 which were not captured in earlier mapping products. These small patches may be more prone to degradation, and are also susceptible to reduced biodiversity, and isolation, which limits species movement and disrupts vital ecological processes such as migration and nutrient cycling (Kundu et al., 2022). Therefore, stronger land use policies and targeted interventions are required in southern Nigeria to protect these vital ecosystems from further degradation.

The highest rate of wetland loss has been primarily attributed to human activities such as agricultural and urban expansion in several cases (Ballut-Dajud et al., 2022; Kundu et al., 2024; Magure et al., 2022). My continental-scale study (Chapter 5) and the resulting WPFI index shows that highly fragmented wetlands are associated with

large populations. I note that a total of 13,000 km^2 of wetlands (Chapter 5) are currently heavily threatened due to their proximity to large population and about 28,700 km^2 of wetland lies in populated areas that suggest a moderate at risk of human interaction. Therefore, being the first study to highlight regions where fragmented wetlands are highly vulnerable to human activities in Africa, this work provides the basis on which policy makers can plan and prioritize innovative policies to preserve and restore wetland ecosystems in proximity to humans.

7.2.3 Estimation of potential carbon stock and carbon loss/uptake from African wetlands

Carbon (C) sequestration is one of the valuable functions of wetlands which helps in climate regulation (Villa and Bernal, 2018; Zou et al., 2022). About one-third of the global organic soil C pool is thought to be stored in wetlands (Villa and Bernal, 2018). The lack of high-resolution data hinders the estimates of the total carbon stored by these wetlands and estimates of the potential for net carbon uptake or loss from African wetlands at a continental scale. Much wetland carbon is below ground, yet potentially fragile and susceptible to rapid loss with wetland degradation (Poulter et al., 2021). Most of the existing estimations are at local level for countries and usually for single categories of wetland (Ouyang and Lee, 2020; Raw et al., 2023). The analysis of carbon storage in African wetlands in this study yielded an important finding that four wetland types of Africa (peatlands, mangroves, swamps and marshes) contain 54 ±11 Gt of carbon which is around 5% to 9% of wetland soil carbon stored globally (520 - 710 Gt C) (Poulter et al., 2021), and about twice that of European wetlands (12-31 Gt) (Malak et al., 2021). It is also revealed that these

wetlands under drained conditions could release up to 260Mt C yr^{-1} (936Mt CO_2 equivalents yr^{-1}) which is equivalent to 2.4% of global net annual CO_2 emissions. These results highlight the importance of protecting African wetlands and provide data critical for both improving land-surface climate models and for wetland conservation.

7.2.4 Wetland changes in the Lake Chad region

The most important factor in the formation and succession of the wetland ecosystem is water, and changes to the water cycle can have a great impact on fragile wetland ecosystems. The Lake Chad region has been reported to experience long-term changes in surface water area (Chapter 6). However, earlier studies did not accurately account for changes in wetland extent in the region. Referring to the fragmentation index in Chapter 5, wetlands within the extreme northern and southern pool areas of Lake Chad fall under the category of high fragmentation.

The results in Chapter 6 showed that there was a net loss of wetland area across the first two decades (2000 – 2020) of the twentieth century, with the most significant change occurring in the northern pool of the lake. Analysis showed that the wetland loss was most likely driven by reduced rainfall and an increased demand for agriculture. The continuous decrease in the wetland area implies that the ongoing management and restoration policy in the region might not be effective. Thus, even with increased future rainfall under climate change, wetlands in the area may be degraded. As noted by Okonkwo and Demoz (2014) and Zieba et al. (2017), the Lake Chad Basin Commission, which oversees policy and coordinates management

plans for this ecosystem, is facing challenges due to limited human, material, and financial resources required for monitoring and assessing the resources and dynamics of the ecosystem. The results of this study can be used as a key reference for scientific monitoring, rational planning of wetland restoration, and development of sustainable management of wetland.

7.3 Research content and methods

In this study, I developed a technique using freely available global satellite datasets from Sentinel-1 SAR and Sentinel-2 optical imagery, by integrating optical indices and SAR polarimetric features from different seasons using a Random Forest classification algorithm. The results from regional wetland mapping in Chapter 4 provide strong evidence of the performance of the technique with about 90% accuracy. The technique in this study identifies small patches of wetland < 1 km^2 which may not have been mapped in earlier mapping products (CIFOR, 2016; Lehner and Döll, 2004; Li et al., 2022). I used different image compositing approaches for different climatic regions as explained in Chapter 3, because similar wetland types may appear differently under different climate settings (Guo et al., 2017).

In the present study, I utilized a Random Forest (RF) classification algorithm for delineating and classifying the wetland type. Compared to previous studies, the classification algorithm used in my study is more universal and robust than other classification algorithms in terms of wetland type, producing a higher accuracy result (Mahdianpari et al., 2018; Potic and Potic, 2017). The RF algorithm is particularly

suitable for handling variation within land cover classes and reducing noise in the data. It does not require prior knowledge of the data distribution compared to other classifiers. With further resources, other accuracy coefficients such as AUROC, TSS, DeLong Test could be used to further test my classification.

To analyze the relationship between wetland patchiness and population I choose to use gridded population data to ease comparison with wetland fragmentation. This approach has the advantage of using a relatively uniform dataset instead of relying on population indicators (like distances to village, city, road) that vary from country to country. However, if a novel set of meaningful population indicator datasets becomes available for comparison it should be used to better highlight the population activities that are drivers of change in wetlands.

Finally in Chapter 6, I use Change Vector Analysis (CVA) approaches to map the types and quantify long-term dynamic changes of the wetlands of the Lake Chad area. CVA has been found to have several advantages over other change detection applications (Karnieli et al., 2014). CVA can measure change in more than two spectral bands, giving it an advantage when mapping rapidly changing and highly diverse wetlands (Gemechu et al., 2022; Klemas, 2013). The CVA approach in this study produces more accurate and reliable change results when compared to other methods such as post classification comparisons as used by previous studies (e.g., Babamaaji and Lee, 2014; Hussaini et al., 2020; Mahamat et al., 2021). My results highlighted the high potential of the CVA to detect wetland dynamics and trends over decades.

7.4 Limitations of the work

7.4.1 Inconsistency of wetland definition

This project focused on high-resolution mapping and assessment of wetlands in Africa and paves the way for global mapping and change detection in the future. However, for certain aspects of this work there are limitations which should be addressed in any future analysis. A key limitation is the absence of a single formal definition of wetland that has been accepted worldwide. Also, there are different classification schemes used to categorize wetland type both at local, country and global scales. Therefore, it is difficult to extract and compare different wetland data products across the region due to non-uniform definitions. Clear and consistent definitions will be very important for ground truth datasets - there was a lack of ground truth data for some wetlands in drier parts of Africa particularly in North Africa; more work is required on the ground to map peatlands and seasonal wetland types in these regions to aid the machine learning classifications. In addition, wetland classification is often based mainly on soil composition resulting in high confusion among wetland classes from EO data. To address this, I used derived indices from EO data that categorize wetland classes in terms of vegetation type, moisture, as well soil composition as observable from satellite imagery.

7.4.2 Exploring the impact of human population at global scale

Inclusion of human-induced population impact mapping which combines the wetland map and population data could be used to indicate areas where detailed data on wetland condition need be collected for better conservation and restoration programmes. My approach could not define the actual drivers of wetland degradation

across Chapters 4-6. It is possible that high resolution remote sensing tools could be developed in the future that allow human impact attribution acquired through other sources of information to be improved for wetlands so that drivers of change can be better understood. This will be important not just for Africa, but for understanding threats to wetlands globally. Upcoming satellite missions such as CHIME (Copernicus Hyperspectral Imaging Mission for the Environment) will complement Copernicus Sentinel-2 for land-cover mapping, and ROSE-L SAR with its longer wavelength L-band will be able to penetrate the canopy and aims to support existing Copernicus C-band SAR systems which will allow for improved wetland mapping in the near future.

7.4.3 Misclassification of wetland types

Despite the high accuracy obtained from the classification model, there are some limitations in the training dataset that may lead to bias in the model. Training data from existing wetland locations can be influenced by ambiguities in wetland class definitions and landscape variation. The fundamental assumption that training data accurately represent a specific class may not always be entirely correct, as individual training points could belong to different wetland classes. To address this, I characterized the training data based on the class composition and internal variability. I then identified the possible outliers from the distribution of each wetland class and filtered them out from the training data. The inequality in the size of my training data for the wetland classes may bias classification accuracy, because the model is sensitive to wetland class with larger numbers of training points. This produces higher accuracy than for wetland classes with small amounts of training

data. Due to the complicated temporal dynamics and spatial and spectral heterogeneity of wetlands, developing classification systems remains a challenging task using remote sensing. The complexity in the differences in remote sensing signals between some wetland classes makes it difficult to discriminate some wetland classes across large geographical ranges. Different wetland types may portray similar signals thereby making them more difficult to discriminate. For example, the distinction between swamp and peat swamp wetlands, especially within the Congo region, was not adequately addressed due to their complex reflectance and given definition. To address this challenge, I mapped the different wetland classes according to climate region in Africa, where wetlands are distinguished based on similar phenological and geographic setting of each climate zone to reduce the bias of class confusion (Chapter 5). Another limitation is the inability to distinguish between bog and fen peatlands due to lack of specific peatland control points. This increases uncertainty in accurately differentiating peatlands from other wetland types. Improving the quality and accuracy of training data through enhanced data collection would likely help mitigate this issue in future studies

7.4.4 Limitation of data sources

Another limitation is related to the production of cloud free seasonal composites in the TWD and TW region of Africa. It is impossible to collect sufficient cloud-free optical data (Sentinel-2 images) to generate full continental coverage, especially for large-scale mapping due to the prevailing cloudy and rainy weather conditions in regions characterized by high rainfall in this study. However, I produced composites

from monthly data with less cloud cover for each season to capture explicit phenological information appropriate for wetland mapping.

The estimation of wetland carbon stock and carbon flux is far from complete due to limited availability of high-quality information on the carbon distribution within African wetlands. My carbon flux estimation includes only three wetland classes due to data constraints - therefore the potential impact of African wetland drainage to the global carbon flux is not fully represented. More work is needed for detailed assessment of the spatial distribution of carbon flux measurements from African wetlands of different types and in different climate zones. In addition, comprehensive data about the current water-table level for different wetland types for different climate zones is needed to improve the estimate of the carbon flux at various water-table conditions. It may be that remote sensing products can support such an assessment in the future (e.g. Burdun et al., 2020).

7.5 Future work

7.5.1 Improving the quality of the data source

Detailed wetland maps at high resolution are important for conservation and climate modelling. However, high resolution, up-to-date data on wetlands at global scales are not available, and good coverage only exists in some well-studied smaller regions. In this thesis I developed a process which could now be rolled out globally to produce a high-resolution global wetland map. There will need to be a concerted effort to gather ground truth data to support the development of such a product. But the fact that this now seems achievable is because of the work conducted in this

thesis. Africa is one of the least developed regions in the world and wetland datasets are often fragmented and inconsistent from one country to another within the continent. Using a standardized methodology developed in this study to compare wetland data across regions or countries makes it possible to collect and verify large amounts of wetland ground control data in Africa and this relatively simple methodology could be applicable to other regions. However, in future studies, more detailed field surveys, new remote sensing data and new classification algorithms will be necessary. In addition, although I used the most recent and highest quality datasets available, ongoing efforts to improve the quality of gridded population data, carbon stock databases, carbon flux datasets and climate change scenarios will further refine future analysis of wetland fragmentation, and estimates of carbon loss from wetlands. It may also be possible to include topographic indices into machine learning for the purpose of classifying wetland type (such as fen and bog peatlands) and forecasting the impacts of drainage on carbon release and wetland degradation.

7.5.2 Dynamic wetland mapping using advanced techniques

It might be possible to automate the algorithms presented here so that a high resolution African and global wetland map and change map can be updated automatically as Sentinel data are collected and updated continuously. This can be achieved by creating a conditional statement to update image collection for a particular time and date to create a seasonal composite. The mapping accuracy can improve dynamically by collecting more ground control points continuously using automatic data entry into a database system to generate more training point and evaluate the accuracy. With increasing availability of high-resolution imagery, such

as Sentinel datasets, global maps that distinguish seasonal/decadal wetland changes from more 'permanent' wetland loss and continuous monitoring of wetland at global scale can be achieved by automation via the Google Earth Engine cloud computing platform. Automated studies to understand of the impacts of wetland restoration programmes would also be welcome. The remote sensing tool developed in this study could also be used to evaluate global wetland protection schemes or treaties, to see if they are successful or not.

7.6 Conclusion

I produced a detailed wetland map both at regional (Chapter 4) and continental (Chapter 5) level using high spatial resolution data (10 m) supported by ground control data that I compiled from a range of sources. The total estimate of wetlands in Africa (947,750 km^2) is larger than that of the coarser global wetland dataset by CIFOR (859,278 km^2) and that of GLWD (934,481 km^2) excluding open water bodies. At regional level, I estimated that the wetlands of southern Nigeria cover a total area of 29,924 km^2 which is less than the estimate by CIFOR (31,829 km^2) but larger than GLWD (24,408 km^2) (Chapter 4). Larger patches of wetland are found along the coastal areas while smaller fragments are mostly located around urban areas suggesting a role for anthropogenic fragmentation of wetlands in southern Nigeria. I identified nine regions with a WFPI value indicating highly fragmented grid cells related to large population size. A total of 3021 km^2 of wetlands are currently heavily threatened by human activity within Africa (WFPI of 0.7 to 1). The carbon stock estimate indicates that African wetland contains about 54 Gt of carbon which is around 5% to 9% of wetland soil carbon stored globally. Drained peatland,

mangrove and marsh in Africa are capable of emitting 260Mt C yr^{-1} (936Mt CO_2-e yr^{-1}) which is equivalent to 2.4% of global net annual CO_2 emissions. The long-term changes in wetlands around Lake Chad were closely linked to the fluctuation of the water level driven by multi-annual climate phases and intensive human activities. The results of this study indicate a net loss of Lake Chad wetlands across all examined five year periods from 2000-2020, including the wettest period when it was anticipated (based on earlier literature) that wetland area would increase. Thus under future climate change with predicted increased rainfall for the region, Lake Chad wetlands are not guaranteed to increase in extent, particularly given that population pressures are growing, with the northern region of the Lake under the greatest pressure.

Reflecting on the sustainable conservation, management, and development of wetlands going forward, there is still a need for historical period classification and dynamic monitoring of wetlands using multi-source remote sensing data to assess the impacts of anthropogenic activities and climate change on wetland dynamics in Africa. The overall approach developed could be expanded to produce a global wetland map at high resolution and for continuous monitoring of changes in wetlands at global scale.

List of References

Acharya, T.D., Subedi, A., Yang, I.T. and Lee, D.H. 2017. Combining Water Indices for Water and Background Threshold in Landsat Image. *Proceedings*. **2**(3), pp.143.

Acreman, M. and Bullock, a. 2003. The role of wetlands in the hydrological cycle. *Hydrology and Earth System Sciences*. **7**(3), pp.358–389.

Acreman, M. and Holden, J. 2013. How wetlands affect floods. *Wetlands*. **33**(5), pp.773–786.

Adame, M.F., Santini, N.S., Tovilla, C., Vázquez-Lule, A., Castro, L. and Guevara, M. 2015. Carbon stocks and soil sequestration rates of tropical riverine wetlands. *Biogeosciences*. **12**(12), pp.3805–3818.

Adekanmbi, O.H. and Ogundipe, O. 2009. Mangrove biodiversity in the restoration and sustainability of the Nigerian natural environment. *Journal of Ecology and Natural Environment*. **1**(3), pp.064–072.

Adekola, O., Whanda, S. and Ogwu, F. 2012. Assessment of policies and legislation that affect management of Wetlands in Nigeria. *Wetlands*. **32**(4), pp.665–677.

Adeyeri, O.E., Lawin, A.E., Laux, P., Ishola, K.A. and Ige, S.O. 2019. Analysis of climate extreme indices over the Komadugu-Yobe basin, Lake Chad region: Past and future occurrences. *Weather and Climate Extremes*. **23**, pp. 194.

Al-Nasrawi, A.K.M., Fuentes, I. and Al-Shammari, D. 2021. Changes in Mesopotamian Wetlands: Investigations Using Diverse Remote Sensing Datasets. *Wetlands*. **41**(7), pp.1–17.

Alfa, N., Adeofun, C. and Ologunorisa, E. 2010. Assessment of changes in Aerial Extent of Lake Chad using Satellite Remote Sensing Data. *Journal of Applied Sciences and Environmental Management*. **12**(1), pp.101–107.

Alshammari, L., Large, D.J., Boyd, D.S., Sowter, A., Anderson, R., Andersen, R. and Marsh, S. 2018. Long-term peatland condition assessment via surface motion monitoring using the ISBAS DInSAR technique over the Flow Country,

Scotland. *Remote Sensing*. **10**(7), pp.1103.

Amani, M., Mahdavi, S., Afshar, M., Brisco, B., Huang, W., Mirzadeh, S.M.J., White, L., Banks, S., Montgomery, J. and Hopkinson, C. 2019. Canadian wetland inventory using Google Earth Engine: The first map and preliminary results. *Remote Sensing*. **11**(7), pp.1–20.

Amani, M., Poncos, V., Brisco, B., Foroughnia, F., Delancey, E.R. and Ranjbar, S. 2021. Insar coherence analysis for wetlands in alberta, canada using time-series sentinel-1 data. *Remote Sensing*. **13**(16), pp.3315.

Amani, M., Salehi, B., Mahdavi, S. and Brisco, B. 2018. Spectral analysis of wetlands using multi-source optical satellite imagery. *ISPRS Journal of Photogrammetry and Remote Sensing*. **144**, pp.119–136.

Amani, M., Salehi, B., Mahdavi, S., Granger, J. and Brisco, B. 2017. Evaluation of multi-temporal landsat 8 data for wetland classification in Newfoundland, Canada. *International Geoscience and Remote Sensing Symposium (IGARSS)*., pp.6229–6231.

Amler, E., Schmidt, M. and Menz, G. 2015. Definitions and mapping of East African Wetlands: A Review. *Remote Sensing*. **7**(5), pp.5256–5282.

Anderson, K., Bennie, J.J., Milton, E.J., Hughes, P.D.M., Lindsay, R. and Meade, R. 2010. Combining LiDAR and IKONOS Data for Eco-Hydrological Classification of an Ombrotrophic Peatland. *Journal of Environmental Quality*. **39**(1), pp.260–273.

Anule, P. and Ujoh, F. 2017. Geospatial analysis of wetlands degradation in Makurdi, Nigeria. *International Archives of the Photogrammetry, Remote Sensing and Spatial Information Sciences - ISPRS Archives*. **42**(2), pp.1075–1081.

Ardha Aryaguna, P. and Danoedoro, P. 2016. Comparison Effectiveness of Pixel Based Classification and Object Based Classification Using High Resolution Image In Floristic Composition Mapping (Study Case: Gunung Tidar Magelang City). *IOP Conference Series: Earth and Environmental Science*. **47**, pp.12042.

Ashraf, M. and Nawaz, R. 2015. A Comparison of Change Detection Analyses Using Different Band Algebras for Baraila Wetland with Nasa's Multi-Temporal Landsat Dataset. *Journal of Geographic Information System*. **07**(01), pp.1–19.

Van Asselen, S., Verburg, P.H., Vermaat, J.E. and Janse, J.H. 2013. Drivers of wetland conversion: A global meta-analysis. *PLoS ONE*. **8**(11), pp.1–13.

Ayanlade, A. 2014. Remote Sensing of Environmental Change in the Niger Delta , Nigeria. *Thesis.* pp.142-145.

Ayanlade, A. and Proske, U. 2016. Assessing wetland degradation and loss of ecosystem services in the Niger Delta, Nigeria. *Marine and Freshwater Research*. **67**(6), pp.828–836.

Babamaaji, R.A. and Lee, J. 2014. Land use/land cover classification of the vicinity of Lake Chad using NigeriaSat-1 and Landsat data. *Environmental Earth Sciences*. **71**(10), pp.4309–4317.

Baghdadi, N., Bernier, M., Gauthier, R. and Neeson, I. 2001. Evaluation of C-band SAR data for wetlands mapping. *International Journal of Remote Sensing*. **22**(1), pp.71–88.

Baird, A.J., Low, R., Young, D., Swindles, G.T., Lopez, O.R. and Page, S. 2017. High permeability explains the vulnerability of the carbon store in drained tropical peatlands. *Geophysical Research Letters*. **44**(3), pp.1333–1339.

Baker, C., Lawrence, R.L., Montagne, C. and Patten, D. 2007. Change detection of wetland ecosystems using Landsat imagery and change vector analysis. *Wetlands*. **27**(3), pp.610–619.

Ballut-Dajud, G.A., Herazo, L.C.S., Fernández-Lambert, G., Marín-Muñiz, J.L., Méndez, M.C.L. and Betanzo-Torres, E.A. 2022. Factors Affecting Wetland Loss: A Review. *Land*. **11**(3), pp.434.

Bassi, N., Kumar, M.D., Sharma, A. and Pardha-Saradhi, P. 2014. Status of wetlands in India: A review of extent, ecosystem benefits, threats and management strategies. *Journal of Hydrology: Regional Studies*. **2**, pp.1–19.

Bastin, J.-F., Berrahmouni, N., Grainger, A., Maniatis, D., Mollicone, D., Moore, R.,

Patriarca, C., Picard, N., Sparrow, B., Abraham, E.M., Aloui, K., Atesoglu, A.., Attore, F., Bassüllü, Ç., Bey, A., Garzuglia, M., Groot, N., Guerin, G., Laestadius, L., Lowe, A.J. and Mamane, B. 2017. The extent of forest in dryland biomes. *Science*. **358**(6365), pp.635–638.

Battaglia, M.J., Banks, S., Behnamian, A., Bourgeau-Chavez, L., Brisco, B., Corcoran, J., Chen, Z., Huberty, B., Klassen, J., Knight, J., Morin, P., Murnaghan, K., Pelletier, K. and White, L. 2021. Multi-source eo for dynamic wetland mapping and monitoring in the great lakes basin. *Remote Sensing*. **13**(4), pp.1–38.

Van Beijma, S., Comber, A. and Lamb, A. 2014. Random forest classification of salt marsh vegetation habitats using quad-polarimetric airborne SAR, elevation and optical RS data. *Remote Sensing of Environment*. **149**, pp.118–129.

Belgiu, M. and Dra, L. 2016. Random forest in remote sensing : A review of applications and future directions. *ISPRS Journal of Photogrammetry and Remote Sensing*. **114**, pp.24–31.

Berhanu, M., Suryabhagavan, K.V. and Korme, T. 2021. Wetland mapping and evaluating the impacts on hydrology, using geospatial techniques: a case of Geba Watershed, Southwest Ethiopia. *Geology, Ecology, and Landscapes*. **6**(3), pp.1–18.

Bey, A., Díaz, A.S.P., Maniatis, D., Marchi, G., Mollicone, D., Ricci, S., Bastin, J.F., Moore, R., Federici, S., Rezende, M., Patriarca, C., Turia, R., Gamoga, G., Abe, H., Kaidong, E. and Miceli, G. 2016. Collect earth: Land use and land cover assessment through augmented visual interpretation. *Remote Sensing*. **8**(10), pp.1–24.

Birkett, C.M. 2000. Synergistic remote sensing of Lake Chad: Variability of basin inundation. *Remote Sensing of Environment*. **72**(2), pp.218–236.

Boone, J.K. and Bhomia, R.K. 2017. Ecosystem carbon stocks of mangroves across broad environmental gradients in West-Central Africa: Global and regional comparisons. *PLoS ONE*. **12**(11), pp.1–17.

Bootsma, A., Elshehawi, S., Grootjans, A., Grundling, P.L., Khosa, S., Butler, M.,

Brown, L. and Schot, P. 2019. Anthropogenic disturbances of natural ecohydrological processes in the Matlabas mountain mire, South Africa. *South African Journal of Science*. **115**(5–6).

Breiman, L.E.O. 2001. Random Forests. *Machine Learning*. **45**, pp.5–32.

Buma, W.G., Lee, S. Il and Seo, J.Y. 2018. Recent surface water extent of lake Chad from multispectral sensors and GRACE. *Sensors (Switzerland)*. **18**(7), pp.2082.

Burdun, I., Bechtold, M., Sagris, V., Lohila, A., Humphreys, E., Desai, A.R., Nilsson, M.B., De Lannoy, G. and Mander, Ü. 2020. Satellite determination of peatland water table temporal dynamics by localizing representative pixels of A SWIR-Based Moisture Index. *Remote Sensing*. **12**(18), pp.2936.

Bwangoy, J.R.B., Hansen, M.C., Roy, D.P., Grandi, G. De and Justice, C.O. 2010. Wetland mapping in the Congo Basin using optical and radar remotely sensed data and derived topographical indices. *Remote Sensing of Environment*. **114**(1), pp.73–86.

Cardoso, G.F., Souza, C. and Souza-Filho, P.W.M. 2014. Using spectral analysis of Landsat-5 TM images to map coastal wetlands in the Amazon River mouth, Brazil. *Wetlands Ecology and Management*. **22**(1), pp.79–92.

Carless, D., Luscombe, D.J., Gatis, N., Anderson, K. and Brazier, R.E. 2019. Mapping landscape-scale peatland degradation using airborne lidar and multispectral data. *Landscape Ecology* . **34**, pp.1329–1345.

Chatziantoniou, A., Petropoulos, G.P. and Psomiadis, E. 2017. Co-Orbital Sentinel 1 and 2 for LULC mapping with emphasis on wetlands in a mediterranean setting based on machine learning. *Remote Sensing*. **9**(12), pp.1259.

Chen, J., Zhu, X., Vogelmann, J.E., Gao, F. and Jin, S. 2011. A simple and effective method for filling gaps in Landsat ETM+ SLC-off images. *Remote Sensing of Environment*. **115**(4), pp.1053–1064.

Chen, L., Jin, Z., Michishita, R., Cai, J., Yue, T., Chen, B. and Xu, B. 2014. Dynamic monitoring of wetland cover changes using time-series remote sensing imagery. *Ecological Informatics*. **24**, pp.17–26.

Chen, Y., Huang, C., Ticehurst, C., Merrin, L. and Thew, P. 2013. An evaluation of MODIS daily and 8-day composite products for floodplain and wetland inundation mapping. *Wetlands*. **33**(5), pp.823–835.

Chico, G., Clutterbuck, B., Lindsay, R., Midgley, N.G. and Labadz, J. 2019. Identification and classification of unmapped blanket bogs in the Cordillera Cantábrica, northern Spain. *Mires and Peat*. **24**, pp.1–12.

Chidumeje, N.P.O., Lalit, K. and Subhashni, T. 2015. The Niger Delta wetland ecosystem: What threatens it and why should we protect it? *African Journal of Environmental Science and Technology*. **9**(5), pp.451–463.

Clark, D.B., Mercado, L.M., Sitch, S., Jones, C.D., Gedney, N., Best, M.J., Pryor, M., Rooney, G.G., Essery, R.L.H., Blyth, E., Boucher, O., Harding, R.J., Huntingford, C. and Cox, P.M. 2011. The Joint UK Land Environment Simulator (JULES), model description – Part 2: Carbon fluxes and vegetation dynamics. *Geoscientific Model Development*. **4**(3), pp.701–722.

Clarkson, B., Peters, M. and Raised, U. 2012. *Wetland Types,* pp.23-42.

Clewley, D., Whitcomb, J., Moghaddam, M., McDonald, K., Chapman, B. and Bunting, P. 2015. Evaluation of ALOS PALSAR data for high-resolution mapping of vegetated wetlands in Alaska. *Remote Sensing*. **7**(6), pp.7272–7297.

Connell, J.O. 2012. Monitoring Changes to Irish Peatlands using Satellite Remote Sensing. *Thesis*, pp.76-142.

Connolly, J. and Holden, N.M. 2017. Detecting peatland drains with Object Based Image Analysis and Geoeye-1 imagery. *Carbon Balance and Management*. **12**(1), pp.2–13.

Costa, J. da S., Liesenberg, V., Schimalski, M.B., de Sousa, R.V., Biffi, L.J., Gomes, A.R., Neto, S.L.R., Mitishita, E. and Bispo, P. da C. 2021. Benefits of combining alos/palsar-2 and sentinel-2a data in the classification of land cover classes in the santa catarina southern plateau. *Remote Sensing*. **13**(2), pp.1–32.

Csillik, O., Reiche, J., De Sy, V., Araza, A. and Herold, M. 2022. Rapid remote

monitoring reveals spatial and temporal hotspots of carbon loss in Africa's rainforests. *Communications Earth & Environment*. **3**(1), pp.1–8.

Dabboor, M., Brisco, B., Banks, S., Murnaghan, K. and White, L. 2017. Multitemporal monitoring of wetlands using simulated radarsat constellation mission compact polarimetric SAR data. *International Geoscience and Remote Sensing Symposium (IGARSS)*. **6**, pp.4586–4589.

Dadaser-Celik, F. and Cengiz, E. 2013. A neural network model for simulation of water levels at the Sultan Marshes wetland in Turkey. *Wetlands Ecology and Management*. **21**(5), pp.297–306.

Dadson, S.J., Ashpole, I., Harris, P., Davies, H.N., Clark, D.B., Blyth, E. and Taylor, C.M. 2010. Wetland inundation dynamics in a model of land surface climate: Evaluation in the Niger inland delta region. *Journal of Geophysical Research Atmospheres*. **115**(23), pp.1–7.

Dan, T.T., Chen, C.F., Chiang, S.H. and Ogawa, S. 2016. Mapping and Change Analysis in Mangrove Forest By Using Landsat Imagery. *ISPRS Annals of Photogrammetry, Remote Sensing and Spatial Information Sciences*. **III–8**, pp.109–116.

Dang, A.T.N., Kumar, L., Reid, M. and Nguyen, H. 2021. Remote sensing approach for monitoring coastal wetland in the mekong delta, vietnam: Change trends and their driving forces. *Remote Sensing*. **13**(17), pp.3359.

Dargie, G.C., Lewis, S.L., Lawson, I.T., Mitchard, E.T.A., Page, S.E., Bocko, Y.E. and Ifo, S.A. 2017. Age, extent and carbon storage of the central Congo Basin peatland complex. *Nature*. **542**(7639), pp.86–90.

Davidson, N.C. 2017. How much wetland has the world lost ? Long-term and recent trends in global wetland area. *Marine and Freshwater Research*. **65**, pp.934–941.

Debanshi, S. and Pal, S. 2020. Wetland delineation simulation and prediction in deltaic landscape. *Ecological Indicators*. **108**(September 2019), pp.105757.

DeLancey, E.R., Kariyeva, J., Bried, J.T. and Hird, J.N. 2019. Large-scale probabilistic identification of boreal peatlands using Google Earth Engine,

open-access satellite data, and machine learning. *PLoS ONE*. **14**(6), pp.1–23.

Demenocal, P., Ortiz, J., Guilderson, T., Adkins, J., Sarnthein, M., Baker, L. and Yarusinsky, M. 2000. Abrupt onset and termination of the African Humid Period: Rapid climate responses to gradual insolation forcing. *Quaternary Science Reviews*. **19**(1–5), pp.347–361.

Dixon, M.J.R., Loh, J., Davidson, N.C., Beltrame, C., Freeman, R. and Walpole, M. 2016. Tracking global change in ecosystem area: The Wetland Extent Trends index. *Biological Conservation*. **193**, pp.27–35.

Dong, Z., Wang, Z., Liu, D., Song, K., Li, L., Jia, M. and Ding, Z. 2014. Mapping Wetland Areas Using Landsat-Derived NDVI and LSWI: A Case Study of West Songnen Plain, Northeast China. *Journal of the Indian Society of Remote Sensing*. **42**(3), pp.569–576.

Dronova, I., Gong, P., Wang, L. and Zhong, L. 2015. Mapping dynamic cover types in a large seasonally flooded wetland using extended principal component analysis and object-based classification. *Remote Sensing of Environment*. **158**, pp.193–206.

Elshehawi, Samer, Barthelmes, A., Beer, F. and Joosten, H. 2019. *Assessment of Carbon (CO2) emissions avoidance potential from the Nile Basin peatlands*.

Elshehawi, S, Gabriel, M., Pretorius, L. and Bukhosini, S. 2019. Ecohydrology and causes of peat degradation at the Vasi peatland , South Africa. *Mires and Peat*. **24**(33), pp.1–21.

Erwin, K.L. 2009. Wetlands and global climate change: The role of wetland restoration in a changing world. *Wetlands Ecology and Management*. **17**(1), pp.71–84.

Estupinan-Suarez, L.M., Florez-Ayala, C., Quinones, M.J., Pacheco, A.M. and Santos, A.C. 2015. Detection and characterization of Colombian wetlands: Integrating geospatial data with remote sensing derived data. Using ALOS PALSAR and MODIS imagery. *International Archives of the Photogrammetry, Remote Sensing and Spatial Information Sciences - ISPRS Archives*. **40**, pp.375–382.

Evans, C.D., Peacock, M., Baird, A.J., Artz, R.R.E., Burden, A., Callaghan, N., Chapman, P.J., Cooper, H.M., Coyle, M., Craig, E., Cumming, A., Dixon, S., Gauci, V., Grayson, R.P., Helfter, C., Heppell, C.M., Holden, J., Jones, D.L., Kaduk, J., Levy, P., Matthews, R., McNamara, N.P., Misselbrook, T., Oakley, S., Page, S.E., Rayment, M., Ridley, L.M., Stanley, K.M., Williamson, J.L., Worrall, F. and Morrison, R. 2021. Overriding water table control on managed peatland greenhouse gas emissions. *Nature*. **593**(7860), pp.548–552.

Evans, T.L. and Costa, M. 2013. Landcover classification of the Lower Nhecolândia subregion of the Brazilian Pantanal Wetlands using ALOS/PALSAR, RADARSAT-2 and ENVISAT/ASAR imagery. *Remote Sensing of Environment*. **128**, pp.118–137.

Fei, S.X., Shan, C.U.I.H. and Hua, G.U.O.Z. 2011. Remote Sensing of Mangrove Wetlands Identification. *Procedia Environmental Sciences*. **10**, pp.2287–2293.

Foerster, V., Vogelsang, R., Junginger, A., Asrat, A., Lamb, H.F., Schaebitz, F. and Trauth, M.H. 2015. Environmental change and human occupation of southern Ethiopia and northern Kenya during the last 20,000 years. *Quaternary Science Reviews*. **129**, pp.333–340.

François, G.G.H., K, G.F., Marcelle, G.S.L., Mooney, H.A., Cropper, A., Leemans, R., Arico, S., Bridgewater, P., Peterson, G., Revenga, C., Rivera, M., Peter, A.W., Fallis, A.., Dubay, L., Point, P., Aboutayeb, H., Mermet, L., Raphaël Billé, Maya Leroy, Poux, X. and Schuyt, K. 2005. Ecosystems and Human Well-being: Wetlands and Water - Synthesis*. Regions and Cohesion*. pp.127-137.

FREL 2019. National Forest Reference Emission Level (FREL) for the Federal Republic of Nigeria. *Report*., pp.1–54.

Friedlingstein, P., Jones, M.W., O'Sullivan, M., Andrew, R.M., Bakker, D.C.E., Hauck, J., L.Q., C., Peters, G.P., Peters, W., Pongratz, J., Sitch, S., Canadell, J.G., Ciais, P., Jackson, R.B., Alin, S.R., Anthoni, P., Bates, N.R., Becker, M., Bellouin, N., Bopp, L., Chau, T.T.T., Chevallier, F., Chini, L.P., Cronin, M., Currie, K.I. and Decharme, B., Djeutchouang, L. M., Dou, X., Evans, W., Feely, R. A., Feng, L., Gasser, T., Gilfillan, D., Gkritzalis, T., Grassi, G.,

Gregor, L., Gruber, N., Gürses, Ö., Harris, I., Houghton, R. A., Hurtt, G. C., Iida, Y., Ilyina, T., Luijkx, I. T., Jain, J. 2022. Global Carbon Budget 2021,. *Earth Syst. Sci. Data*. **14**, pp.1917–2005.

Gallant, A.L. 2015. The challenges of remote monitoring of wetlands. *Remote Sensing*. **7**(8), pp.10938–10950.

Gao, Q., Zribi, M., Escorihuela, M.J. and Baghdadi, N. 2017. Synergetic use of sentinel-1 and sentinel-2 data for soil moisture mapping at 100 m resolution. *Sensors (Switzerland)*. **17**(9), pp.1966.

Garba, S.I., Ebmeier, S.K., Bastin, J.F., Mollicone, D. and Holden, J. 2023. Wetland mapping at 10 m resolution reveals fragmentation in southern Nigeria. *Wetlands Ecology and Management*. **31**(3), pp.329–345.

Gbetkom, P.G., Crétaux, J.F., Tchilibou, M., Carret, A., Delhoume, M., Bergé-Nguyen, M. and Sylvestre, F. 2023. Lake Chad vegetation cover and surface water variations in response to rainfall fluctuations under recent climate conditions (2000−2020). *Science of the Total Environment*. **857**(October 2022).

Gemechu, G.F., Rui, X. and Lu, H. 2022. Wetland Change Mapping Using Machine Learning Algorithms, and Their Link with Climate Variation and Economic Growth: A Case Study of Guangling County, China. *Sustainability (Switzerland)*. **14**(1).

Gitau, W., Camberlin, P., Ogallo, L. and Bosire, E. 2017. Trends of intraseasonal descriptors of wet and dry spells over equatorial eastern Africa. *International Journal of Climatology*. **1200**(September 2017), pp.1189–1200.

Gómez, C., White, J.C. and Wulder, M.A. 2016. ISPRS Journal of Photogrammetry and Remote Sensing Optical remotely sensed time series data for land cover classification : A review. *ISPRS Journal of Photogrammetry and Remote Sensing*. **116**, pp.55–72.

Gorelick, N., Hancher, M., Dixon, M., Ilyushchenko, S., Thau, D. and Moore, R. 2017. Remote Sensing of Environment Google Earth Engine : Planetary-scale geospatial analysis for everyone. *Remote Sensing of Environment*. **202**,

pp.18–27.

Griffiths, P., van der Linden, S., Kuemmerle, T. and Hostert, P. 2013. A Pixel-Based Landsat Compositing Algorithm for Large Area Land Cover Mapping. *IEEE Journal of Selected Topics in Applied Earth Observations and Remote Sensing*. **6**(5), pp.2088–2101.

Gulácsi, A. and Kovács, F. 2020. Sentinel-1-imagery-based high-resolutionwater cover detection on wetlands, aided by google earth engine. *Remote Sensing*. **12**(10), pp.1–20.

Gumbricht, T. 2018. Detecting trends in Wetland extent from MODIS derived soil moisture estimates. *Remote Sensing*. **10**(4), pp.611.

Gumbricht, T., Roman-Cuesta, R.M., Verchot, L., Herold, M., Wittmann, F., Householder, E., Herold, N. and Murdiyarso, D. 2017. An expert system model for mapping tropical wetlands and peatlands reveals South America as the largest contributor. *Global Change Biology*. **23**(9), pp.3581–3599.

Guo, M., Li, J., Sheng, C., Xu, J. and Wu, L. 2017. A review of wetland remote sensing. *Sensors (Switzerland)*. **17**(4), pp.1–36.

Gxokwe, S., Dube, T. and Mazvimavi, D. 2020. Multispectral remote sensing of wetlands in semi-arid and arid areas: A review on applications, challenges and possible future research directions. *Remote Sensing*. **12**(24), pp.1–19.

Halabisky, M., Moskal, L.M., Gillespie, A. and Hannam, M. 2016. Reconstructing semi-arid wetland surface water dynamics through spectral mixture analysis of a time series of Landsat satellite images (1984-2011). *Remote Sensing of Environment*. **177**, pp.171–183.

Hassan, T.., Majid, M.., Davidson, S.A.. and Medugu, N.. 2014. The Role of Wetlands in Mitigating the Effect of Climate Change in Nigeria. *Handbook of Climate Change Adaptation*., pp.551–564.

Hedjal, S., Zouini, D. and Benamara, A. 2018. Hydrochemical assessment of water quality for irrigation: A case study of the wetland complex of Guerbes-Sanhadja, North-East of Algeria. *Journal of Water and Land Development*. **38**(1), pp.43–52.

Herbst, D.L. 2015. Wetlands: An ecosystem service South Africa can afford to protect ‘ A critical evaluation of the current legal regime and mechanisms to facilitate the use of payment for ecosystem services to the conservation of wetlands in South Africa’.*Thesis* , pp.1–89.

Hird, J.N., Delancey, E.R. and Mcdermid, G.J. 2017. Google Earth Engine , Open-Access Satellite Data , and Machine Learning in Support of Large-Area Probabilistic Wetland Mapping. *Remote Sensing*. **9**(1315), pp.1315.

Hirschmugl, M., Gallaun, H., Dees, M., Datta, P., Deutscher, J., Koutsias, N. and Schardt, M. 2017. Methods for Mapping Forest Disturbance and Degradation from Optical Earth Observation Data: a Review. *Current Forestry Reports*. **3**(1), pp.32–45.

Hribljan, J.A., Suarez, E., Bourgeau-Chavez, L., Endres, S., Lilleskov, E.A., Chimbolema, S., Wayson, C., Serocki, E. and Chimner, R.A. 2017. Multidate, multisensor remote sensing reveals high density of carbon-rich mountain peatlands in the páramo of Ecuador. *Global Change Biology*. **23**(12), pp.5412–5425.

Hu, S., Niu, Z. and Chen, Y. 2017. Global Wetland Datasets: a Review. *Wetlands*. **37**(5), pp.807–817.

Hu, S., Niu, Z., Chen, Y., Li, L. and Zhang, H. 2017. Global wetlands: Potential distribution, wetland loss, and status. *Science of the Total Environment*. **586**, pp.319–327.

Huang, L. 2019. Local incidence angle referenced classification on polarimetric synthetic aperture radar images in mountain glacier areas. *Applied Remote sensing*. **10**(2), pp.5015.

Hulme, P.E. 2005. Adapting to climate change: is there scope for ecological management in the face of. *Journal of Applied Ecology 2005 42, 784-794*. **42**(5), pp.784–794.

Hussain, M., Chen, D., Cheng, A., Wei, H. and Stanley, D. 2013. Change detection from remotely sensed images: From pixel-based to object-based approaches. *ISPRS Journal of Photogrammetry and Remote Sensing*. **80**, pp.91–106.

Hussaini, A., Mahmud, M.R. and Tang, K.K.W. 2020. Change Detection for the Past Three Decades Using Geospatial Approach in Lake Chad, Central Africa. *IOP Conference Series: Earth and Environmental Science*. **540**(1), pp.2001.

Hussaini, A., Mahmud, M.R., Tang, K.K.W. and Abubakar, A.G. 2019. Water Level Fluctuation Assessment of Lake Chad for Environmental Sustainability using Remote Sensing and Geographic Information System Technique. *International Archives of the Photogrammetry, Remote Sensing and Spatial Information Sciences - ISPRS Archives*. **42**, pp.261–266.

IAEA 2017. Integrated and Sustainable Management of Shared Aquifer Systems and Basins of the Sahel Region. Lake Chad Basin. RAF/7/011. Vienna, Austria.

Igu, N. and Marchant, R. 2017. Freshwater swamp forest use in the Niger Delta : perception and insights. *Journal of Forest Research*. **22**(1), pp.44–52.

IPCC Task Force on National Greenhouse Gas Inventories 2014. *Methodological Guidance on Lands with Wet and Drained Soilds, and Constructed Wetlands for Wastewater.*

Jamali, A. and Mahdianpari, M. 2022. Swin Transformer and Deep Convolutional Neural Networks for Coastal Wetland Classification Using Sentinel-1 , Sentinel-2 , and LiDAR Data. *Remote Sensingote sensing*. **14**(359), pp.359.

Jamali, A., Mahdianpari, M., Brisco, B., Granger, J., Mohammadimanesh, F. and Salehi, B. 2021. Comparing solo versus ensemble convolutional neural networks for wetland classification using multi-spectral satellite imagery. *Remote Sensing*. **13**(11), pp.2046.

Jochems, L.W., Brandt, J., Monks, A., Cattau, M., Kolarik, N., Tallant, J. and Lishawa, S. 2021. Comparison of different analytical strategies for classifying invasive wetland vegetation in imagery from unpiloted aerial systems (Uas). *Remote Sensing*. **13**(23), pp.4733.

Jones, T. 1997. The European Region: An Overview of European Wetlands. *Wetlands, Biodiversity and the Ramsar Convention*. pp.80-86.

Junk, W.J., An, S., Finlayson, C.M., Gopal, B., Květ, J., Mitchell, S.A., Mitsch, W.J.

and Robarts, R.D. 2013. Current state of knowledge regarding the world's wetlands and their future under global climate change: A synthesis. *Aquatic Sciences*. **75**(1), pp.151–167.

Kaplan, G. and Avdan, U. 2017. Mapping and Monitoring wetlands using Sentinel-2 satellite imagery. *ISPRS Annals of the Photogrammetry, Remote Sensing and Spatial Information Sciences*. **4**, pp.271–277.

Kaplan, G. and Avdan, U. 2018a. Monthly analysis of wetlands dynamics using remote sensing data. *ISPRS International Journal of Geo-Information*. **7**(10), pp.411.

Kaplan, G. and Avdan, U. 2018b. Sentinel-1 and Sentinel-2 Data Fusion for Mapping and Monitoring Wetlands. *The International Archives of the Photogrammetry*. **XLII**(3), pp.7–10.

Kaplan, G., Yigit Avdan, Z. and Avdan, U. 2019. Mapping and Monitoring Wetland Dynamics Using Thermal, Optical, and SAR Remote Sensing Data. *Wetlands Management - Assessing Risk and Sustainable Solutions*. **264**, pp.13.

Kariyasa, K. and Dewi, Y.A. 2011. Wetlands of the Nile Basin Distribution, functions and contribution to livelihoods. *Journal of Gender, Agriculture and Food Security*. **1**(3), pp.1–22.

Karnieli, A., Qin, Z., Wu, B., Panov, N. and Yan, F. 2014. Spatio-temporal dynamics of land-use and land-cover in the Mu Us Sandy Land, China, using the change vector analysis technique. *Remote Sensing*. **6**(10), pp.9316–9339.

Kelly, M., Tuxen, K.A. and Stralberg, D. 2011. Mapping changes to vegetation pattern in a restoring wetland: Finding pattern metrics that are consistent across spatial scale and time. *Ecological Indicators*. **11**(2), pp.263–273.

Kim, J., Grunwald, S., Rivero, R.G. and Robbins, R. 2012. Multi-scale Modeling of Soil Series Using Remote Sensing in a Wetland Ecosystem. *Soil Science Society of America Journal*. **76**(6), pp.2327.

Klemas, V. 2013. Remote sensing of emergent and submerged wetlands: an overview. *International Journal of Remote Sensing*. **34**(18), pp.6286–6320.

Klemas, V. 2011. Remote Sensing of Wetlands: Case Studies Comparing Practical Techniques. *Journal of Coastal Research*. **27**(3), pp.418–427.

Klemas, V. 2016. Using Remote sensing to select and monitor restoration site: An Overview. . **29**(5), pp.1016–1028.

Kovács, G.M., Horion, S. and Fensholt, R. 2022. Characterizing ecosystem change in wetlands using dense earth observation time series. *Remote Sensing of Environment*. **281**, pp. 3267.

Kuenzer, C., Bluemel, A., Gebhardt, S., Quoc, T.V. and Dech, S. 2011. Remote sensing of mangrove ecosystems: A review. *Remote Sensing*. **3**(5), pp.878–928.

Kundu, S., Pal, S., Mandal, I. and Talukdar, S. 2022. How far damming induced wetland fragmentation and water richness change affect wetland ecosystem services? *Remote Sensing Applications: Society and Environment*. **27**, pp. 777.

Laine, J., Silvola, J., Tolonen, K., Alm, J., Nykänen, H., Vasander, H., Sallantaus, T., Savolainen, I., Sinisalo, J. and Martikainen, P.J. 1996. Effect of water-level drawdown on global climatic warming: Northern peatlands. *Ambio*. **25**(3), pp.179–184.

Landmann, T., Schramm, M., Colditz, R.R., Dietz, A. and Dech, S. 2010. Wide area wetland mapping in semi-arid Africa using 250-meter MODIS metrics and topographic variables. *Remote Sensing*. **2**(7), pp.1751–1766.

Landmann, T., Schramm, M., Huettich, C. and Dech, S. 2013. MODIS-based change vector analysis for assessing wetland dynamics in Southern Africa. *Remote Sensing Letters*. **4**(2), pp.104–113.

Langan, C., Farmer, J., Rivington, M. and Smith, J.U. 2018. Tropical wetland ecosystem service assessments in East Africa; A review of approaches and challenges. *Environmental Modelling and Software*. **102**, pp.260–273.

LaRocque, A., Phiri, C., Leblon, B., Pirotti, F., Connor, K. and Hanson, A. 2020. Wetland mapping with landsat 8 OLI, Sentinel-1, ALOS-1 PALSAR, and LiDAR data in Southern New Brunswick, Canada. *Remote Sensing*. **12**(13),

pp.1–30.

Leblanc, M., Lemoalle, J., Bader, J.C., Tweed, S. and Mofor, L. 2011. Thermal remote sensing of water under flooded vegetation: New observations of inundation patterns for the ‘Small’ Lake Chad. *Journal of Hydrology*. **404**(1–2), pp.87–98.

Lee, T.M. and Yeh, H.C. 2009. Applying remote sensing techniques to monitor shifting wetland vegetation: A case study of Danshui River estuary mangrove communities, Taiwan. *Ecological Engineering*. **35**(4), pp.487–496.

Leemhuis, C., Amler, E., Diekkrüger, B., Gabiri, G. and Näschen, K. 2016. East African wetland-catchment data base for sustainable wetland management. *Proceedings of the International Association of Hydrological Sciences*. **374**, pp.123–128.

Lefebvre, G., Davranche, A., Willm, L., Campagna, J., Redmond, L., Merle, C., Guelmami, A. and Poulin, B. 2019. Introducing WIW for detecting the presence of water in wetlands with landsat and sentinel satellites. *Remote Sensing*. **11**(19), pp.10–14.

Lehner, B. and Döll, P. 2004a. Development and validation of a global database of lakes, reservoirs and wetlands. *Journal of Hydrology*. **296**(1), pp.1–22.

Lehner, B. and Döll, P. 2004b. Global Lakes and Wetlands Database GLWD. *Wetlands*. **296**(4), pp.1–7.

Lemoalle, J. 2005. The Lake Chad basin. *The World’s Largest Wetlands: Ecology and Conservation*. pp.316–346.

Lemoalle, J., Bader, J.C., Leblanc, M. and Sedick, A. 2012. Recent changes in Lake Chad: Observations, simulations and management options (1973-2011). *Global and Planetary Change*. **80**–**81**, pp.247–254.

Li, A., Song, K., Chen, S., Mu, Y., Xu, Z. and Zeng, Q. 2022. Mapping African wetlands for 2020 using multiple spectral, geo-ecological features and Google Earth Engine. *ISPRS Journal of Photogrammetry and Remote Sensing*. **193**, pp.252–268.

Li, L., Vrieling, A., Skidmore, A., Wang, T., Muñoz, A.R. and Turak, E. 2015. Evaluation of MODIS Spectral Indices for Monitoring Hydrological Dynamics of a Small, Seasonally-Flooded Wetland in Southern Spain. *Wetlands*. **35**(5), pp.851–864.

Li, Z., Chen, H., White, J.C., Wulder, M.A. and Hermosilla, T. 2020. Discriminating treed and non-treed wetlands in boreal ecosystems using time series Sentinel-1 data. *International Journal of Applied Earth Observation and Geoinformation*. **85**, pp.102007.

Limpert, K.E., Carnell, P.E., Trevathan-Tackett, S.M. and Macreadie, P.I. 2020. Reducing Emissions From Degraded Floodplain Wetlands. *Frontiers in Environmental Science*. **8**, pp.1–18.

Liu, D., Chen, W., Menz, G. and Dubovyk, O. 2020. Development of integrated wetland change detection approach: In case of Erdos Larus Relictus National Nature Reserve, China. *Science of the Total Environment*. **731**, pp.139166.

Liu, Y., Gong, W., Hu, X. and Gong, J. 2018. Forest Type Identification with Random Forest Using Sentinel-1A, Sentinel-2A, Multi-Temporal Landsat-8 and DEM Data. *Remote Sensing*. **10**(946), pp.1–25.

Liu, Y., Liu, Yongxue, Li, J., Sun, C., Xu, W. and Zhao, B. 2020. Trajectory of coastal wetland vegetation in Xiangshan Bay, China, from image time series. *Marine Pollution Bulletin*. **160**(163), pp.11697.

Lu, D. and Chang, J. 2023. Examining human disturbances and inundation dynamics in China's marsh wetlands by using time series remote sensing data. *Science of the Total Environment*. **863**, pp.160961.

Lu, D., Mausel, P., Brondízio, E. and Moran, E. 2004. Change detection techniques. *International Journal of Remote Sensing*. **25**(12), pp.2365–2407.

Ma, L., Li, M., Ma, X., Cheng, L., Du, P. and Liu, Y. 2017. A review of supervised object-based land-cover image classification. *ISPRS Journal of Photogrammetry and Remote Sensing*. **130**, pp.277–293.

Magrin, G. 2016. The disappearance of Lake Chad: History of a myth. *Journal of Political Ecology*. **23**(1), pp.204–222.

Magure, M., Gumindoga, W., Makurira, H. and Rwasoka, D.T. 2022. Impacts of wetland loss and fragmentation on the hydrology of Zimbabwe's highveld. *Water Practice and Technology*. **17**(11), pp.2463–2483.

Mahamat, A.-A.A., Al-Hurban, A. and Saied, N. 2021. Change Detection of Lake Chad Water Surface Area Using Remote Sensing and Satellite Imagery. *Journal of Geographic Information System*. **13**(05), pp.561–577.

Mahdavi, S., Salehi, B., Granger, J., Amani, M., Brisco, B. and Huang, W. 2018. Remote sensing for wetland classification: a comprehensive review. *GIScience and Remote Sensing*. **55**(5), pp.623–658.

Mahdianpari, Masoud, Granger, J.E., Mohammadimanesh, F., Salehi, B., Brisco, B., Homayouni, S., Gill, E., Huberty, B. and Lang, M. 2020. Meta-analysis of wetland classification using remote sensing: A systematic review of a 40-year trend in North America. *Remote Sensing*. **12**(11), pp.1882.

Mahdianpari, M, Jafarzadeh, H., Granger, J.E., Mohammadimanesh, F., Brisco, B., Salehi, B., Homayouni, S. and Weng, Q. 2020. A large-scale change monitoring of wetlands using time series Landsat imagery on Google Earth Engine: a case study in Newfoundland. *GIScience and Remote Sensing*. **57**(8), pp.1102–1124.

Mahdianpari, M., Salehi, B., Mohammadimanesh, F., Homayouni, S. and Gill, E. 2018. The First Wetland Inventory Map of Newfoundland at a Spatial Resolution of 10 m Using Sentinel-1 and Sentinel-2 Data on the Google Earth Engine Cloud Computing Platform. *Remote Sensing*. **11**(43), pp.3390.

Mahdianpari, M., Salehi, B., Mohammadimanesh, F. and Motagh, M. 2017. Random forest wetland classification using ALOS-2 L-band , RADARSAT-2 C-band , and TerraSAR-X imagery. *ISPRS Journal of Photogrammetry and Remote Sensing*. **130**, pp.13–31.

Maina, N.S. and Mwangi, J.W. 2023. Influence of Agricultural Practices and Activities on Conservation of the Ol-Bollosat Wetland in Kenya Njagi. . **4**(1), pp.11–24.

Malak, D.A., Marín, A.I., Trombetti, M. and San Román, S. 2021. Carbon pools and

sequestration potential of wetlands in the European Union. *ETC/ULS Report.* pp.8-21.

Mandishona, E. and Knight, J. 2022. Inland wetlands in Africa: A review of their typologies and ecosystem services. *Progress in Physical Geography*. **46**(4), pp.547–565.

Mao, D., Wang, Z., Du, B., Li, L., Tian, Y., Jia, M., Zeng, Y., Song, K., Jiang, M. and Wang, Y. 2020. National wetland mapping in China: A new product resulting from object-based and hierarchical classification of Landsat 8 OLI images. *ISPRS Journal of Photogrammetry and Remote Sensing*. **164**, pp.11–25.

Mapeshoane, B.E. 2013. Soil Hydrology and Hydric soil indicators of the Bokong wetlands in Lesotho. *Thesis*, pp.9-101.

Matema, S., Eilers, C.H.A.M., van der Zijpp, A.J. and Giller, K.E. 2022. Wetlands in drylands: Use and conflict dynamics at the human–wildlife interface in Mbire District, Zimbabwe. *African Journal of Ecology*. **60**(4), pp.1184–1200.

Maxwell, A.E. and Warner, T.A. 2020. Thematic classification accuracy assessment with inherently uncertain boundaries: An argument for center-weighted accuracy assessment metrics. *Remote Sensing*. **12**(12), pp.1905.

Maxwell, S.K. and Sylvester, K.M. 2012. Identification of 'ever-cropped' land (1984-2010) using Landsat annual maximum NDVI image composites: Southwestern Kansas case study. *Remote Sensing of Environment*. **121**, pp.186–195.

McCarthy, M.J., Radabaugh, K.R., Moyer, R.P. and Muller-Karger, F.E. 2018. Enabling efficient, large-scale high-spatial resolution wetland mapping using satellites. *Remote Sensing of Environment*. **208**, pp.189–201.

Meng, L., Roulet, N., Zhuang, Q., Christensen, T.R. and Frolking, S. 2016. Focus on the impact of climate change on wetland ecosystems and carbon dynamics Focus on the impact of climate change on wetland ecosystems and carbon dynamics. *Environmental Research letters*. **11**, pp.201.

Metz, T. 2017. An overview of African ethics. *Themes, Issues and Problems in African Philosophy*., pp.61–75.

Mitchell, S.A. 2013. The status of wetlands, threats and the predicted effect of global climate change: The situation in Sub-Saharan Africa. *Aquatic Sciences*. **75**(1), pp.95–112.

Mitsch, W.J., Bernal, B., Nahlik, A.M., Mander, Ü., Zhang, L., Anderson, C.J., Jørgensen, S.E. and Brix, H. 2013. Wetlands, carbon, and climate change. *Landscape Ecology*. **28**(4), pp.583–597.

Mitsch, W.J. and Gosselink, J.G. 2015. *Wetlands Fifth Edition*. pp.721.

Mitsch, W.J. and Mander, Ü. 2018. Wetlands and carbon revisited. *Ecological Engineering*. **114**, pp.1–6.

Mohammadimanesh, F., Salehi, B., Mahdianpari, M. and Brisco, B. 2018. ISPRS Journal of Photogrammetry and Remote Sensing backscatter analysis of wetlands. *ISPRS Journal of Photogrammetry and Remote Sensing*. **142**, pp.78–93.

Moser, L., Schmitt, A., Wendleder, A. and Roth, A. 2016. Monitoring of the Lac Bam wetland extent using dual-polarized X-band SAR data. *Remote Sensing.* **8**(302), pp.1-31.

Moser, L., Voigt, S., Schoepfer, E. and Palmer, S. 2014. Multitemporal wetland monitoring in sub-Saharan West-Africa using medium resolution optical satellite data. *IEEE Journal of Selected Topics in Applied Earth Observations and Remote Sensing*. **7**(8), pp.3402–3415.

Murray-Hudson, M., Wolski, P., Cassidy, L., Brown, M.T., Thito, K., Kashe, K. and Mosimanyana, E. 2015. Remote Sensing-derived hydroperiod as a predictor of floodplain vegetation composition. *Wetlands Ecology and Management*. **23**(4), pp.603–616.

Murray-Hudson, M., Wolski, P. and Ringrose, S. 2006. Scenarios of the impact of local and upstream changes in climate and water use on hydro-ecology in the Okavango Delta, Botswana. *Journal of Hydrology*. **331**(1–2), pp.73–84.

Musasa, T. and Marambanyika, T. 2022. Assessing the sustainability of land uses in Driefontein and Intunjambili wetlands, Zimbabwe. *Scientific African*. **16**, pp.95.

Musasa, T. and Marambanyika, T. 2021. Drivers of Wetland Utilisation Patterns and The Current Status of Provisioning and Cultural Services In Driefontein and Intunjambili Wetlands , Zimbabwe. *Research Square*, pp.1–24.

Mwita, E. 2010. Remote sensing based assessment of small wetlands in East Africa.*Thesis*, pp.22-52.

Mwita, E., Menz, G., Misana, S., Becker, M., Kisanga, D. and Boehme, B. 2012. Mapping small wetlands of Kenya and Tanzania using remote sensing techniques. *International Journal of Applied Earth Observation and Geoinformation*. **21**(1), pp.173–183.

Mwita, E.J. 2013. Land Cover and Land Use Dynamics of Semi Arid Wetlands: A Case of Rumuruti (Kenya) and Malinda (Tanzania). *Geophysics and Remote Sensing*. **S1**, pp.1–9.

Na, X., Zang, S., Wu, C., Tian, Y. and Li, W. 2018. Hydrological regime monitoring and mapping of the Zhalong wetland through integrating time series Radarsat-2 and landsat imagery. *Remote Sensing*. **10**(5).

Navarro, A., Young, M., Macreadie, P.I., Nicholson, E. and Ierodiaconou, D. 2021. Mangrove and saltmarsh distribution mapping and land cover change assessment for south-eastern australia from 1991 to 2015. *Remote Sensing*. **13**(8), pp.1450.

Ndayisaba, F., Nahayo, L., Guo, H., Bao, A., Kayiranga, A., Karamage, F. and Nyesheja, E.M. 2017. Mapping and monitoring the Akagera wetland in Rwanda. *Sustainability (Switzerland)*. **9**(2), pp.1–13.

Nhamo, L., Magidi, J. and Dickens, C. 2017. Determining wetland spatial extent and seasonal variations of the inundated area using multispectral remote sensing. *Water SA*. **43**(4), pp.1816–7950.

Niu, Z.G., Zhang, H.Y., Wang, X.W., Yao, W.B., Zhou, D.M., Zhao, K.Y., Zhao, H., Li, N.N., Huang, H.B., Li, C.C., Yang, J., Liu, C.X., Liu, S., Wang, L., Li, Z., Yang, Z.Z., Qiao, F., Zheng, Y.M., Chen, Y.L., Sheng, Y.W., Gao, X.H., Zhu, W.H., Wang, W.Q., Wang, H., Weng, Y.L., Zhuang, D.F., Liu, J.Y., Luo, Z.C., Cheng, X., Guo, Z.Q. and Gong, P. 2012. Mapping wetland changes in China

between 1978 and 2008. *Chinese Science Bulletin*. **57**(22), pp.2813–2823.

Nsengimana, V., Weihler, S. and Kaplin, B.A. 2017. Perceptions of Local People on the Use of Nyabarongo River Wetland and Its Conservation in Rwanda. *Society and Natural Resources*. **30**(1), pp.3–15.

Oberholster, P.J., McMillan, P., Durgapersad, K., Botha, A.M. and De Klerk, A.R. 2014. The development of a Wetland Classification and Risk Assessment Index (WCRAI) for non-wetland specialists for the management of natural freshwater wetland ecosystems. *Water, Air, and Soil Pollution*. **225**(2), pp.1833.

Obiefuna, J.N., Nwilo, P.C., Atagbaza, A.O. and Okolie, C.J. 2013. Land Cover Dynamics Associated with the Spatial Changes in the Wetlands of Lagos/Lekki Lagoon System of Lagos, Nigeria. *Journal of Coastal Research*. **288**(3), pp.671–679.

Ogilvie, A., Belaud, G., Delenne, C., Bailly, J.S., Bader, J.C., Oleksiak, A., Ferry, L. and Martin, D. 2015. Decadal monitoring of the Niger Inner Delta flood dynamics using MODIS optical data. *Journal of Hydrology*. **523**, pp.368–383.

Ohimain, E. 1996. Environmental Impacts of Dredging in the Niger Delta. *Habitat*., pp.9–19.

Ojaghi, S., Farnood Ahmadi, F., Ebadi, H. and Bianchetti, R. 2017. Wetland cover change detection using multi-temporal remotely sensed data. *Arabian Journal of Geosciences*. **10**(21), pp.470.

Okpara, U.T., Stringer, L.C. and Dougill, A.J. 2016. Lake drying and livelihood dynamics in Lake Chad: Unravelling the mechanisms, contexts and responses. *Ambio*. **45**(7), pp.781–795.

Olalekan, E.I., Abimbola, L.-H.M., Saheed, M. and Damilola, O.A. 2014. Wetland Resources of Nigeria: Case Study of the Hadejia-Nguru Wetlands. *Poultry, Fisheries & Wildlife Sciences*. **2**(2), pp.123.

Olusola, A., Muyideen, A. and Abel, O. 2016. An Assessment of Wetland Loss in Lagos Metropolis , Nigeria. *Developing Country Studies*. **6**(7), pp.1–7.

Onamuti, O.Y., Okogbue, E.C. and Orimoloye, I.R. 2017. Remote sensing appraisal of Lake Chad shrinkage connotes severe impacts on green economics and socio-economics of the catchment area. *Royal Society Open Science*. **4**(11), pp.0–10.

Ondiek, R.A., Vuolo, F., Kipkemboi, J., Kitaka, N., Lautsch, E., Hein, T. and Schmid, E. 2020. Socio-Economic Determinants of Land Use/Cover Change in Wetlands in East Africa: A Case Study Analysis of the Anyiko Wetland, Kenya. *Frontiers in Environmental Science*. **7**(207), pp.1-16.

Ouyang, X. and Lee, S.Y. 2020. Improved estimates on global carbon stock and carbon pools in tidal wetlands. *Nature Communications*. **11**(1), pp.1–7.

Ozesmi, S.L. and Bauer, M.E. 2002. Satellite remote sensing of wetlands. *Wetlands Ecology and Management*. **10**(5), pp.381–402.

Page, S.E., Rieley, J.O. and Banks, C.J. 2011. Global and regional importance of the tropical peatland carbon pool. *Global Change Biology*. **17**(2), pp.798–818.

Penfound, E. and Vaz, E. 2021. Analysis of Wetland Landcover Change in Great Lakes Urban Areas Using Self-Organizing Maps. *Remote Sensing*. **13**(1), pp.4960.

Petrescu, A.M.R., Lohila, A., Tuovinen, J.P., Baldocchi, D.D., Desai, A.R., Roulet, N.T., Vesala, T., Dolman, A.J., Oechel, W.C., Marcolla, B., Friborg, T., Rinne, J., Matthes, J.H., Merbold, L., Meijide, A., Kiely, G., Sottocornola, M., Sachs, T., Zona, D., Varlagin, A., Lai, D.Y.F., Veenendaal, E., Parmentier, F.J.W., Skiba, U., Lund, M., Hensen, A., Van Huissteden, J., Flanagan, L.B., Shurpali, N.J., Grünwald, T., Humphreys, E.R., Jackowicz-Korczyński, M., Aurela, M.A., Laurila, T., Grüning, C., Corradi, C.A.R., Schrier-Uijl, A.P., Christensen, T.R., Tamstorf, M.P., Mastepanov, M., Martikainen, P.J., Verma, S.B., Bernhofer, C. and Cescatti, A. 2015. The uncertain climate footprint of wetlands under human pressure. *Proceedings of the National Academy of Sciences of the United States of America*. **112**(15), pp.4594–4599.

Pham-duc, B., Sylvestre, F., Papa, F., Frappart, F., Bouchez, C. and Cr, J. 2020. The Lake Chad hydrology under current climate change. *naure research*.

10(5498), pp.1–10.

Policelli, F., Hubbard, A., Jung, H.C., Zaitchik, B. and Ichoku, C. 2018. Lake Chad total surface water area as derived from Land Surface Temperature and radar remote sensing data. *Remote Sensing*. **10**(2), pp.1–16.

Poortinga, A., Aekakkararungroj, A., Kityuttachai, K., Nguyen, Q., Bhandari, B., Thwal, N.S., Priestley, H., Kim, J., Tenneson, K., Chishtie, F., Towashiraporn, P. and Saah, D. 2020. Predictive analytics for identifying land cover change hotspots in the mekong region. *Remote Sensing*. **12**(9), pp.1–17.

Poulter, B., Fluet-Chouinard, E., Hugelius, G., Koven, C., Fatoyinbo, L., Page, S.E., Rosentreter, J.A., Smart, L.S., Taillie, P.J., Thomas, N., Zhang, Z. and Wijedasa, L.S. 2021. A Review of Global Wetland Carbon Stocks and Management Challenges. *Wetland Carbon and Environmental Management* , pp.1–20.

Powell, M., Hodgins, G., Danaher, T., Ling, J., Hughes, M. and Wen, L. 2019. Mapping wetland types in semiarid floodplains: A statistical learning approach. *Remote Sensing*. **11**(6), pp.609.

Qu, Y., Zheng, Y., Gong, P., Shi, J., Li, L., Wang, S., Luo, C., Zhang, H. and Xu, L. 2022. Estimation of wetland biodiversity based on the hydrological patterns and connectivity and its potential application in change detection and monitoring: A case study of the Sanjiang Plain, China. *Science of the Total Environment*. **805**, pp.150291.

Rahman, S. and Mesev, V. 2019. Change vector analysis, tasseled cap, and NDVI-NDMI for measuring land use/cover changes caused by a sudden short-term severe drought: 2011 Texas event. *Remote Sensing*. **11**(19), pp.2217.

Raines, G.L., Sawatzky, D.L. and Bonham-Carter, G.F. 2010. New fuzzy logic tools in ArcGIS 10. *ArcUser*., pp.8–13.

Ramsey, E.W. and Laine, S.C. 1997. Comparison of Landsat Thematic Mapper and High Resolution Photography to Identify Change in Complex Coastal Wetlands. *Journal of Coastal Research*. **13**(2), pp.281–292.

Rebelo, A.J., Le Maitre, D.C., Esler, K.J. and Cowling, R.M. 2015. Hydrological

responses of a valley-bottom wetland to land-use/land-cover change in a South African catchment: Making a case for wetland restoration. *Restoration Ecology*. **23**(6), pp.829–841.

Rebelo, L.M., McCartney, M.P. and Finlayson, C.M. 2010. Wetlands of Sub-Saharan Africa: Distribution and contribution of agriculture to livelihoods. *Wetlands Ecology and Management*. **18**(5), pp.557–572.

Ritchie, M. and Das, S. 2015. *A Brief Review of Remote Sensing Data and Techniques for Wetlands Identification*. pp.1-5.

Rodriguez-Galiano, V.F., Ghimire, B., Rogan, J., Chica-Olmo, M. and Rigol-Sanchez, J.P. 2012. An assessment of the effectiveness of a random forest classifier for land-cover classification. *ISPRS Journal of Photogrammetry and Remote Sensing*. **67**(1), pp.93–104.

Rongoei, P.J.K., Kipkemboi, J., Okeyo-Owuor, J.B. and van Dam, a a 2013. Ecosystem services and drivers of change in Nyando floodplain wetland , Kenya. *African Journal of Environmental Science and Technology*. **7**, pp.274–291.

Roy, D.P., Kovalskyy, V., Zhang, H.K., Vermote, E.F., Yan, L., Kumar, S.S. and Egorov, A. 2016. Characterization of Landsat-7 to Landsat-8 reflective wavelength and normalized difference vegetation index continuity. *Remote Sensing of Environment*. **185**, pp.57–70.

Rüetschi, M. and Schaepman, M.E. 2018. Using Multitemporal Sentinel-1 C-band Backscatter to Monitor Phenology and Classify Deciduous and Coniferous Forests in Northern Switzerland. *Remote Sensing*. **10**, pp.55.

Sahour, H., Kemink, K.M. and O'Connell, J. 2022. Integrating SAR and Optical Remote Sensing for Conservation- Targeted Wetlands Mapping. *Remote Sensing*. **14**, pp.159.

Salehi, B., Mahdianpari, M., Amani, M., M. Manesh, F., Granger, J., Mahdavi, S. and Brisco, B. 2019. A Collection of Novel Algorithms for Wetland Classification with SAR and Optical Data *Intechopen*. **688**, pp.110-125.

Salih, A.A.M., Ganawa, E.T. and Elmahl, A.A. 2017. Spectral mixture analysis

(SMA) and change vector analysis (CVA) methods for monitoring and mapping land degradation/desertification in arid and semiarid areas (Sudan), using Landsat imagery. *Egyptian Journal of Remote Sensing and Space Science*. **20**, pp. 21–29.

Salimi, S. and Scholz, M. 2021. Impact of future climate scenarios on peatland and constructed wetland water quality: A mesocosm experiment within climate chambers. *Journal of Environmental Management*. **289**, pp. 2459.

Sánchez-Espinosa, A. and Schröder, C. 2019. Land use and land cover mapping in wetlands one step closer to the ground: Sentinel-2 versus landsat 8. *Journal of environmental management*. **247**, pp.484–498.

Sarch, M.T. and Birkett, C. 2000. Fishing and farming at Lake Chad: Responses to lake-level fluctuations. *Geographical Journal*. **166**(2), pp.156–172.

Saunders, M.J., Kansiime, F. and Jones, M.B. 2012. Agricultural encroachment: Implications for carbon sequestration in tropical African wetlands. *Global Change Biology*. **18**(4), pp.1312–1321.

Scharsich, V., Mtata, K., Hauhs, M., Lange, H. and Bogner, C. 2017. Analysing land cover and land use change in the Matobo National Park and surroundings in Zimbabwe. *Remote Sensing of Environment*. **194**, pp.278–286.

Schmitt, A., Wendleder, A., Roth, A. and Brisco, B. 2014. Water extent monitoring and water level estimation using multi-frequency, multi-polarized, and multi-temporal SAR data. *International Geoscience and Remote Sensing Symposium (IGARSS)*., pp.1175–1178.

Schmitt, L. and Simpson, N. 2018. *IPCC WGII Sixth Assessment Report*.

Schuijt, K. 2002. Land and water use of wetlands in Africa: Economic values of African wetlands. *Interim Report*. pp.10-27.

Schuyt, K.D. 2005. Economic consequences of wetland degradation for local populations in Africa. *Ecological Economics*. **53**(2), pp.177–190.

Sica, Y. V., Quintana, R.D., Radeloff, V.C. and Gavier-Pizarro, G.I. 2016. Wetland loss due to land use change in the Lower Paraná River Delta, Argentina.

Science of the Total Environment. **568**, pp.967–978.

Singh, S. and Talwar, R. 2014. A comparative study on change vector analysis. *Sadhana*. **39**, pp.1311–1331.

Sjögersten, S., de la Barreda-Bautista, B., Brown, C., Boyd, D., Lopez-Rosas, H., Hernández, E., Monroy, R., Rincón, M., Vane, C., Moss-Hayes, V., Gallardo-Cruz, J.A., Infante-Mata, D., Hoyos-Santillan, J., Vidal Solórzano, J., Peralta-Carreta, C. and Moreno-Casasola, P. 2021. Coastal wetland ecosystems deliver large carbon stocks in tropical Mexico. *Geoderma*. **403**, pp. 173.

Slagter, B., Tsendbazar, N.E., Vollrath, A. and Reiche, J. 2020. Mapping wetland characteristics using temporally dense Sentinel-1 and Sentinel-2 data: A case study in the St. Lucia wetlands, South Africa. *International Journal of Applied Earth Observation and Geoinformation*. **86**, pp. 2009.

Steele-Dunne, S.C., McNairn, H., Monsivais-Huertero, A. and Member, S. 2017. Radar Remote Sensing of Agricultural Canopies : A Review. *IEEE Journal of Selected Topics in Applied Earth Observations and Remote Sensing*. **10**(2), pp.2249–2273.

Steinbach, S., Cornish, N., Franke, J., Hentze, K., Strauch, A., Thonfeld, F., Zwart, S.J. and Nelson, A. 2021. A New Conceptual Framework for Integrating Earth Observation in Large-scale Wetland Management in East Africa. *Wetlands*. **41**(7), pp.93.

Stoyanov, A. 2022. Application of Tasseled Cap Transformation of Sentinel-2—MSI Data for Forest Monitoring and Change Detection on Territory of Natural Park “BLUE STONES”. *Environmental Science Proceedings*. **22**, pp.42.

Suiter, A.E. 2015. Remote Sensing Based detection of Forested Wetlands: An Evaluation of Lidar, Aerial Imagery, and their data fusion. *Thesis,* pp.52-61.

Sun, C., Liu, Y., Zhao, S., Zhou, M., Yang, Y. and Li, F. 2016. Classification mapping and species identification of salt marshes based on a short-time interval NDVI time-series from HJ-1 optical imagery. *International Journal of Applied Earth Observation and Geoinformation*. **45**, pp.27–41.

Sylvestre, F., Mahamat-nour, A., Naradoum, T., Alcoba, M., Gal, L., Paris, A.,

Cretaux, J., Pham-duc, B., Lescoulier, C., Recouvreur, R., Ahmat, M.M. and Gaya, D. 2024. Strengthening of the hydrological cycle in the Lake Chad Basin under current climate change*. Nature Scientific Report* , pp.1–13.

Taiwo, O.J. and Areola, O. 2009. A spatial temporal analysis of wetland losses in the lagos coastal region, Southwestern Nigeria, using multi-date satellite imagery. *International Geoscience and Remote Sensing Symposium (IGARSS)*. **3**, pp.928–930.

Tana, G., Letu, H., Cheng, Z. and Tateishi, R. 2013. Wetlands mapping in north america by decision rule classification using MODIS and ancillary data. *IEEE Journal of Selected Topics in Applied Earth Observations and Remote Sensing*. **6**(6), pp.2391–2401.

Taylor, A.R.D., Howard, G.W. and Begg, G.W. 2018. Developing Wetland Inventories in Southern Africa : A Review. . **118**(1), pp.57–79.

Tewkesbury, A.P., Comber, A.J., Tate, N.J., Lamb, A. and Fisher, P.F. 2015. A critical synthesis of remotely sensed optical image change detection techniques. *Remote Sensing of Environment*. **160**, pp.1–14.

Thakkar, A.K., Desai, V.R., Patel, A. and Potdar, M.B. 2016. An effective hybrid classification approach using tasseled cap transformation (TCT) for improving classification of land use/land cover (LU/LC) in semi-arid region: a case study of Morva-Hadaf watershed, Gujarat, India. *Arabian Journal of Geosciences*. **9**(3), pp.180.

Van Tricht, K., Gobin, A., Gilliams, S. and Piccard, I. 2018. Synergistic use of radar sentinel-1 and optical sentinel-2 imagery for crop mapping: A case study for Belgium. *Remote Sensing*. **10**(10), pp.1–22.

Turpie, J. and Kleynhans, M. 2010. Wetland Valuation Volume IV. A protocol for the quantification and valuation of wetland ecosystem services. *Report,* pp.74.

Uloacha, N.. and I.. O. 2004. Implications of wetlands degradation for water resources management. *GeoJournal*. **61**(2), pp.151–154.

Villa, J.A. and Bernal, B. 2018. Carbon sequestration in wetlands , from science to practice : An overview of the biogeochemical process , measurement methods

, and policy framework. *Ecological Engineering*. **114**, pp.115–128.

Vinet, L. and Zhedanov, A. 2010. Global biodiversity status of the earth's living resources. *Climate Change - The Physical Science Basis*. **1**, pp.624.

Wang, X., Xiao, X., Zou, Z., Hou, L., Qin, Y., Dong, J., Doughty, R.B., Chen, B., Zhang, X., Chen, Y., Ma, J., Zhao, B. and Li, B. 2020. Mapping coastal wetlands of China using time series Landsat images in 2018 and Google Earth Engine. *ISPRS Journal of Photogrammetry and Remote Sensing*. **163**, pp.312–326.

White, L., Brisco, B., Dabboor, M., Schmitt, A. and Pratt, A. 2015. A collection of SAR methodologies for monitoring wetlands. *Remote Sensing.* **7**(6), pp. 7615-7645

Wilen, A.B.O. and Bates, M.K. 1995. The US Fish and Wildlife Service's National Wetlands Inventory Project. *Vegetatio*. **118**(1), pp.153–169.

Woodson, R.D. 2012. Basic Information. *Concrete Portable Handbook*., pp.1–3.

Wright, C. and Gallant, A. 2007. Improved wetland remote sensing in Yellowstone National Park using classification trees to combine TM imagery and ancillary environmental data. *Remote Sensing of Environment*. **107**(4), pp.582–605.

Wu, N., Shi, R., Zhuo, W., Zhang, C., Zhou, B., Xia, Z., Tao, Z., Gao, W. and Tian, B. 2021. A classification of tidal flat wetland vegetation combining phenological features with google earth engine. *Remote Sensing*. **13**(3), pp.1–22.

Wu, W., Zhi, C., Gao, Y., Chen, C., Chen, Z., Su, H., Lu, W. and Tian, B. 2022. Increasing fragmentation and squeezing of coastal wetlands: Status, drivers, and sustainable protection from the perspective of remote sensing. *Science of the Total Environment*. **811**, pp. 339.

Wulder, M.A., Li, Z., Campbell, E.M., White, J.C., Hobart, G., Hermosilla, T. and Coops, N.C. 2018. A National Assessment of Wetland Status and Trends for Canada's Forested Ecosystems Using 33 Years of Earth Observation Satellite Data. *Remote Sensing*. **10**(10), pp.1623.

WWF 2014. Managing rivers wisely: Lake Chad case study. *Wwf.Panda.Org*.

38(3), pp.269.

Xia, L., Ruan, R. and Zhang, X. 2002. Change Detection of Wetland in Hongze Lake Using. *Water.*, pp.1734–1737.

Xing, L., Tang, X., Wang, H., Fan, W. and Gao, X. 2018. Mapping Wetlands of Dongting Lake in China Using Landsat and Sentinel-1 Time Series At 30M. *ISPRS - International Archives of the Photogrammetry, Remote Sensing and Spatial Information Sciences*. **XLII**–**3**, pp.1971–1976.

Xiu, L., Yan, C., Li, X., Qian, D. and Feng, K. 2019. Changes in wetlands and surrounding land cover in a desert area under the influences of human and climatic factors: A case study of the Hongjian Nur region. *Ecological Indicators*. **101**, pp.261–273.

Xu, H. 2006. Modification of normalised difference water index (NDWI) to enhance open water features in remotely sensed imagery. *International Journal of Remote Sensing*. **27**(14), pp.3025–3033.

Xu, J., Morris, P.J., Liu, J. and Holden, J. 2018. PEATMAP: Refining estimates of global peatland distribution based on a meta-analysis. *Catena*. **160**, pp.134–140.

Ye, S., Chen, D. and Yu, J. 2016. A targeted change-detection procedure by combining change vector analysis and post-classification approach. *ISPRS Journal of Photogrammetry and Remote Sensing*. **114**, pp.115–124.

Yoon, G.W., Yun, Y.B. and Park, J.H. 2003. Change Vector Analysis: Detecting of Areas Associated with Flood Using Landsat TM. *International Geoscience and Remote Sensing Symposium (IGARSS)*. **5**, pp.3386–3388.

Young, D.M., Baird, A.J., Morris, P.J., Dargie, G.C., Mampouya Wenina, Y.E., Mbemba, M., Boom, A., Cook, P., Betts, R., Burke, E., Bocko, Y.E., Chadburn, S., Crabtree, D.E., Crezee, B., Ewango, C.E.N., Garcin, Y., Georgiou, S., Girkin, N.T., Gulliver, P., Hawthorne, D., Ifo, S.A., Lawson, I.T., Page, S.E., Jovani-Sancho, A.J., Schefuß, E., Sciumbata, M., Sjögersten, S. and Lewis, S.L. 2023. Simulating carbon accumulation and loss in the central Congo peatlands. *Global Change Biology*. **29**(23), pp.6812–6827.

Zabala, S. 2017. Comparison of multi-temporal and multispectral Sentinel-2 and Unmanned Aerial Vehicle imagery for crop type mapping. *Msc Thesis*, pp.7-18.

Zeleke, T.T., Zakaria Wani Lukwasa, A., Ture Beketie, K. and Yayeh Ayal, D. 2024. Analysis of spatio-temporal precipitation and temperature variability and trend over Sudd-Wetland, Republic of South Sudan. *Climate Services*. **34**, pp. 451.

Zhang, X., Liu, L., Zhao, T., Chen, X., Lin, S., Wang, J., Mi, J. and Liu, W. 2023. GWL_FCS30: a global 30 m wetland map with a fine classification system using multi-sourced and time-series remote sensing imagery in 2020. *Earth System Science Data*. **15**(1), pp.265–293.

Zhao, B., Yan, Y., Guo, H., He, M., Gu, Y. and Li, B. 2009. Monitoring rapid vegetation succession in estuarine wetland using time series MODIS-based indicators: An application in the Yangtze River Delta area. *Ecological Indicators*. **9**(2), pp.346–356.

Zhu, W., Jia, S., Lall, U., Cao, Q. and Mahmood, R. 2019. Relative contribution of climate variability and human activities on the water loss of the Chari/Logone River discharge into Lake Chad: A conceptual and statistical approach. *Journal of Hydrology*. **569**, pp.519–531.

Zhu, W., Yan, J. and Jia, S. 2017. Monitoring recent fluctuations of the southern pool of lake chad using multiple remote sensing data: Implications for water balance analysis. *Remote Sensing*. **9**(10), pp.1032.

Zhu, Z. and Woodcock, C.E. 2014. Remote Sensing of Environment Continuous change detection and classi fi cation of land cover using all available Landsat data. *Remote Sensing of Environment*. **144**, pp.152–171.

Zou, J., Ziegler, Alan D, Chen, D., McNicol, G., Ciais, P., Jiang, X., Zheng, C., Wu, Jie, Wu, Jin, Lin, Z., He, X., Brown, L.E., Holden, J., Zhang, Z., Ramchunder, S.J., Chen, A. and Zeng, Z. 2022. Rewetting global wetlands effectively reduces major greenhouse gas emissions. *Nature Geoscience*. **15**(8), pp.627–632.

Appendix A

Supplementary table for Chapter 4

Table A.1 Ground control point for Wetland and non-wetland in southern Nigeria. The class code is the identifier for each landcover type. 1 for Forest, 2 for Mangrove, 3 for Marsh, 4 for Swamp, 5 for Cultivated land, 6 for Built up, 7 for Deep water, 8 for Shallow water.

Class code	Landcover type	Location x	Location y
1	Forest	5.9164	4.4032
1	Forest	7.1486	4.3947
1	Forest	7.0028	5.3445
1	Forest	7.7691	4.9326
1	Forest	7.922	4.796
1	Forest	7.1591	5.6148
1	Forest	7.7759	5.7465
1	Forest	7.1603	5.7506
1	Forest	8.6973	5.4693
1	Forest	8.385	4.9287
1	Forest	8.0826	5.6088
1	Forest	8.2333	5.2008
1	Forest	8.0815	5.4731
1	Forest	9.0093	6.0105
1	Forest	8.6941	5.0623
1	Forest	9.0104	6.1464
1	Forest	9.1653	6.2814
1	Forest	8.3916	5.7426
1	Forest	8.0849	5.8804
1	Forest	9.3192	6.2805
1	Forest	8.8565	6.1473
1	Forest	7.6117	4.5271
1	Forest	4.703	6.3117
1	Forest	6.6877	4.5332
1	Forest	5.0081	6.0376
1	Forest	5.4595	4.9485

Class code	Landcover type	Location x	Location y
1	Forest	6.2245	4.401
1	Forest	5.6186	5.4899
1	Forest	6.9969	4.6666
1	Forest	8.2289	4.6586
1	Forest	6.2269	4.6719
1	Forest	5.6173	5.3542
1	Forest	5.9177	4.5386
1	Forest	5.7675	4.9462
1	Forest	6.3882	5.4844
1	Forest	6.6985	5.7537
1	Forest	6.2319	5.2141
1	Forest	5.9252	5.352
1	Forest	6.6973	5.618
1	Forest	6.0767	5.0796
1	Forest	6.3821	4.8063
1	Forest	6.541	5.3476
1	Forest	6.3834	4.9419
1	Forest	6.3858	5.213
1	Forest	6.387	5.3487
1	Forest	5.6198	5.6256
1	Forest	5.3159	6.0353
1	Forest	5.471	6.17
1	Forest	5.9314	6.0308
1	Forest	8.3883	5.3355
1	Forest	7.6174	5.2047
1	Forest	7.6197	5.4761
1	Forest	6.5434	5.619
1	Forest	8.7037	6.2842
1	Forest	7.1544	5.0722
1	Forest	7.9209	4.6605
1	Forest	8.0804	5.3374
1	Forest	7.9287	5.6098
1	Forest	7.1532	4.9366
1	Forest	8.5423	5.3345
1	Forest	8.8523	5.604
1	Forest	8.3894	5.4712

Class code	Landcover type	Location x	Location y
1	Forest	8.5455	5.7417
1	Forest	8.2344	5.3364
1	Forest	8.8544	5.8756
1	Forest	8.3927	5.8784
1	Forest	8.8554	6.0114
1	Forest	8.8576	6.2832
1	Forest	9.0125	6.4183
1	Forest	9.1663	6.4174
1	Forest	8.8533	5.7398
1	Forest	8.6951	5.1979
1	Forest	8.2355	5.4721
1	Forest	5.7637	4.5397
1	Forest	8.23	4.7941
1	Forest	5.4608	5.084
1	Forest	7.1521	4.8011
1	Forest	6.5349	4.6698
1	Forest	5.9214	4.9451
1	Forest	6.2282	4.8074
1	Forest	5.9227	5.0807
1	Forest	6.6949	5.3466
1	Forest	6.5458	5.8906
1	Forest	5.4698	6.0341
1	Forest	5.9327	6.1667
1	Forest	5.7801	6.3037
1	Forest	5.0107	6.3094
1	Forest	5.162	6.0364
1	Forest	5.4672	5.7625
1	Forest	8.5498	6.2851
1	Forest	7.3119	5.4781
1	Forest	8.5433	5.4702
1	Forest	5.4659	5.6267
1	Forest	5.9239	5.2163
1	Forest	7.0052	5.6159
1	Forest	7.7737	5.4751
1	Forest	8.3861	5.0642
1	Forest	8.6994	5.7407

Class code	Landcover type	Location x	Location y
1	Forest	8.3905	5.6069
1	Forest	8.8512	5.4683
1	Forest	9.0114	6.2823
1	Forest	8.5444	5.6059
1	Forest	8.7026	6.1483
1	Forest	8.7005	5.8765
1	Forest	8.3872	5.1998
1	Forest	9.3202	6.4165
1	Forest	8.6962	5.3336
1	Forest	8.6983	5.605
1	Forest	8.5466	5.8775
1	Forest	5.3107	5.4921
1	Forest	7.7658	4.5261
1	Forest	5.9189	4.6741
1	Forest	5.611	4.6763
1	Forest	7.4577	4.5281
1	Forest	6.0729	4.673
1	Forest	6.2343	5.4855
1	Forest	5.9202	4.8096
1	Forest	5.77	5.2174
1	Forest	6.6913	4.9397
1	Forest	5.7687	5.0818
1	Forest	6.3846	5.0774
1	Forest	6.8465	5.0743
1	Forest	5.4723	6.306
1	Forest	5.7788	6.1678
1	Forest	4.8568	6.3105
1	Forest	5.9277	5.6234
1	Forest	5.6249	6.1689
1	Forest	8.0871	6.1521
1	Forest	7.9298	5.7456
1	Forest	8.0771	4.9306
1	Forest	7.3153	5.8854
1	Forest	8.5401	5.0633
1	Forest	8.2366	5.6078
1	Forest	9.0135	6.5543

Class code	Landcover type	Location x	Location y
1	Forest	4.0902	6.5885
1	Forest	4.2427	6.4512
1	Forest	3.7867	6.9993
1	Forest	3.0176	7.0055
1	Forest	4.5558	6.9932
1	Forest	4.8582	6.4465
1	Forest	6.547	6.0264
1	Forest	2.8638	7.0068
1	Forest	5.4749	6.5779
1	Forest	4.7096	6.992
1	Forest	4.5544	6.8571
1	Forest	4.3993	6.7221
1	Forest	5.1672	6.5802
1	Forest	3.7853	6.8631
1	Forest	3.6329	7.0005
1	Forest	4.7083	6.8559
1	Forest	3.4776	6.8656
1	Forest	4.8608	6.7186
1	Forest	4.4006	6.8583
1	Forest	6.0891	6.4375
1	Forest	6.0878	6.3015
1	Forest	4.8595	6.5825
1	Forest	5.0172	6.9897
1	Forest	6.7033	6.2972
1	Forest	7.9332	6.1531
1	Forest	7.7838	6.698
1	Forest	4.3979	6.5861
1	Forest	3.321	6.5946
1	Forest	7.63	6.6991
1	Forest	4.0888	6.4525
1	Forest	5.1698	6.8524
1	Forest	4.0943	6.9968
1	Forest	5.7826	6.5757
1	Forest	6.3968	6.4353
1	Forest	5.63	6.7129
1	Forest	5.0133	6.5814

Class code	Landcover type	Location x	Location y
1	Forest	4.5504	6.4489
1	Forest	5.6287	6.5768
1	Forest	4.8634	6.9909
1	Forest	3.7825	6.5909
1	Forest	5.3236	6.8513
1	Forest	5.4736	6.4419
1	Forest	3.479	7.0017
1	Forest	4.7056	6.5837
1	Forest	2.8609	6.7345
1	Forest	5.3249	6.9874
1	Forest	6.7021	6.1613
1	Forest	6.5506	6.4342
1	Forest	5.0146	6.7174
1	Forest	7.4761	6.7001
1	Forest	5.7813	6.4397
1	Forest	7.4715	6.1561
1	Forest	3.6301	6.7282
1	Forest	5.7838	6.7118
1	Forest	5.4762	6.714
1	Forest	6.094	6.9818
1	Forest	3.7839	6.727
1	Forest	5.9389	6.8468
1	Forest	4.2441	6.5873
1	Forest	3.9405	6.998
1	Forest	2.8016	6.618
1	Forest	2.9254	6.5064
1	Forest	5.3197	6.4431
1	Forest	5.1711	6.9886
1	Forest	4.8621	6.8547
1	Forest	6.7009	6.0254
1	Forest	5.9339	6.3026
1	Forest	7.1684	6.7021
1	Forest	7.4727	6.292
1	Forest	6.4016	6.9796
1	Forest	4.093	6.8607
1	Forest	7.3211	6.565

Class code	Landcover type	Location x	Location y
2	Mangrove	4.5969	6.2581
2	Mangrove	6.4229	4.4307
2	Mangrove	3.2227	6.4334
2	Mangrove	8.5207	4.7569
2	Mangrove	6.5951	4.461
2	Mangrove	5.0929	5.7338
2	Mangrove	5.7538	4.5801
2	Mangrove	5.3203	5.4314
2	Mangrove	6.0731	4.4317
2	Mangrove	5.9869	4.478
2	Mangrove	5.1142	5.7702
2	Mangrove	6.3582	4.4087
2	Mangrove	5.3125	5.7776
2	Mangrove	5.9576	4.4294
2	Mangrove	6.6497	4.4068
2	Mangrove	5.5246	5.4939
2	Mangrove	6.1876	4.6369
2	Mangrove	5.8049	4.4879
2	Mangrove	6.786	4.7289
2	Mangrove	6.3583	4.3749
2	Mangrove	5.7602	4.8374
2	Mangrove	6.6801	4.3891
2	Mangrove	4.6058	6.2445
2	Mangrove	5.4801	5.4685
2	Mangrove	5.7752	4.7916
2	Mangrove	4.6318	6.2378
2	Mangrove	8.4065	4.7456
2	Mangrove	5.7904	4.8362
2	Mangrove	6.6688	4.4095
2	Mangrove	6.0939	4.3273
2	Mangrove	5.4326	5.4878
2	Mangrove	5.7529	4.4876
2	Mangrove	5.4902	5.4783
2	Mangrove	5.2861	5.4592
2	Mangrove	5.9599	4.4775
2	Mangrove	5.7912	4.8183

Class code	Landcover type	Location x	Location y
2	Mangrove	5.2891	5.4331
2	Mangrove	5.7367	4.8096
2	Mangrove	5.7523	4.8299
2	Mangrove	5.1372	5.8994
2	Mangrove	5.7596	4.4985
2	Mangrove	3.4281	6.5654
2	Mangrove	6.2991	4.3795
2	Mangrove	5.5208	5.4787
2	Mangrove	6.7553	4.7698
2	Mangrove	3.1756	6.436
2	Mangrove	6.0964	4.4017
2	Mangrove	6.3785	4.3999
2	Mangrove	7.1294	4.5707
2	Mangrove	6.0705	4.4021
2	Mangrove	6.5365	4.4611
2	Mangrove	8.3184	4.8443
2	Mangrove	5.7244	4.7864
2	Mangrove	6.1099	4.3507
2	Mangrove	5.9976	4.4532
2	Mangrove	5.4596	5.4705
2	Mangrove	6.6865	4.3978
2	Mangrove	6.5666	4.4005
2	Mangrove	4.9469	5.9543
2	Mangrove	6.1935	4.3422
2	Mangrove	5.437	5.5138
2	Mangrove	8.2729	4.8987
2	Mangrove	7.0143	4.7386
2	Mangrove	6.7512	4.7387
2	Mangrove	5.5146	5.5165
2	Mangrove	5.2752	5.4414
2	Mangrove	6.0372	4.4353
2	Mangrove	5.5058	5.5019
2	Mangrove	8.3644	4.8635
2	Mangrove	6.7779	4.7633
2	Mangrove	6.3051	4.3948
2	Mangrove	3.4561	6.6147

Class code	Landcover type	Location x	Location y
2	Mangrove	5.7662	4.8107
2	Mangrove	5.1965	5.9296
2	Mangrove	5.73	4.83
2	Mangrove	8.2841	4.9192
2	Mangrove	6.5465	4.4337
2	Mangrove	6.0937	4.4344
2	Mangrove	5.2667	5.9227
2	Mangrove	6.1838	4.4756
2	Mangrove	4.5492	6.2969
2	Mangrove	6.53	4.4173
2	Mangrove	6.4071	4.3765
2	Mangrove	6.7952	4.7176
2	Mangrove	5.8754	4.4143
2	Mangrove	5.8027	4.7849
2	Mangrove	6.3602	4.4282
2	Mangrove	6.666	4.3747
2	Mangrove	6.6868	4.4051
2	Mangrove	3.2174	6.4179
2	Mangrove	8.3449	4.8243
2	Mangrove	5.7466	4.5419
2	Mangrove	4.7048	5.7919
2	Mangrove	6.5104	4.3701
2	Mangrove	6.0445	4.3998
2	Mangrove	6.6867	4.3815
2	Mangrove	6.8095	4.7294
2	Mangrove	8.2449	4.9454
2	Mangrove	7.0525	4.7327
2	Mangrove	6.7473	4.721
2	Mangrove	5.8419	4.5108
2	Mangrove	6.0427	4.3623
2	Mangrove	3.4783	6.5752
2	Mangrove	6.8132	4.7504
2	Mangrove	4.5565	6.2849
2	Mangrove	6.3212	4.4213
2	Mangrove	5.2258	5.8992
2	Mangrove	8.2361	4.9657

Class code	Landcover type	Location x	Location y
2	Mangrove	5.1629	5.89
2	Mangrove	5.756	4.8267
2	Mangrove	6.5913	4.4368
2	Mangrove	5.5193	5.4627
2	Mangrove	8.4454	4.7427
2	Mangrove	6.4212	4.3934
2	Mangrove	5.4646	5.491
2	Mangrove	6.6662	4.3947
2	Mangrove	5.9309	4.4433
2	Mangrove	6.3111	4.3737
2	Mangrove	5.2022	5.9692
2	Mangrove	8.2513	4.9075
2	Mangrove	6.0516	4.4194
2	Mangrove	6.0516	4.4194
2	Mangrove	5.9509	4.4513
2	Mangrove	6.3343	4.3851
2	Mangrove	7.0518	4.7058
2	Mangrove	8.1978	4.9478
2	Mangrove	5.489	5.4922
2	Mangrove	7.0722	4.5423
2	Mangrove	5.7468	4.7862
2	Mangrove	8.3025	4.8114
2	Mangrove	6.5487	4.3611
2	Mangrove	3.1634	6.4143
2	Mangrove	5.7906	4.563
2	Mangrove	7.0132	4.6997
2	Mangrove	8.3001	4.9
2	Mangrove	4.9843	5.8916
2	Mangrove	5.7766	4.4786
2	Mangrove	6.0589	4.4383
2	Mangrove	6.5325	4.3989
2	Mangrove	6.6777	4.409
2	Mangrove	7.026	4.7198
3	Marsh	6.8171	6.674
3	Marsh	6.7593	6.6764
3	Marsh	6.7612	6.6228

Class code	Landcover type	Location x	Location y
3	Marsh	6.9302	6.6395
3	Marsh	6.8744	6.6706
3	Marsh	6.8656	6.6125
3	Marsh	6.923	6.5504
3	Marsh	6.9171	6.5323
3	Marsh	6.8625	6.3713
3	Marsh	6.8221	6.313
3	Marsh	6.7858	6.3382
3	Marsh	6.7914	6.2361
3	Marsh	6.7836	6.2015
3	Marsh	6.7153	6.2592
3	Marsh	6.7273	6.2164
3	Marsh	6.6002	6.0099
3	Marsh	6.6767	5.9811
3	Marsh	6.6121	5.9593
3	Marsh	6.6	5.9755
3	Marsh	6.6432	6.0217
3	Marsh	6.6594	6.0389
3	Marsh	6.6066	6.0695
3	Marsh	6.5861	6.026
3	Marsh	6.6582	6.1171
3	Marsh	6.7206	6.1465
3	Marsh	6.702	6.1193
3	Marsh	6.7533	6.1533
3	Marsh	6.7853	6.108
3	Marsh	6.7389	6.087
3	Marsh	6.8055	6.0699
3	Marsh	6.8061	6.013
3	Marsh	6.7225	5.9541
3	Marsh	6.6696	5.9138
3	Marsh	6.684	5.9402
3	Marsh	6.7071	5.9316
3	Marsh	6.3795	5.6138
3	Marsh	6.376	5.5713
3	Marsh	6.3379	5.5527
3	Marsh	6.3695	5.534

Class code	Landcover type	Location x	Location y
3	Marsh	6.3561	5.4371
3	Marsh	6.2945	5.4677
3	Marsh	6.1753	5.3274
3	Marsh	6.179	5.3921
3	Marsh	7.9725	5.8752
3	Marsh	7.9423	5.8301
3	Marsh	7.9634	5.7361
3	Marsh	8.005	5.6571
3	Marsh	5.3638	6.255
3	Marsh	5.2999	6.0943
3	Marsh	5.0874	6.2506
3	Marsh	5.0492	6.2776
3	Marsh	5.4193	5.8413
3	Marsh	5.2537	5.5119
3	Marsh	5.4726	5.1737
3	Marsh	6.913	7.0532
3	Marsh	6.9066	6.9298
3	Marsh	6.7435	6.9865
3	Marsh	6.6405	7.0592
3	Marsh	6.615	6.6966
3	Marsh	6.7036	6.343
3	Marsh	6.5832	6.93
3	Marsh	6.7142	7.2137
3	Marsh	5.6742	5.4757
3	Marsh	4.3966	6.4501
3	Marsh	3.3163	6.8397
3	Marsh	3.3883	6.5681
3	Marsh	3.1917	6.5747
3	Marsh	2.9819	6.4672
3	Marsh	2.887	6.4136
4	Swamp	5.8648	4.9509
4	Swamp	5.9022	4.8458
4	Swamp	5.7809	4.8689
4	Swamp	5.7494	4.9648
4	Swamp	5.8392	5.0151
4	Swamp	5.9165	5.0518

Class code	Landcover type	Location x	Location y
4	Swamp	5.9285	4.9565
4	Swamp	6.0302	4.8952
4	Swamp	6.0574	4.8266
4	Swamp	6.0604	4.7284
4	Swamp	6.0513	4.6385
4	Swamp	6.0109	4.3343
4	Swamp	6.0459	4.3032
4	Swamp	6.4975	5.002
4	Swamp	6.5022	4.9337
4	Swamp	6.5526	4.8434
4	Swamp	6.6097	4.9079
4	Swamp	6.7622	4.9271
4	Swamp	6.7752	4.971
4	Swamp	6.7602	5.011
4	Swamp	6.7387	5.0453
4	Swamp	6.6895	5.0793
4	Swamp	6.6533	5.1354
4	Swamp	6.7081	5.1865
4	Swamp	6.6005	5.2032
4	Swamp	6.5268	5.19
4	Swamp	6.3621	5.1991
4	Swamp	6.3727	4.6142
4	Swamp	6.2116	4.7356
4	Swamp	6.1724	4.7061
4	Swamp	5.8487	4.6991
4	Swamp	5.526	4.8608
4	Swamp	5.4822	4.9006
4	Swamp	5.5552	4.9382
4	Swamp	5.495	4.9883
4	Swamp	5.5186	5.0721
4	Swamp	5.6	5.244
4	Swamp	5.7925	6.2427
4	Swamp	5.8963	6.2181
4	Swamp	5.8782	6.2228
4	Swamp	5.9172	6.2129
4	Swamp	5.9886	6.2469

Class code	Landcover type	Location x	Location y
4	Swamp	5.9614	6.2321
4	Swamp	6.0549	6.3085
4	Swamp	5.7499	6.192
4	Swamp	5.7622	6.2754
4	Swamp	5.6759	6.166
4	Swamp	5.6655	6.0497
4	Swamp	5.5977	6.0317
4	Swamp	5.5523	5.9852
4	Swamp	5.4485	5.9576
4	Swamp	5.3003	5.8896
4	Swamp	5.3541	5.9365
4	Swamp	5.3107	6.0215
4	Swamp	5.2287	5.9439
4	Swamp	5.1953	5.9505
4	Swamp	5.1374	5.9448
4	Swamp	5.0413	6.038
4	Swamp	4.8875	6.0787
4	Swamp	4.7447	6.1761
4	Swamp	4.7533	6.2854
4	Swamp	4.6857	6.3385
4	Swamp	4.6705	6.4481
4	Swamp	4.6702	6.4191
4	Swamp	7.0434	6.4051
4	Swamp	7.0256	6.4478
4	Swamp	7.0846	6.3523
4	Swamp	7.1162	6.3076
4	Swamp	7.1372	6.2817
4	Swamp	6.7218	5.7635
4	Swamp	6.7409	5.7074
4	Swamp	6.68	5.7106
4	Swamp	6.6772	5.7525
4	Swamp	6.6891	5.6051
4	Swamp	6.6284	5.559
4	Swamp	6.6745	5.5273
4	Swamp	6.7325	5.8435
4	Swamp	6.6787	5.7979

Class code	Landcover type	Location x	Location y
4	Swamp	6.6788	5.8258
4	Swamp	6.7355	5.9054
4	Swamp	6.7545	5.8751
4	Swamp	6.6195	5.868
4	Swamp	6.6526	5.9506
4	Swamp	6.6507	6
4	Swamp	6.6931	6.0004
4	Swamp	6.6812	5.9808
4	Swamp	6.4351	5.9644
4	Swamp	6.3856	5.9338
4	Swamp	5.9991	5.6681
4	Swamp	5.8992	5.5839
4	Swamp	5.8905	5.5407
4	Swamp	5.9383	5.5732
4	Swamp	5.8341	5.4556
4	Swamp	5.7708	5.4332
4	Swamp	5.6368	5.3524
4	Swamp	5.6698	5.2547
4	Swamp	5.538	5.1596
4	Swamp	5.5368	5.1091
4	Swamp	5.576	5.1389
4	Swamp	5.6135	5.0254
4	Swamp	5.6281	4.9863
4	Swamp	5.7521	4.8835
4	Swamp	5.7648	4.8408
4	Swamp	5.2918	6.1706
4	Swamp	5.2578	6.1323
4	Swamp	5.3492	6.1862
4	Swamp	5.3621	6.2395
4	Swamp	5.4139	6.2723
4	Swamp	5.3537	6.2659
4	Swamp	5.437	6.2913
4	Swamp	5.4401	6.3356
4	Swamp	5.4526	6.3953
4	Swamp	5.295	6.074
4	Swamp	5.291	6.1126

Class code	Landcover type	Location x	Location y
4	Swamp	5.2155	6.0208
4	Swamp	5.0674	5.9897
4	Swamp	5.087	6.0094
4	Swamp	4.3466	6.4873
4	Swamp	4.2901	6.438
4	Swamp	4.2137	6.4742
4	Swamp	7.4914	4.8349
4	Swamp	7.5426	4.7184
4	Swamp	7.5485	4.6267
4	Swamp	7.5735	4.6064
4	Swamp	8.1309	5.0533
4	Swamp	8.096	5.0063
4	Swamp	8.0466	5.1144
4	Swamp	8.017	5.0729
4	Swamp	8.0854	5.1031
4	Swamp	8.1953	4.8861
5	Cultivated land	7.4669	5.6128
5	Cultivated land	6.85	5.4812
5	Cultivated land	7.6288	6.563
5	Cultivated land	8.5412	5.1989
5	Cultivated land	8.8586	6.4192
5	Cultivated land	6.3895	5.6201
5	Cultivated land	4.5531	6.721
5	Cultivated land	5.775	5.7602
5	Cultivated land	7.9254	5.2027
5	Cultivated land	7.9276	5.4741
5	Cultivated land	7.3142	5.7496
5	Cultivated land	7.9231	4.9316
5	Cultivated land	7.6152	4.9336
5	Cultivated land	7.313	5.6138
5	Cultivated land	7.7703	5.0681
5	Cultivated land	6.8512	5.6169
5	Cultivated land	7.614	4.798
5	Cultivated land	6.6997	5.8895
5	Cultivated land	8.0782	5.0662
5	Cultivated land	7.4635	5.2057

Class code	Landcover type	Location x	Location y
5	Cultivated land	7.7714	5.2037
5	Cultivated land	7.7816	6.426
5	Cultivated land	6.5543	6.8424
5	Cultivated land	8.5477	6.0133
5	Cultivated land	8.7015	6.0124
5	Cultivated land	8.0793	5.2018
5	Cultivated land	8.8597	6.5552
5	Cultivated land	6.2294	4.9429
5	Cultivated land	6.5398	5.212
5	Cultivated land	6.5373	4.9408
5	Cultivated land	5.1685	6.7163
5	Cultivated land	6.5446	5.7548
5	Cultivated land	6.3992	6.7074
5	Cultivated land	2.8623	6.8706
5	Cultivated land	5.9264	5.4876
5	Cultivated land	6.2441	6.5724
5	Cultivated land	6.3931	6.0275
5	Cultivated land	5.1646	6.3082
5	Cultivated land	5.3146	5.8994
5	Cultivated land	6.0853	6.0297
5	Cultivated land	7.0099	6.1592
5	Cultivated land	7.6254	6.1551
5	Cultivated land	6.7045	6.4332
5	Cultivated land	6.9993	4.9376
5	Cultivated land	3.1671	6.5959
5	Cultivated land	6.5482	6.1623
5	Cultivated land	7.1649	6.2941
5	Cultivated land	6.8548	6.0243
5	Cultivated land	6.8536	5.8885
5	Cultivated land	7.0004	5.0732
5	Cultivated land	7.0111	6.2951
5	Cultivated land	7.4612	4.9346
5	Cultivated land	7.4623	5.0701
5	Cultivated land	7.46	4.799
5	Cultivated land	7.7725	5.3394
5	Cultivated land	6.8489	5.3455

Class code	Landcover type	Location x	Location y
5	Cultivated land	7.6231	5.8833
5	Cultivated land	7.3072	4.9356
5	Cultivated land	7.3107	5.3424
5	Cultivated land	7.3061	4.8
5	Cultivated land	6.8572	6.2961
5	Cultivated land	7.777	5.8823
5	Cultivated land	7.6277	6.427
5	Cultivated land	8.0915	6.6961
5	Cultivated land	7.7849	6.8342
5	Cultivated land	7.7804	6.29
5	Cultivated land	8.397	6.4221
5	Cultivated land	8.2432	6.423
5	Cultivated land	7.6311	6.8352
5	Cultivated land	8.0882	6.288
5	Cultivated land	7.7793	6.1541
5	Cultivated land	7.0146	6.7031
5	Cultivated land	7.4704	6.0202
5	Cultivated land	7.6266	6.291
5	Cultivated land	7.9354	6.425
5	Cultivated land	8.3992	6.6941
5	Cultivated land	8.7069	6.6922
5	Cultivated land	7.0134	6.5671
5	Cultivated land	8.0904	6.56
5	Cultivated land	7.7827	6.562
5	Cultivated land	2.7992	6.397
5	Cultivated land	7.32	6.429
5	Cultivated land	8.0837	5.7446
5	Cultivated land	8.7058	6.5562
5	Cultivated land	8.2322	5.0652
5	Cultivated land	5.7713	5.3531
5	Cultivated land	6.8453	4.9387
5	Cultivated land	6.0779	5.2152
5	Cultivated land	6.5386	5.0764
5	Cultivated land	6.6961	5.4822
5	Cultivated land	5.7864	6.984
5	Cultivated land	6.3943	6.1634

Class code	Landcover type	Location x	Location y
5	Cultivated land	3.1714	7.0042
5	Cultivated land	4.7069	6.7198
5	Cultivated land	6.0829	5.758
5	Cultivated land	3.3252	7.003
5	Cultivated land	6.5494	6.2983
5	Cultivated land	6.2417	6.3004
5	Cultivated land	5.7775	6.0319
5	Cultivated land	5.9377	6.7107
5	Cultivated land	6.0841	5.8938
5	Cultivated land	6.2454	6.7085
5	Cultivated land	6.2478	6.9807
5	Cultivated land	3.17	6.8681
5	Cultivated land	5.1659	6.4442
5	Cultivated land	3.0133	6.5972
5	Cultivated land	6.3956	6.2993
5	Cultivated land	3.3238	6.8668
5	Cultivated land	5.3184	6.3071
5	Cultivated land	6.2392	6.0286
5	Cultivated land	6.0816	5.6223
5	Cultivated land	7.7669	4.6615
5	Cultivated land	7.4646	5.3414
5	Cultivated land	7.6129	4.6625
5	Cultivated land	7.0016	5.2088
5	Cultivated land	7.6186	5.3404
5	Cultivated land	7.6163	5.0691
5	Cultivated land	8.241	6.1511
5	Cultivated land	6.6925	5.0753
5	Cultivated land	6.0791	5.3509
5	Cultivated land	5.7763	5.896
5	Cultivated land	2.8004	6.5075
5	Cultivated land	5.6275	6.4408
5	Cultivated land	5.321	6.5791
6	Built up/bare land	7.359	4.8765
6	Built up/bare land	7.0692	5.0097
6	Built up/bare land	6.8789	5.0044
6	Built up/bare land	6.8156	5.1117

Class code	Landcover type	Location x	Location y
6	Built up/bare land	6.667	5.0882
6	Built up/bare land	6.4005	5.0362
6	Built up/bare land	6.3273	4.9334
6	Built up/bare land	6.2842	4.831
6	Built up/bare land	6.0724	4.7991
6	Built up/bare land	5.9192	5.6637
6	Built up/bare land	5.8882	5.5801
6	Built up/bare land	5.8219	5.609
6	Built up/bare land	5.8821	5.5044
6	Built up/bare land	5.7999	5.4853
6	Built up/bare land	5.8184	5.5409
6	Built up/bare land	5.7191	5.52
6	Built up/bare land	5.7023	5.5613
6	Built up/bare land	5.6499	5.6446
6	Built up/bare land	4.9789	5.9091
6	Built up/bare land	4.8199	6.0912
6	Built up/bare land	7.011	4.9465
6	Built up/bare land	7.1702	4.8734
6	Built up/bare land	7.1663	4.778
6	Built up/bare land	7.0886	4.7404
6	Built up/bare land	7.0307	4.7353
6	Built up/bare land	7.0334	4.9323
6	Built up/bare land	6.9339	4.8754
6	Built up/bare land	6.9232	4.9388
6	Built up/bare land	6.9538	4.7926
6	Built up/bare land	7.1324	4.792
6	Built up/bare land	7.0758	4.8511
6	Built up/bare land	7.3359	5.0618
6	Built up/bare land	7.4381	5.1424
6	Built up/bare land	7.3138	5.1667
6	Built up/bare land	5.7266	6.5836
6	Built up/bare land	5.6324	6.5183
6	Built up/bare land	5.5925	6.4622
6	Built up/bare land	5.6551	6.4177
6	Built up/bare land	5.5659	6.3684
6	Built up/bare land	5.7688	6.411

Class code	Landcover type	Location x	Location y
6	Built up/bare land	5.743	6.3273
6	Built up/bare land	5.7114	6.273
6	Built up/bare land	5.6311	6.1973
6	Built up/bare land	5.5317	6.2769
6	Built up/bare land	5.6112	6.4106
6	Built up/bare land	6.0341	6.3139
6	Built up/bare land	6.1897	6.1393
6	Built up/bare land	6.3028	6.0841
6	Built up/bare land	6.2836	6.0267
6	Built up/bare land	6.2345	5.9697
6	Built up/bare land	6.1679	5.8541
6	Built up/bare land	6.1305	5.8033
6	Built up/bare land	6.0526	5.7021
6	Built up/bare land	5.8803	5.4513
6	Built up/bare land	5.9185	5.3745
6	Built up/bare land	7.9729	4.6398
6	Built up/bare land	7.9096	4.6902
6	Built up/bare land	7.94	5.0212
6	Built up/bare land	8.3389	4.9881
6	Built up/bare land	7.8361	5.6237
6	Built up/bare land	7.8407	5.6638
6	Built up/bare land	7.8569	5.5476
6	Built up/bare land	7.6253	5.625
6	Built up/bare land	7.5038	5.5004
6	Built up/bare land	7.5492	5.3912
6	Built up/bare land	7.2624	5.4651
6	Built up/bare land	7.036	5.5162
6	Built up/bare land	7.1472	5.6425
6	Built up/bare land	6.8487	5.966
6	Built up/bare land	7.0721	5.9109
6	Built up/bare land	7.1073	5.7579
6	Built up/bare land	6.9344	5.779
6	Built up/bare land	6.8964	5.6435
6	Built up/bare land	6.8966	5.5673
6	Built up/bare land	3.3201	6.6425
6	Built up/bare land	3.2488	6.5767

Class code	Landcover type	Location x	Location y
6	Built up/bare land	3.2928	6.4768
6	Built up/bare land	2.8679	6.3889
6	Built up/bare land	2.71	6.4306
6	Built up/bare land	4.6511	6.59
6	Built up/bare land	4.9077	6.4827
6	Built up/bare land	4.8055	6.3468
6	Built up/bare land	4.8768	6.7094
6	Built up/bare land	4.8767	6.8028
6	Built up/bare land	4.998	6.7747
6	Built up/bare land	5.1925	7.4286
6	Built up/bare land	5.2474	7.3337
6	Built up/bare land	5.1723	7.3481
6	Built up/bare land	5.1133	7.3495
6	Built up/bare land	5.1666	7.2288
6	Built up/bare land	5.1287	7.2557
6	Built up/bare land	5.2349	7.1891
6	Built up/bare land	5.2691	7.2503
6	Built up/bare land	5.1524	7.2897
6	Built up/bare land	7.6964	5.2108
6	Built up/bare land	7.768	5.138
6	Built up/bare land	7.7156	5.1734
6	Built up/bare land	7.7172	5.1182
6	Built up/bare land	7.7719	5.018
6	Built up/bare land	7.8441	4.984
6	Built up/bare land	7.8672	5.0576
6	Built up/bare land	7.9787	5.0373
6	Built up/bare land	7.901	5.0028
6	Built up/bare land	7.9961	4.9841
6	Built up/bare land	8.0321	5.0371
6	Built up/bare land	8.0501	4.9066
6	Built up/bare land	7.9501	4.9075
6	Built up/bare land	7.9143	4.8708
6	Built up/bare land	8.3346	4.9275
6	Built up/bare land	8.333	5.0369
6	Built up/bare land	8.3805	4.9721
6	Built up/bare land	8.3336	5.3426

Class code	Landcover type	Location x	Location y
6	Built up/bare land	8.3798	5.2345
6	Built up/bare land	7.8556	4.8302
6	Built up/bare land	7.0087	6.0233
6	Built up/bare land	7.3165	6.0212
6	Built up/bare land	7.1614	5.8864
6	Built up/bare land	6.8524	5.7527
6	Built up/bare land	7.0063	5.7516
6	Built up/bare land	7.004	5.4802
6	Built up/bare land	7.1579	5.4791
6	Built up/bare land	7.1568	5.3434
6	Built up/bare land	7.4681	5.7486
6	Built up/bare land	7.7748	5.6108
6	Built up/bare land	7.3095	5.2068
6	Built up/bare land	7.9309	5.8814
6	Built up/bare land	6.0804	5.4865
6	Built up/bare land	6.2331	5.3498
6	Built up/bare land	6.9981	4.8021
6	Built up/bare land	3.0504	6.5054
6	Built up/bare land	3.6287	6.5922
6	Built up/bare land	3.0161	6.8694
6	Built up/bare land	3.6315	6.8643
6	Built up/bare land	3.1685	6.732
6	Built up/bare land	3.3224	6.7307
6	Built up/bare land	3.4762	6.7295
6	Built up/bare land	3.9377	6.7258
6	Built up/bare land	5.6224	5.8972
6	Built up/bare land	5.7738	5.6245
6	Built up/bare land	5.6262	6.3048
6	Built up/bare land	5.1633	6.1723
6	Built up/bare land	7.3223	6.7011
6	Built up/bare land	8.3959	6.2861
6	Built up/bare land	3.1657	6.4599
6	Built up/bare land	3.3195	6.4586
6	Built up/bare land	3.4734	6.4574
6	Built up/bare land	4.5491	6.3129
6	Built up/bare land	4.7016	6.1758

Class code	Landcover type	Location x	Location y
6	Built up/bare land	7.1509	4.6656
6	Built up/bare land	7.3049	4.6645
6	Built up/bare land	7.4589	4.6635
7	Deep water	3.4748	6.5934
7	Deep water	5.4506	5.3798
7	Deep water	5.5029	5.3989
7	Deep water	5.5075	5.4551
7	Deep water	5.5045	5.4188
7	Deep water	5.5007	5.4405
7	Deep water	5.4242	5.4384
7	Deep water	5.4415	5.4109
7	Deep water	5.3942	5.4842
7	Deep water	5.4006	5.515
7	Deep water	5.4319	5.4892
7	Deep water	5.3114	5.5632
7	Deep water	5.3116	5.6268
7	Deep water	5.3271	5.5935
7	Deep water	5.275	5.6034
7	Deep water	5.302	5.6093
7	Deep water	5.3258	5.6988
7	Deep water	5.303	5.6567
7	Deep water	5.3166	5.6663
7	Deep water	5.3195	5.6895
7	Deep water	5.3134	5.6889
7	Deep water	5.3059	5.6725
7	Deep water	5.3263	5.7307
7	Deep water	5.3285	5.7118
7	Deep water	5.2953	5.7094
7	Deep water	5.2994	5.6981
7	Deep water	5.2854	5.7303
7	Deep water	5.5736	5.9348
7	Deep water	5.6101	5.9117
7	Deep water	5.5483	5.9433
7	Deep water	5.5091	5.9379
7	Deep water	5.5193	5.9125
7	Deep water	5.5061	5.9236

Class code	Landcover type	Location x	Location y
7	Deep water	5.3823	5.8581
7	Deep water	5.4137	5.8254
7	Deep water	5.3338	5.8462
7	Deep water	5.2385	5.8678
7	Deep water	5.2491	5.8481
7	Deep water	5.1886	5.8506
7	Deep water	5.2145	5.8867
7	Deep water	5.2731	5.8989
7	Deep water	5.2668	5.8769
7	Deep water	5.2729	5.8653
7	Deep water	5.1564	5.8235
7	Deep water	5.084	5.7893
7	Deep water	5.1151	5.8196
7	Deep water	5.1472	5.7908
7	Deep water	5.0813	5.7558
7	Deep water	5.0755	5.7864
7	Deep water	3.4587	6.4975
7	Deep water	3.5198	6.4744
7	Deep water	3.513	6.53
7	Deep water	3.4354	6.5653
7	Deep water	3.4137	6.5411
7	Deep water	3.4016	6.4154
7	Deep water	3.357	6.4282
7	Deep water	3.3456	6.4358
7	Deep water	3.3495	6.4074
7	Deep water	3.3804	6.4129
7	Deep water	3.4241	6.4401
7	Deep water	2.8993	6.5135
7	Deep water	2.8943	6.5125
7	Deep water	2.8833	6.5396
7	Deep water	2.8481	6.4311
7	Deep water	2.8894	6.4087
7	Deep water	2.8791	6.4096
7	Deep water	2.8246	6.4457
7	Deep water	2.8202	6.4501
7	Deep water	3.1038	6.4826

Class code	Landcover type	Location x	Location y
7	Deep water	7.2258	4.6484
7	Deep water	7.1755	4.6353
7	Deep water	7.2482	4.6113
7	Deep water	7.2061	4.6397
7	Deep water	6.6603	5.8435
7	Deep water	6.6458	5.8043
7	Deep water	6.6268	5.8101
7	Deep water	6.6421	5.8421
7	Deep water	6.6438	5.7614
7	Deep water	6.6356	5.7194
7	Deep water	6.599	5.6771
7	Deep water	6.6181	5.6473
7	Deep water	6.6258	5.6949
7	Deep water	6.5285	5.5254
7	Deep water	6.5395	5.4846
7	Deep water	6.5417	5.4423
7	Deep water	6.477	5.4118
7	Deep water	6.4936	5.3725
7	Deep water	6.3732	5.3102
7	Deep water	6.458	5.3298
7	Deep water	6.4107	5.2645
7	Deep water	6.3355	5.2291
7	Deep water	6.3409	5.1686
7	Deep water	6.3561	5.149
7	Deep water	6.3091	5.097
7	Deep water	6.261	5.0848
7	Deep water	6.2363	5.0581
7	Deep water	6.1929	5.0121
7	Deep water	6.1613	5.0338
7	Deep water	6.1205	5.0601
7	Deep water	6.0529	5.0042
7	Deep water	6.0807	4.9887
7	Deep water	6.1283	4.9414
7	Deep water	6.0868	4.9037
7	Deep water	6.1286	4.9087
7	Deep water	6.1766	4.8649

Class code	Landcover type	Location x	Location y
7	Deep water	6.1488	4.8613
7	Deep water	6.1112	4.8382
7	Deep water	6.123	4.8699
7	Deep water	6.1863	4.8516
7	Deep water	6.1948	4.8584
7	Deep water	5.4914	4.8505
7	Deep water	5.5433	4.8228
7	Deep water	5.6323	4.8408
7	Deep water	5.6523	4.8006
7	Deep water	5.6395	4.8588
7	Deep water	5.6772	4.8846
7	Deep water	5.6271	4.886
7	Deep water	5.6085	4.8209
7	Deep water	5.572	4.8111
7	Deep water	5.5572	4.8302
7	Deep water	6.074	4.3715
7	Deep water	6.0787	4.2996
7	Deep water	-62.3907	-62.3907
7	Deep water	3.707	6.5819
7	Deep water	4.056	6.469
7	Deep water	5.1887	5.5912
7	Deep water	5.3946	5.6015
7	Deep water	5.9714	4.3489
7	Deep water	6.2407	4.3394
7	Deep water	7.6028	4.4675
7	Deep water	8.3786	4.5997
7	Deep water	6.5373	5.4689
7	Deep water	6.6985	5.9479
7	Deep water	3.3944	6.4699
7	Deep water	7.0664	4.3879
8	Shallow water	6.8011	5.7038
8	Shallow water	6.7783	5.7082
8	Shallow water	6.7974	5.7098
8	Shallow water	6.8512	5.6844
8	Shallow water	6.7276	5.6344
8	Shallow water	5.5942	5.1193

Class code	Landcover type	Location x	Location y
8	Shallow water	5.6488	5.0899
8	Shallow water	5.6052	5.0998
8	Shallow water	5.4514	5.4089
8	Shallow water	5.4763	5.9223
8	Shallow water	5.4895	5.905
8	Shallow water	5.4487	5.9119
8	Shallow water	5.4452	5.9179
8	Shallow water	5.4176	6.001
8	Shallow water	5.3461	6.0123
8	Shallow water	5.8555	6.2274
8	Shallow water	5.817	6.2264
8	Shallow water	5.8103	6.2283
8	Shallow water	7.1896	4.6574
8	Shallow water	5.6697	6.7693
8	Shallow water	5.6571	6.7808
8	Shallow water	5.6241	6.7562
8	Shallow water	5.5726	6.7002
8	Shallow water	5.5439	6.6904
8	Shallow water	5.5851	6.7219
8	Shallow water	5.4438	6.3461
8	Shallow water	5.4571	6.3223
8	Shallow water	6.5621	5.8333
8	Shallow water	6.5241	5.8124
8	Shallow water	6.5232	5.8062
8	Shallow water	6.4836	5.7747
8	Shallow water	6.4944	5.7665
8	Shallow water	6.5047	5.7857
8	Shallow water	6.5046	5.7775
8	Shallow water	6.4777	5.7419
8	Shallow water	6.4782	5.7321
8	Shallow water	6.4637	5.7273
8	Shallow water	6.4672	5.7239
8	Shallow water	6.4489	5.7418
8	Shallow water	6.4623	5.7194
8	Shallow water	6.448	5.7321
8	Shallow water	6.4984	5.7079

Class code	Landcover type	Location x	Location y
8	Shallow water	6.4989	5.7056
8	Shallow water	6.4996	5.7028
8	Shallow water	6.5184	5.6401
8	Shallow water	6.5257	5.6447
8	Shallow water	6.5303	5.6443
8	Shallow water	6.5361	5.649
8	Shallow water	6.5518	5.6441
8	Shallow water	6.5587	5.6405
8	Shallow water	6.5603	5.6442
8	Shallow water	6.5471	5.637
8	Shallow water	6.4642	5.585
8	Shallow water	6.477	5.5736
8	Shallow water	6.4314	5.552
8	Shallow water	6.4476	5.5696
8	Shallow water	6.4521	5.5641
8	Shallow water	6.483	5.6173
8	Shallow water	6.5009	5.6205
8	Shallow water	6.4845	5.6252
8	Shallow water	6.4837	5.62
8	Shallow water	6.56	5.4693
8	Shallow water	6.5723	5.4832
8	Shallow water	6.0912	4.3835
8	Shallow water	6.1068	4.3744
8	Shallow water	6.129	4.3795
8	Shallow water	6.123	4.3846
8	Shallow water	6.5275	5.3286
8	Shallow water	6.7053	5.6791
8	Shallow water	6.6934	5.6869
8	Shallow water	6.7245	5.692
8	Shallow water	6.7043	5.7142
8	Shallow water	6.7321	5.5676
8	Shallow water	6.7239	5.5674
8	Shallow water	6.6945	5.5504
8	Shallow water	6.567	5.5117
8	Shallow water	6.456	5.5495
8	Shallow water	6.4307	5.5461

Class code	Landcover type	Location x	Location y
8	Shallow water	6.4191	5.5455
8	Shallow water	6.4757	5.5479
8	Shallow water	6.4728	5.5587
8	Shallow water	6.433	5.561
8	Shallow water	5.2665	5.988
8	Shallow water	4.8943	6.3122
8	Shallow water	4.9341	6.3303
8	Shallow water	7.1601	5.6102
8	Shallow water	7.1428	5.5614
8	Shallow water	7.4915	5.9722
8	Shallow water	6.8003	6.6063
8	Shallow water	6.7187	7.0431
8	Shallow water	6.0039	5.5043
8	Shallow water	5.9944	5.5015
8	Shallow water	5.9991	5.5028
8	Shallow water	5.9701	5.4954
8	Shallow water	5.7209	5.5566

Appendix B

Supplementary tables for Chapter 5

Table B.1 The spatial extent of wetland cover in different African climate zones. Classification of satellite imagery was based on training which was independent for each climate zone

Climate zone	Total area (km^2)	Wetland area	Percentage wetland cover
TW	1,948,865	448,210	23.0
TWD	11,302,156	362,980	3.2
SARD	6,685,370	93811	1.4
ARD/DST	8,962,030	35,853	0.4
MED/HST	1,202,970	8,276	0.7

Table B.2 The description of each wetland type used in this study.

Wetland class	Soil systems	Water sources	Typical settings and features	Plant species
Marsh	Mineral	Direct flow from lakes, streams, precipitation	Edges of lakes and streams, Coastal zone (salt/tidal marshes)	Herbaceous
Swamp	Mineral or Organic	Precipitation, groundwater, freshwater flooding from rivers or lakes	Along large rivers or on the shores of large lakes	Woody, forested
Mangrove	Organic	Precipitation, groundwater and tidal flow.	Coastal zone mostly grows in sheltered low lying coasts estuaries, and lagoons	Trees and shrubs
Peatland	Organic	Groundwater inflow or precipitation	Standing water of lakes or margins of slow flowing rivers,	Herbaceous plants, Shrubs, small trees.
Seasonal wetland	Organic or mineral	Precipitation	Low lying areas and open fields.	Herbaceous

Table B.3 Confusion matrix for wetlands of Tropical wet and dry (TWD) climate zone after applying RF.

Wetland class	Marsh	Mangrove	Swamp	Peatland	Seasonal wetlands	Deep water	Total	User`s Accuracy
Marsh	510	4	2	0	10	0	526	0.97
Mangrove	4	171	9	6	0	0	190	0.90
Swamp	9	10	141	36	4	0	200	0.71
Peatland	6	4	23	117	0	0	150	0.78
Seasonal wetlands	13	2	2	0	124	6	147	0.84
Deep water	0	0	0	0	12	384	396	0.97
Total	542	191	177	159	153	390	1609	
Producer`s Accuracy	0.94	0.90	0.80	0.74	0.81	0.98		
Overall accuracy (%)								89

Table B.4 Confusion matrix for wetlands of Tropical wet (TW) climate zone after applying RF

Wetland class	Marsh	Mangrove	Swamp	Peatland	Seasonal wetlands	Deep water	Total	User Accuracy
Marsh	249	0	1	0	5	0	255	0.97
Mangrove	8	120	10	1	6	0	145	0.83
Swamp	10	9	107	29	6	0	161	0.66
Peatland	18	7	65	347	2	0	439	0.79
Seasonal wetlands	26	11	14	14	118	17	200	0.59
Deep water	0	0	0	0	2	73	75	0.95
Total	311	147	197	391	139	90	1275	
Producer Accuracy	0.80	0.82	0.54	0.89	0.85	0.81		
Overall accuracy								84

Table B.5 Confusion matrix for wetlands of Semi-Arid climate zone after applying RF

Wetland class	Marsh	Mangrove	Swamp	Peatland	Seasonal wetlands	Deep water	Total	User`s Accuracy
Marsh	64	3	7	2	4	0	80	0.80
Mangrove	0	25	4	2	0	0	31	0.81
Swamp	2	3	32	11	2	0	48	0.64
Peatland	2	3	9	34	2	0	55	0.70
Seasonal wetlands	15	2	3	4	99	5	128	0.90
Deep water	0	0	0	0	8	75	82	0.95
Total	83	36	55	53	115	80	424	
Producer`s Accuracy	0.77	0.69	0.58	0.64	0.86	0.94		
Overall Accuracy (%)								79

Table B.6 Confusion matrix for wetlands of Arid/Desert climate zone after applying RF

Wetland class	Marsh	Mangrove	Swamp	Peatland	Seasonal wetlands	Deep water	Total	User`s Accuracy
Marsh	131	2	4	5	3	0	145	0.90
Mangrove	0	64	5	3	0	0	73	0.88
Swamp	5	9	101	32	6	0	153	0.66
Peatland	2	2	8	35	0	0	47	0.74
Seasonal wetlands	7	2	5	3	40	7	64	0.63
Deep water	0	0	0	0	1	89	90	0.99
Total	145	79	123	78	50	96	572	
Producer`s Accuracy	0.90	0.81	0.82	0.45	0.80	0.93		
Overall Accuracy (%)								77

Table B.7 Confusion matrix for wetlands of Mediterranean/Humid subtropical climate zone after applying RF

Wetland class	Marsh	Mangrove	Swamp	Peatland	Seasonal wetlands	Deep water	Total	User`s Accuracy
Marsh	31	1	2	2	3	0	39	0.79
Mangrove	1	17	5	2	0	0	25	0.68
Swamp	1	2	28	10	2	0	43	0.65
Peatland	2	3	11	29	0	0	45	0.64
Seasonal wetlands	10	0	2	4	43	4	63	0.68
Deep water	0	0	0	0	2	51	53	0.96
Total	45	23	48	47	50	55	268	
Producer`s Accuracy	0.84	0.86	0.95	0.80	0.89	0.98		0.88
Overall Accuracy(%)								78